THERMODYNAMIC MODELLING AND OPTIMIZATION OF BIOMASS GASIFICATION SYSTEM FOR FISCHER-TROPSCH SYNTHESIS

EMMANUEL YERI KOMBE

J98/39229/2016

A Research Thesis Submitted in Partial Fulfilment of the Requirements for the Award of the Degree of Doctor of Philosophy in the School of Engineering and Architecture of Kenyatta University

June, 2023

Declaration

This thesis is my original work and has not been presented for a degree at any other University.

Signature ..... Date 08/06/2023

Emmanuel Yeri Kombe

J98/39229/2016

Supervisors

We confirm that the work reported in this thesis was carried out by the student under our supervision.

Signature..... Date 08.06.2023

Dr. Nickson K. Lang'at

Agriculture and Biosystem Engineering Department

Kenyatta University

Signature..... Date 08.06.2023

Dr. Paul M. Njogu

Institute of Energy and Environmental Technology

Jomo Kenyatta University of Agriculture and Technology

Dedication

This work is dedicated to my dear wife Magdaline Musanga, our sons Innocent Kakai and Eleazar Baraka and my family members for their unwavering support and understanding throughout my studies. Above all, our Almighty God, who provided strength, health and favour to enable me see this through.

Acknowledgement

I sincerely thank the Federal Ministry for Economic Cooperation and Development (BMZ) for funding my doctoral study (Grant personal Ref. 91672311). I express sincere gratitude to my supervisors, Dr. Nickson Lang'at and Dr. Paul Njogu, for their guidance and diligent supervision. My appreciation goes to Dr. Francis Njoka, Chairman Energy Technology Department, Prof. Christian-Toralf Weber of the Department of Engineering and Industrial Design, Hochschule Magdeburg-Stendal, Magdeburg, Germany, and Prof. Reiner Malessar of the Department of Engineering, Technische Hochschule Brandenburg Fachbereich Technik, University of Applied Sciences, Brandenburg, Germany for their support and contribution at various stages of my research work. The student also expresses gratitude for the access to computing resources provided by Otto-von-Guericke-University, Instrumental and Environmental Technology Department under the supervision of Prof. Ulrich Krause.

Table of contents

List of Figures

List of Tables

Nomenclature

y	Number of atoms of Oxygen
z	Number of atoms of Nitrogen
x	Number of atoms of Hydrogen
k	Number of atoms of Sulphur
C	Percentage mass of carbon in the biomass.
Cl	Percentage mass of chlorine in the biomass
H	Percentage mass of hydrogen in the biomass.
N	Percentage mass of nitrogen in the biomass
O	Percentage mass of oxygen in the biomass.
R	Universal gas constant, 8.314 kJ/kmol.K
S	Percentage mass of sulfur in the biomass.
k_1	Equilibrium constant for Methane formation
k_2	Equilibrium constant for water-gas shift reaction
f_i	Fugacity of species i
n_i	The numbers of moles of species i
μ_i	The chemical potential of species i
X_i	Volume fraction of syngas component on a dry basis
G^t	Total Gibbs free energy
ΔG^0	Standard Gibbs function
ΔH^0	Heat of formation
G_i^0	Standard Gibbs free energy
f_i^0	Standard fugacity of species i
$\emptyset$	Coefficient of fugacity

Abbreviations and Acronyms

Adj SS	Adjusted sum of squares
ANN	Artificial Neural Network
Aspen Plus	Advanced System for Process Engineering Plus
BBD	Box-Behnken design
CCD	Central composite design
CCRD	Central composite rotatable design
CGE	Cold gas efficiency
DF	Degree of freedom
EES	Engineering Equation Solver
EIA	Energy Information Administration
ER	Equivalence ratio
HHV	Higher heating value
IEA	International Energy Agency
IME	Institute of Mechanical Engineers
MC	Moisture Content
LHV_{bm}	Lower heating value of biomass feedstock (MJ/kg)
LHV_{Syngas}	Lower heating value of syngas (MJ/Nm^3)
RMSE	Root mean square error
RSM	Response surface methodology
S/B	Steam to biomass ratio
SS_R	Sum of squares of residual
SS_T	Total sum of squares
UN	United Nations

Abstract

Biomass is a feasible route for producing transport fuels through Fischer-Tropsch synthesis (FTs). Production of transport fuels from biomass gasification output gas by FTs has become more attractive due to its ability to substitute fossil fuel in the energy market. Gasification technology is at the forefront of biomass conversion among other technologies due to its high flexibility in utilizing various biomass materials. In this work, a thermodynamic model of air gasification of rice husk in a downdraft gasifier was developed using Aspen Plus software and Engineering Equation Solver at various operating conditions. Experiments were conducted to validate the model. The influence of gasification temperature, equivalence ratio (ER), and moisture content (MC) on the composition of syngas, hydrogen to carbon monoxide ratio (H_2/CO), and lower heating value of syngas was studied. Response surface methodology was applied to study the combined effects of the main operating parameters and thus determine the optimized zone of the operating conditions for Fischer-Tropsch synthesis. The R^2 values of the generated regression models from the ANOVA tool were observed to be 98.47% for LHV_{Syngas}, 98.93% for H_2, 96.94% for CO and 89.91% for H_2/CO molar ratio with corresponding Adj-R^2 values of 98.28%, 98.80%, 96.56%, and 88.64%, respectively. This result indicates that the regression models determined the response variables with a high accuracy level. By using Response Surface Methodology (RSM), an optimization of the parameters was achieved. The RSM analysis results showed optimal conditions at gasification temperatures between 720 ^oC and 780 ^oC, ER in the range of 0.06 and 0.095, and MC in the range of 10% and 16%. The findings of this study reveal that a blend of simulation with advanced optimization tools can indeed achieve optimal operating conditions of a gasification system at a more refined precision. These analyses could form a basis for future practical development and implementation of biomass-based gasification systems through the selection of the best possible conditions in on-field plant operations.

CHAPTER ONE: INTRODUCTION

1.1 Background Information

1.1.1 Energy crisis and climate change

The global energy demand increases daily, causing an energy crisis due to the persistent rise in the global population (Coyle & Simmons, 2014). Since 2012 the International Energy Agency (IEA) has asserted that petroleum and natural gas produce about 81 percent of the world's overall principal energy supply (IEA, 2014). With the constant rise in the global population, the energy consumption imposed on the current energy producers will worsen in years to come (Homchat & Ramphueiphad 2022).

Fossil fuel reserves have been estimated to last for some years, therefore, the need to develop more diverse energy generation technologies is becoming increasingly vital (Veziroglu, 2008). Moreover, burning fossil fuels emits extensive greenhouse gases into the environment (Park et al., 2021), which causes severe environmental issues (Davis & Caldeira, 2010). Efforts have been made to develop cleaner and environmentally friendly biofuels such as diesel, jet fuel and gasoline to meet the ever-growing global energy demand while reducing environmental pollution. This is possible through FTs of linear hydrocarbons from a synthetic gas patented by Franz Fischer and Hans Tropsch (Dasappa et al., 2004).

Biomass conversion to synthesis gas and subsequent conversion to transport fuel via Fischer-Tropsch synthesis (FTs) has gained increasing attention in recent years. FTs have gained interest in producing high-added value liquid biofuels by exploiting natural gas, biomass, and coal (Buragohain et al., 2010; Martín & Grossmann, 2011). Biomass to liquid through Fischer-Tropsch synthesis (BTL-FTs) produces cleaner and environmentally friendly biofuels such as gasoline, jet fuel, and diesel. In the BTL-

FTs process, the biomass feedstock is first converted into bio-synthetic gas through gasification. Then, the bio-synthetic gas is cleaned to remove impurities such as tar to produce a clean synthetic gas that meets the FTs requirements. The purified synthetic gas is finally used in an FT catalytic reactor to produce clean biofuels.

The biomass gasification product mainly comprises carbon dioxide, carbon monoxide, hydrogen, and methane as the main gas-phase products; other impurities such as tar and char, which account for less than 1%, are the main by-products (Chiodini et al., 2017). Considering FTs application, it is vital to find optimum operating conditions of the gasification system, which allow high hydrogen to carbon monoxide ratio.

1.1.2 Biomass as a renewable energy resource

Biomass is any carbon-based material originating from plants or animals which exist renewably. It is an energy resource that is theoretically limitless with repeated consumption. Extracting energy from biomass can be achieved through conversion technologies based on thermochemical (Pyrolysis, Combustion, and Gasification) or biological (Anaerobic Digestion, Fermentation, and Composting) conversion processes.

The conversion of biomass energy is considered a "carbon-neutral process". During biomass growth, quantities of Carbon Dioxide are absorbed, and when gasified, only the Carbon Dioxide absorbed is released resulting in a net-zero rise in the levels of global Carbon Dioxide. Even after deducting this aspect, the intensity of carbon in fossil-based fuels is substantially higher than that of biomass (Basu, 2013).

1.1.3 Gasification

From a theoretical point of view, gasification is a thermochemical process that converts raw biomass materials to a gaseous fuel by partially oxidizing them with

gasifying agents such as oxygen, steam, air, or their mixtures (Bridgwater, 2003). It is characterized by drying (100 °C – 200 °C), pyrolysis (200 °C – 500 °C), oxidation, and reduction stages (Faraji & Saidi, 2021). The potential application of the gasification product gas depends on its composition and quality. There are several gasifiers available which vary in terms of gasification medium, operating temperature, pressure, and heat source. The three widely approved types of gasification systems, which produce variable tar output, are downdraft, fluidized bed and updraft systems.

Among the various biomass conversion technologies, gasification remains to be the most viable alternative for bioenergy utilization (Kaewluan & Pipatmanomai, 2011: Heidenreich & Foscolo, 2015). Biomass gasification is highly flexible in utilizing various kinds of fresh biomass feedstocks (Heidenreich & Foscolo, 2015). It can upgrade a lower-energy-value biomass feedstock to a higher-energy-value synthetic gas (Kuo et al., 2014), which can be utilized to generate electricity through gas engines and gas turbines.

1.2 Problem Statement

Rice husk is the key waste produced by the rice milling industry. Annually, the world generates above 120 million tons (Jain & Goss, 2000; Yoon et al., 2012) of rice husk. According to the Government of Kenya (2009); Njogu et al. (2015), Kenya produces between 45 to 50 thousand tons of rice annually. A couple of years back, rice husk was regarded to be of no economic value to millers (Njogu et al., 2015) and was often dumped off or burned in open fields, thus creating both land and air pollution (Bakar et al., 2016; Kate & Chaurasia, 2018).

Biomass conversion to synthesis gas and subsequent conversion to transport fuel via Fischer-Tropsch synthesis (FTs) is a promising technology for producing cleaner and

environmentally friendly biofuels. However, it is not viable in the current context of biofuel production due to low syngas yields from biomass gasification, lack of reproducibility in gasification systems, presence of tar, a troublesome compound in syngas, and lack of economic competitiveness with respect to fossil fuels thus the need for this work. Presently, rice husk is commonly used in fillers, compost, and stall mats. Owing to the rise in energy demand, many researchers are actively participating in the search for alternative routes of using rice husk as fuel for energy production.

From a brief literature survey, it was established that many of the previous simulation studies on process modelling and simulation for Fischer Tropsch synthesis applications have focused on the fundamental process. Moreover, most of the research studies employed the single-parameter optimization technique which is not efficient in determining the optimal working parameters of a process. To our knowledge, no work has considered the inclusion of a comprehensive syngas purification coupled with RSM optimization for Fischer Tropsch synthesis application from air-gasification of rice husk. Furthermore, 400 runs of Aspen Plus simulated results were used to construct an RSM design matrix, offering another mileage of the present study.

1.3 Justification

A substantial amount of agro-industrial, municipal, and forestry waste is discarded each year; instead, it can be recovered and converted into energy via thermochemical or biological conversion methods (Li et al., 2019). Generally, the consistent yearly production of rice husks makes it possible to secure a sustainable raw material supply (Yoon et al., 2012). Moreover, rice husk does not require a pre-treatment process, and this reduces the need for pre-treatment costs (Yoon et al., 2012). Furthermore, rice husk has a uniform particle size and chemical composition, consequently enabling efficient combustion (Natarajan et al., 1998; Yoon et al., 2012). Gasification of solid

fuels is widely acknowledged as the most efficient method of generating energy from a variety of wastes (Faraji & Saidi, 2021). It is incredibly adaptable when it comes to using different types of fresh biomass feedstocks (Heidenreich & Foscolo, 2015). The use of rice husks for the generation of transport fuel will not only improves the efficiency of energy recovery from waste but also enhances the efficiency of waste management.

1.4 Research Objectives

1.4.1 General objective

The general research objective is to develop a thermodynamic simulation model for fixed bed gasification systems with the ability to perform a multi-objective optimization of the operating conditions of a gasification process for Fischer Tropsch synthesis applications.

1.4.2 Specific objectives

The specific objectives of the study were:

i. To develop a robust numerical simulation model of a fixed bed gasifier using Engineering Equation Solver and Aspen Plus.
ii. To validate the simulation model experimentally.
iii. To analyse the model's sensitivity on syngas composition, syngas yield and gasifier's performance.
iv. To investigate the optimized zone of the operating conditions for Fischer Tropsch synthesis application based on the response surface methodology.

1.5 Significance of the Study

Among the various kinds of biomass feedstocks identified for bioenergy production, agricultural residue and process waste have a better environmental impact during the

life cycle (Raheem et al., 2019; Ramirez & Rainey, 2019). Using agricultural residue as feedstock instead of disposal will reduce the net impacts and emissions. This will further improve the efficiency of waste management and offers excellent potential for producing environmentally friendly renewable and low-carbon energy (Kumar & Samadder, 2017).

1.6 Scope of the Study

There are several applications of syngas generated from biomass gasification but this study focuses on generating syngas for FTs application. This study is restricted to thermodynamic modelling and optimization of air-gasification of biomass in a fixed bed gasification system to establish the optimal conditions that yield maximum H_2 to CO ratio which are the raw material for liquid transport fuel synthesis. Hence, this study is limited to establishing an optimum condition of a gasification system to predict the feasibility of generating biofuels from air-gasification of biomass through simulation blended with advanced optimization tools.

CHAPTER TWO: LITERATURE REVIEW

2.1 Introduction

In order to establish an optimal gasifier condition to enhance syngas quality, developing a gasification model to control the distribution of tar is paramount. This chapter comprehensively discusses biomass as a renewable source of energy, biomass gasification, the operating conditions influencing the yields and composition of the syngas, syngas application, gasification models and process optimization based on response surface methodology.

2.2 Biomass as a Renewable Energy Source

Biomass is the world's principal energy source after fossil fuel (Tavares et al., 2020). It refers to organic materials originating from living or recently lived organisms like plants, animals, and wastes, which can be used as a clean and sustainable energy source (Mathieu & Dubuisson, 2002; Balat, 2005; Bassyouni et al., 2014). Its major characteristics are the apparent net-zero carbon dioxide (Roy et al., 2019) and worldwide availability (Zaman et al., 2020). The potential reduction in global carbon dioxide emissions using alternative fuels to fossil fuels makes biomass a promising energy resource (Favas et al., 2017). It is a valuable, sustainable energy resource alternative to fossil fuels (Begum et al., 2014) convertible to electricity, heat, syngas, liquid transportation biofuels, and biogas (Converti et al., 2009) through energy conversion technologies such as combustion, gasification, fermentation and anaerobic digestion. The conventional sources of biomass (Gunnarsson & Petersen, 2007) include fuelwood, energy crops, agricultural residue, and municipal wastes (Balat, 2005; Demirbas, 2008).

The efficient utilization of biomass has been considered the most promising carbon dioxide neutral energy option, as well as offering an alternative route for reducing the

overdependence on fossil fuels**.** However, the relatively low density of most biomass resources makes its transport, handling, and processing difficult (Broer & Brown, 2015). Furthermore, growing biomass feedstock for energy production requires large amounts of nitrogenous fertilisers, which are the by-products of fossil fuel energy production; this leaves a question of how suitable Bio-energy is a sustainable and environmentally sensible substitute for fossil fuels (Younger, 2015).

2.2.1 Rice husk

Among the various kinds of biomass feedstocks identified for bioenergy production, agricultural residue and process waste have a better environmental impact during the life cycle (Raheem et al., 2019; Ramirez & Rainey, 2019). Using agricultural residue as feedstock instead of disposal reduces the net impacts and emissions when compared to using dedicated energy crops. Rice husk is the key waste produced by the rice milling industry. Annually, the world generates above 120 million tons (Jain & Goss, 2000; Yoon et al., 2012) of rice husk. According to the Government of Kenya (2009); Njogu et al. (2015), Kenya produces between 45 to 50 thousand tons of rice annually.

A couple of years back, rice husk was regarded to be of no economic value to millers (Njogu et al., 2015) and was often dumped off or burned in open fields, thus creating both land and air pollution (Bakar et al., 2016; Kate & Chaurasia, 2018).

Rice husk has a relatively high ash content and low energy density. The rice husk ash contains 95 % silica (Yoon et al., 2012) with several industrial applications such as carrier for catalyst, reinforcement of rubber and thickening of paints etc. (Alvarez et al., 2014; Kate & Chaurasia, 2018). Previously, studies have been conducted on the manufacturing of catalyst-supporting material (Ismagilov et al., 2009), solar-grade

silicon (Amick, 1982; Hunt et al., 1984), ceramics (Bondioli et al., 2010), zeolite (Wittayakun et al., 2008) from rice husk silica. Presently, rice husk is commonly used in fillers, compost, and stall mats. Owing to the rise in energy demand, many researchers are actively participating in the search for alternative routes of using rice husk as fuel for energy production. In order to generate different forms of energy like electricity, heat, liquid fuel, and hydrogen from rice husk, research on combustion (Albina, 2006), pyrolysis (Zheng et al., 2006) and gasification(Wu et al., 2008; Zhao et al., 2009) have been done.

Generally, the consistent yearly production of rice husks makes it possible to secure a raw material supply (Yoon et al., 2012). Moreover, rice husk does not require a pre-treatment process, and this reduces the need for pre-treatment costs (Yoon et al., 2012). Furthermore, rice husk has a uniform particle size and chemical composition, consequently enabling efficient combustion (Natarajan et al., 1998; Yoon et al., 2012).

2.3 Biomass Gasification

For biomass utilisation toward a clean fuel source, biomass gasification is a promising conversion technology (Heidenreich & Foscolo, 2015). Biomass gasification is highly flexible in utilizing various kinds of biomass feedstock (Heidenreich & Foscolo, 2015). Gasification is a process through which complex hydrocarbons contained in the feedstock are thermally broken down into a valuable mixture of gases (syngas) which comprise mainly Carbon Monoxide (CO), Methane (CH_4), Hydrogen (H_2) and Carbon Dioxide (CO_2) (Heidenreich & Foscolo, 2015; Al-Rahbi et al., 2016; Đurišić-Mladenović et al., 2016). The biomass gasification process is characterized by four stages comprising drying, pyrolysis, oxidation and reduction (Basu, 2013; Han et al., 2017), as shown in Figure 2.1.

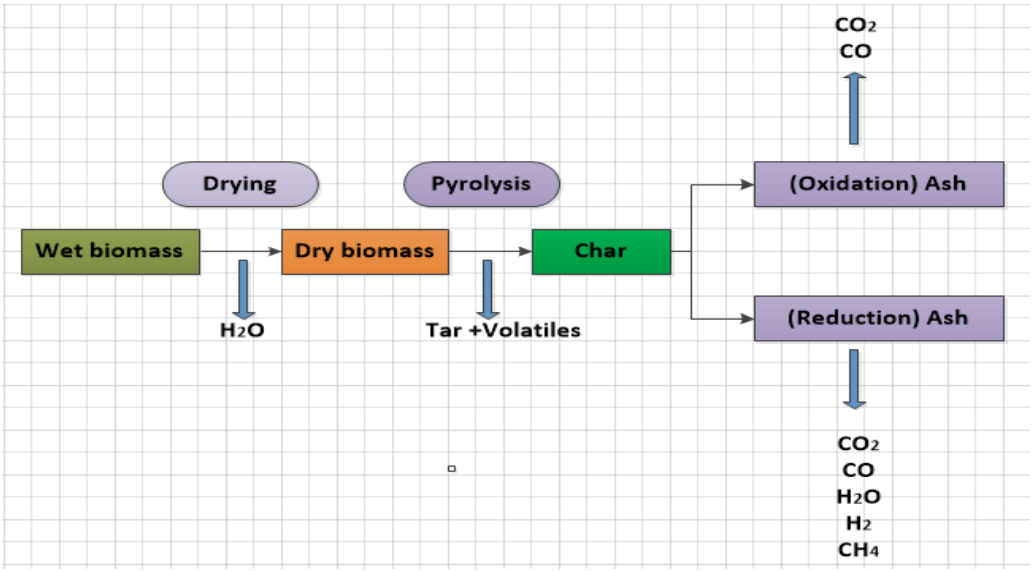

Figure 2.1 Biomass gasification process reaction paths

Fresh biomass feedstock usually has a moisture content exceeding 50% (Basu, 2013; Asadullah, 2014). Moisture content exceeding 40% reduces the gasification system performance as lots of unrecoverable energy is utilised in evaporating the water contained in the biomass. It is, therefore, necessary to pre-dry the biomass feedstock to the desired moisture content before feeding it into the gasifier. Drying occurs at a temperature between 100 ℃ – 200 ℃. The dried biomass then undergoes the pyrolysis process. During pyrolysis, the biomass feedstock is thermally broken down in the absence of air into volatiles, char, ash and tar (Diyoke et al., 2018). Char is combusted with oxygen after pyrolysis. Combustion occurs at a temperature of between 700 ℃– 1500 ℃ and is the key reaction occurring in a gasifier (Doherty et al., 2009; Han et al., 2017; Pala et al., 2017). The combustible substances present in the feedstock react with the supplied oxygen yielding CO_2 and H_2O. The remaining char finally reacts with the combustion products in the gasification zone. In this zone (800℃ – 1000℃), a series of endothermic reactions fuelled by thermal energy from combustion takes place. H_2, CO and CH_4 are the combustible gases produced during gasification (Zainal et al., 2001; Altafini et al., 2003; Melgar et al., 2007). The major gasification

reactions are methanation, shift conversion, boudouard, reforming and water-gas shift (Doherty et al., 2009; Han et al., 2017; Pala et al., 2017) as summarised in Table 2.1.

Table 2.1 Main gasification reactions

Reaction ID	Chemical reaction	Reaction Name	Reaction heat
Heterogeneous reactions:			
R_1	$C + 0.5O_2 \rightarrow CO$	Char partial combustion	$(-111\ kJ/mol)$
R_2	$C + CO_2 \leftrightarrow 2CO$	Boudouard reaction	$(+172\ kJ/mol)$
R_3	$C + H_2O \leftrightarrow H_2 + CO$	Water gas reaction	$(+131\ kJ/mol)$
R_4	$C + 2H_2 \leftrightarrow CH_4$	Methanation	$(-75\ kJ/mol)$
Homogeneous reactions:			
R_5	$CO + 0.5O_2 \rightarrow CO_2$	CO partial combustion	$(-283\ kJ/mol)$
R_6	$H_2 + 0.5O_2 \rightarrow H_2O$	H_2 partial combustion	$(-242\ kJ/mol)$
R_7	$CO + H_2O \leftrightarrow CO_2 + H_2$	Water-gas shift reaction	$(-41\ kJ/mol)$
R_8	$CH_4 + H_2O \leftrightarrow CO + 3H_2$	Steam-methane reforming	$(+206\ kJ/mol)$
Hydrogen sulfide (H_2S) and ammonia (NH_3) formation reactions:			
R_9	$H_2 + S \rightarrow H_2S$	H_2S formation	nr*
R_{10}	$0.5N_2 + 1.5H_2 \leftrightarrow NH_3$	NH_3 formation	nr*

nr* = not reported
Heat of reaction is in standard conditions

2.4 Factors Affecting Syngas Yield

The quality of syngas varies based on the type of gasifier, the type of biomass feedstock and the gasifier operating conditions which include the oxidant, gasification temperature, moisture content of the biomass feedstock, equivalence ratio etc. (Heidenreich & Foscolo, 2015; Đurišić-Mladenović et al., 2016).

2.4.1 Temperature

Gasification temperature affects the rates of chemical reactions occurring during gasification. High gasification temperatures ranging from 800-850 ℃ yield syngas abundant in H_2 and CO with little amounts of CH_4 and little or no tar formed (Mahishi & Goswami, 2007). According to Xiang et al. (2018), the yield of H_2 and CO_2 increases in composition while that of CO_2 and H_2O decreases as the gasification

temperature increase from 700 to 1100 ℃. This is because high temperature triggers the thermal cracking of tar compounds into H_2, CO and other controllable lightweight gases (Han & Kim, 2008).

2.4.2 Equivalence ratio

ER is among the key parameter that influences the performance of a gasifier. This parameter determines the formation of volatiles by fixing the actual air required for combustion. Subsequently, the combustion of volatiles provides the heat needed to drive water gas and Boudouard reactions. ER calculates the quantity of air needed for gasification. This parameter determines both available oxygen for combustion and the gasification temperature attained. It is defined as per Eqn. (2.1) (Jangsawang et al., 2015; Diyoke et al., 2018; Upadhyay et al., 2019).

$$\text{ER} = \frac{(\frac{Air}{Fuel})_{stoichiometric}}{(\frac{Air}{Fuel})_{actual}} \tag{2.1}$$

A study by Chang et al. (2011) and Diyoke et al., (2018) showed that a higher ER provides lower hydrogen yields as it favours complete combustion. The standard values of equivalence ratio for biomass gasification range from 0.2 and 0.4. Using a downdraft gasifier, Gai & Dong (2012) observed that a rise in equivalence ratio from 0.18 to 0.32 increased the mole fraction of H_2 from 6.91 to 13.51%, and that of CO increased from 11.35 to 19.81% (Pereira et al., 2012). A study by Mahishi & Goswami (2007) showed that enhancing the equivalence ratio factor from 0.1 to 0.2 increases the mole fraction of H_2 and CO and beyond equivalence ratio factor 0.2, they also observed a decrease in the mole fraction of H_2 and CO.

2.4.3 Biomass moisture

Biomass moisture content is among the major factors affecting the quality and composition of syngas. A study by Brammer & Bridgwater (2002) on the impact of biomass moisture content on gasification process performance proved that excess moisture content compromises the output gas quality and the performance of the gasification system, as lots of the energy is utilised in evaporating the water contained in the biomass. According to Reed & Das (1988), a moisture content lower than 33% is preferred for high-quality combustible syngas production. According to Brammer & Bridgwater (2002); Pereira et al. (2012), moisture content below 30% is suitable for gasification. Plis & Wilk (2011) observed that dry biomass produces higher CO content in the syngas, while CO_2 content escalates with biomass moisture enhancement. Low moisture content causes high oxidation zone temperature which further favours the formation of CO and H_2 (Diyoke et al., 2018).

2.4.4 Pressure

From equilibrium studies, pressure enhancement decreases the hydrogen and carbon monoxide yield (Mahishi & Goswami, 2007). A simulation carried out by Mahishi & Goswami (2007) on the impact of lowering pressure below 1 atm showed a negligible increase in hydrogen and carbon monoxide yield, and for this reason, all analyses were performed at a constant pressure of 1 atm.

2.4.5 Types of gasifiers

Based on the type of combustion bed, gasification systems are classified into three, namely: fixed or moving bed, fluidised bed and entrained-flow bed gasifiers (Basu, 2013), as illustrated in Figure 2.2. In this section, no discussion will be provided for entrained flow gasifiers due to their unsuitability for biomass.

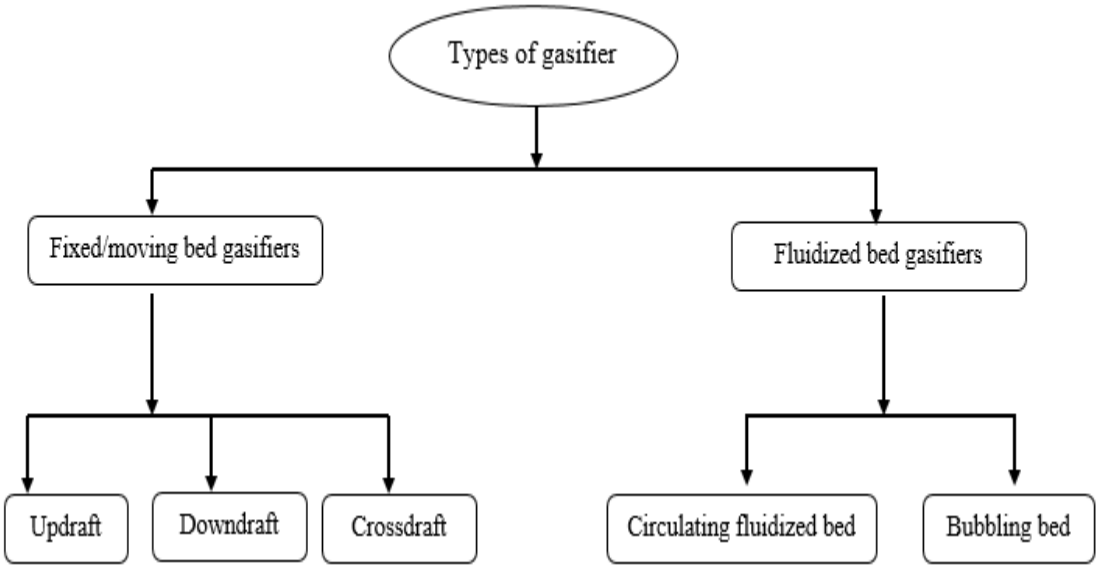

Figure 2.2 Gasification system classifications

2.4.5.1 Fixed bed gasification system

This type of gasification technology is the most commonly used in synthetic gas production. These gasifiers consist of a simple cylindrical reactor and are easy to construct and operate. In a fixed-bed gasifier, the biomass fuel and producer gas move either downward or upward. These reactors are further classified based on how the gasification medium is introduced into the reactor to gasify the biomass fuel as downdraft, updraft and crossdraft gasifiers.

Downdraft gasifier: This gasifier is highly suitable for converting high volatile fuel such as biomass to a low tar content syngas, making it the most suitable gasification system for power production. In this reactor, the gasifying agent is introduced into downward-flowing biomass fuel at the combustion zone, and the syngas is extracted at the bottom (Panwar et al., 2012), as shown in Figure 2.3 (a). The product gas passes through the reduction zone before exiting the reactor resulting in a low tar content syngas as most of the tar is cracked (Elakiya et al., 2016).

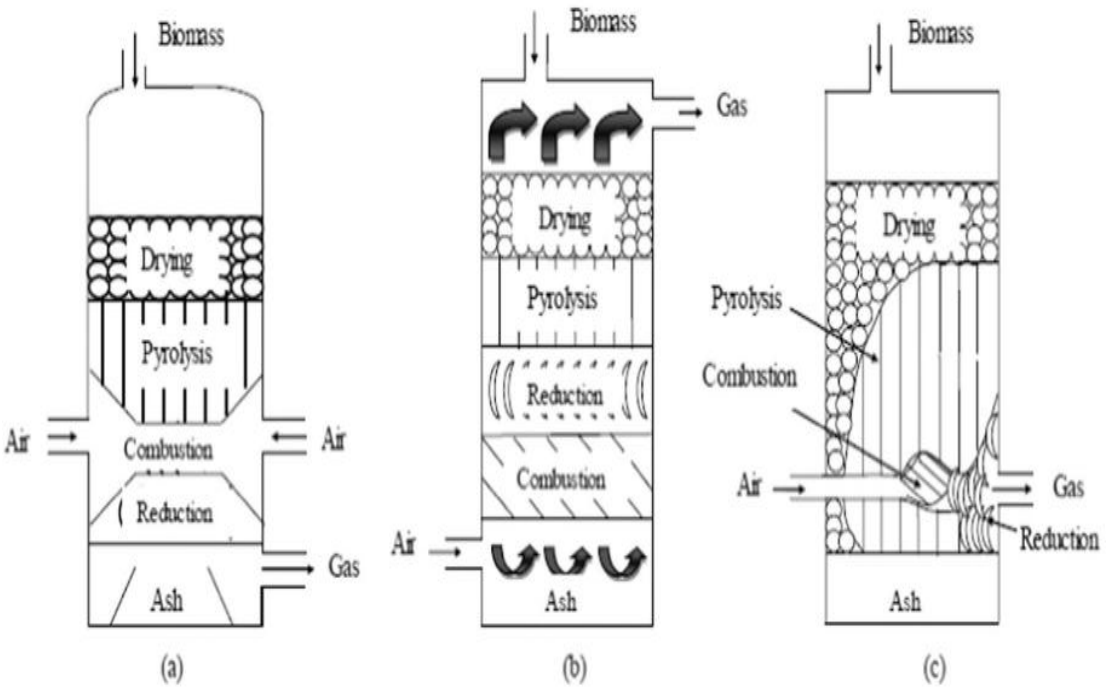

Figure 2.3 Fixed bed gasifiers: (a) Downdraft, (b) Updraft, and (c) Crossdraft gasifier (Sansaniwal et al., 2017).

Updraft gasifier: In this reactor, the gasifying agent is introduced at the bottom, and the product gas leaves at the top, as shown in Figure 2.3 (b). As the product gas passes through the unburnt fuel before exiting the reactor, it contains no ash but has more tar and water vapour. Therefore, this design is appropriate for charcoal, a tar-free fuel (Elakiya et al., 2016).

Crossdraft gasifier: In this reactor, fuel is fed at the top while the gasification agent enters through the sides of the reactor, and the producer gas is then drawn off from the opposite side of the reactor, as shown in Figure 2.3 (c).

2.4.5.2 Fluidised bed gasifiers

This design has been extensively used for many years in coal gasification. This gasifier achieves uniform temperature distribution in the gasification zone, making it

advantageous over fixed-bed gasifiers (McKendry, 2002; Basu, 2013). These gasifiers are further classified as bubbling and circulating fluidised bed gasifiers.

Bubbling bed gasifier: This gasifier consists of a reactor containing a grate fixed at the bottom through which the gasification agent is introduced, as shown in Figure 2.4 (a). A moving bed above the grate through which biomass feeding takes place. The bed temperature is maintained at 700-900 ^{o}C by varying the air/biomass ratio. These gasifiers promote tar and particulate formation, which require the reactor to be coupled with a cyclone (Motta et al., 2018).

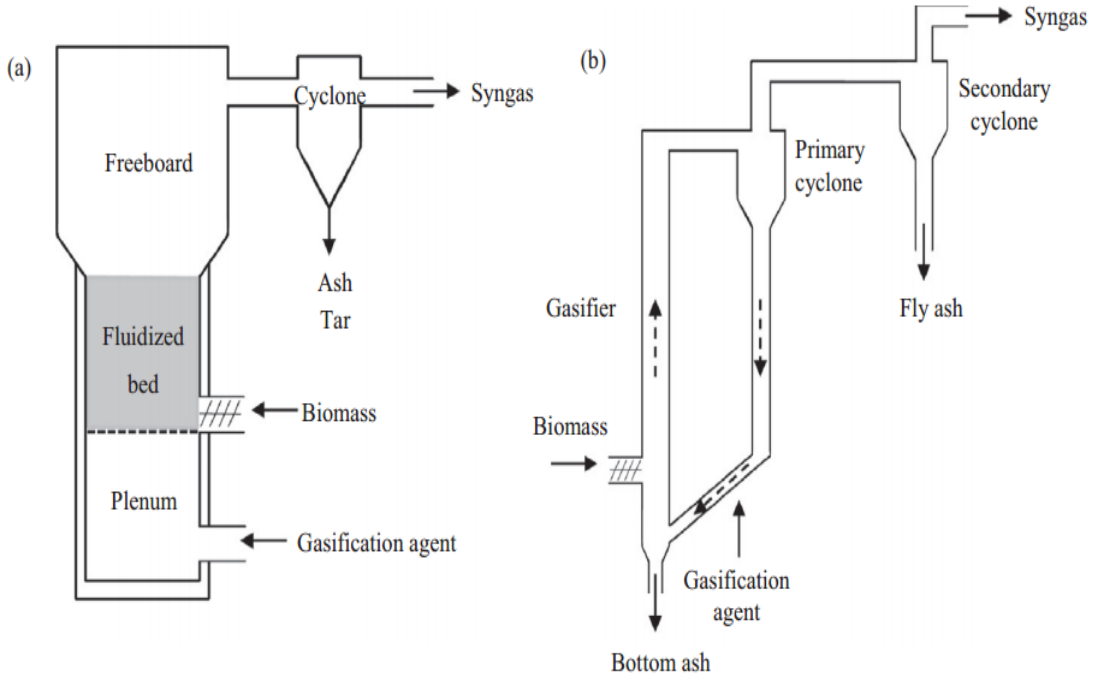

Figure 2.4 Fluidised bed gasifiers: (a) Bubbling bed; (b) Circulating bed gasifiers (Motta et al., 2018).

Circulating fluidised bed gasifier: This gasification system Figure 2.4 (b) can withstand high-capacity inputs and has been widely used for the gasification of forestry residues in the paper industry. In this gasifier, the feedstock is circulated between the reactor and a cyclone coupled to the gasifier to separate ash from char

and bed material (McKendry, 2002; Motta et al., 2018). This reactor is appropriate for syngas applications, such as a gas turbine, where a compressed product gas is required (McKendry, 2002).

2.5 Analytical Techniques

Analysing the characteristics of feedstock is a crucial part of a process. It provides important information which helps in understanding the best choice for the biomass conversion process. This section discusses the analytical procedures for establishing the characteristics of biomass feedstock and the composition of syngas generated through biomass gasification.

2.5.1 Analytical techniques for biomass characterization

For accurate and consistent fuel characterization, the use of a standardized method is paramount. Various analytical methods have been used to characterize solid fuels. In these characterization analyses, different standard procedures such as ASTM, ISO, DIN, BS, and others have been used (Higman & Burgt, 2003).

Table 2.2 Analytical methods for biomass fuel characterization.

Property	**Analytical method**
Heating value	ASTM D 2015, E 711
Particle size distribution	ASTM E828
Proximate analysis	
Moisture	ASTM E871, DIN 51718
Ash	ASTM E 1755, ASTM D1102, DIN 51719
Volatiles	ASTM E 872–82, ASTM E 897, DIN 51720
Fixed carbon	by difference
Ultimate analysis	
Carbon	ASTM E 777
Hydrogen	ASTM E 777
Nitrogen	ASTM E 778
Sulphur	ASTM E 775
Chlorine	ASTM E 776
Oxygen	By difference
Ash elemental	ASTM D3682, ASTM D2795, ASTM D4278, AOAC 14.7

Table 2.2 summarizes the most frequently used analytical method to determine the main properties of biomass fuels (Jenkins et al., 1998; Demirbas, 2004; Virmond et al., 2012; Basu, 2013; Yusuf & Inambao, 2020; Zinla et al., 2021). Though some methods were developed for specific fuels such as coal, they are generally applicable for biomass fuel characterization (Jenkins et al., 1998).

2.5.2 Analytical techniques for gas analysis

There are two wide-ranging analysis methods developed by several institutions and employed for syngas analysis (Dayton & Foust, 2020). These are offline and online analysis techniques. Offline syngas analysis involves indirectly analysing an extracted gas, whereas online procedures engage directly with a gas stream generated from a reactor for purposes of providing live data. Online gas analysis is always preferred if analytical instruments are available. If not, producer gas can be sampled and stored in vessels for post-process analysis. This chapter critically reviews two syngas analysers: Gas Chromatography coupled to a thermocouple detector system (GC-TCD) and Fourier Transform Infrared (FTIR) spectroscopy gas analysers.

2.5.2.1 Gas chromatography coupled to a thermocouple detector (GC-TCD)

GC-TCD is used to qualitatively and quantitatively measure chemical composition within complex mixtures of either gas or liquid solutions. Gas samples are mixed with a carrier gas, usually helium (Snavely & Subramaniam, 1998). GC-TCD incorporates a gas chromatograph system and a Thermocouple Detector, which provide a higher degree of species identification. By using a fused silica capillary column, the GC block separates the diverse sample mixture constituents in stages along the column's length and elutes at different times. Following elution, the TCD captures the various components, broken down into fragments and analysed based on the difference between their thermal conductivities and that of the carrier gas (Snavely &

Subramaniam, 1998; Budiman et al., 2015). These procedures produce a vast amount of illustrative data represented in gas chromatogram form with peaks identifiable to various components within the analysed mixture. The quantity of various distinctive constituents of the analysed mixture can then be extrapolated from the gas chromatograms through calibration standards. This makes GC-TCD instrumental in syngas components quantification (Harvey, 2000).

2.5.2.2 Fourier transform infrared gas analysers (FTIR)

FTIR is a spectroscopy technique for real-time monitoring of infrared active gas phase species (Dayton & Foust, 2020). It works on the principle that different gas compounds vibrate within their chemical structures depending on their unique functional groups after absorbing energy (Willard et al., 1986). Since a large number of compounds in the producer gas are infrared active, equipment working in this range, such as FTIR, is very useful (Granada et al., 2012). FTIR is a suitable producer gas analyser due to its speed and accuracy (Granada et al., 2012). This makes FTIR an ideal technique for syngas analysis.

Infrared radiation is passed through a gas sample contained in a gas sample cell. During this process, individual gas components absorb radiation, thereby transmitting a percentage of the incident radiation. With the in-built library containing FTIR data for many gas phase molecules, the obtained spectrum can be matched to identify individual components in the producer gas. Modern FTIRs can determine gas concentrations based on Beer's Law without the need for calibration (Dayton & Foust, 2020).

2.6 Syngas Utilization

Syngas can be used for various applications like biofuel production through Fischer-Tropsch synthesis, energy production by running a gas turbine and the production of different chemicals (Bahng et al., 2009; Damartzis & Zabaniotou, 2011). Apart from syngas, biomass gasification also yields solids (ash or slag), and condensable polycyclic aromatic hydrocarbon (tar), which is a significant contaminant in the output gas (Basu, 2013). In addition to tar, the product also contains small amounts of Nitrogen gas (N_2), oxygen gas (O_2) and Hydrogen Sulphide (H_2S) (Kraussler et al., 2016). The potential syngas' application varies based on the quality and composition of syngas (Đurišić-Mladenović et al., 2016). Figure 2.5 illustrates the biomass gasification process pathways and the application of the output gas.

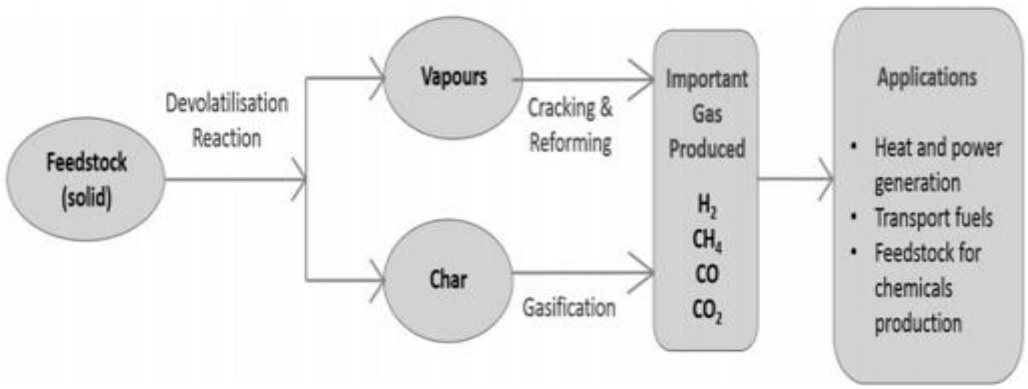

Figure 2.5 Biomass gasification process routes and applications (Ahmad et al., 2016).

2.6.1 Fischer-Tropsch synthesis (FTs)

FTs is a set of catalytic processes for manufacturing transport fuels such as gasoline and diesel from syngas (CO and H_2) derived from biomass, coal or natural gas (Buragohain et al., 2010). Producing transport fuels from biomass gasification output gas by FTs has become more attractive in the industry and academia due to its ability to substitute fossil fuel in the energy market; such biofuels can meet the rising global energy demand and the strict environmental regulations (Ail & Dasappa, 2016).

In the Biomass to liquid through FTs, the biomass feedstock is first converted into bio-synthetic gas through gasification. Then, the bio-synthetic gas is cleaned to remove impurities such as tar to produce a clean synthetic gas which meets the FTs requirements. The purified synthetic gas is finally used in an FT catalytic reactor to produce clean biofuels such as gasoline and diesel. Figure 2.6 illustrates the process of producing biofuel from biomass through FTs.

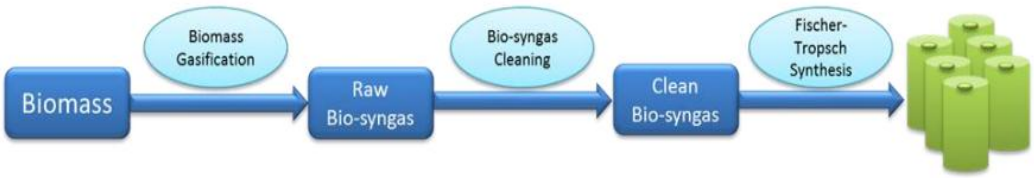

Figure 2.6 Flow sheet for biofuel production from biomass through Fischer–Tropsch Synthesis (Hu et al., 2012).

2.7 Biomass Gasification Models

Gasification is a complex chemical process. Therefore, gasification models are essential in understanding and predicting the behaviour as well as analyzing the effects of various operating parameters on gasification process performance (Gómez-Barea & Leckner, 2010; Couto et al., 2013). Gasification models also help prevent high experimentation costs by allowing researchers to study various scenarios while saving time and avoiding costly procedures (Couto et al., 2015). These models are classified into kinetics, neural network, and thermodynamic equilibrium models (Zhong et al., 2009; Puig-Arnavat et al., 2010).

2.7.1 Kinetic models

This model offers crucial kinetic-based mechanisms information explaining the conversion process occurring in a gasifier (Sharma, 2008; Karmakar & Datta, 2011). Such a model can estimate the syngas composition with varying operation parameters,

which is vital information for designing, evaluating and enhancing of gasification system (Karmakar & Datta, 2011). Kinetic models give accurate and detailed results; however, they are computationally demanding and contain factors limiting their applicability to different process plants (Schuster et al., 2001; Ahmed et al., 2012).

2.7.2 Artificial Neural network (ANN) model

ANN is a mathematical modelling technique which compares input and output streams to and from a processing unit using regression (Puig-Arnavat et al., 2010). It has been widely applied in function approximation, pattern recognition, signal processing, and process simulation (Ahmed et al., 2012). While neural network modelling plays an essential role in various application fields, recently, it has attracted attention as a system modelling tool in renewable energy (Kalogirou, 2001). ANN models are reported to accurately predict syngas composition (Puig-Arnavat et al., 2010). However, they require a large amount of experimental data, which is unavailable in the literature (Ahmed et al., 2012).

2.7.3 Thermodynamic equilibrium model

The kinetic-based models give accurate results. However, they contain factors which limit their applicability to various process plants (Schuster et al., 2001). Thus, this modelling technique, which is independent of the gasification system design and not restricted to a specific range of operating parameters (Ratnadhariya & Channiwala, 2009), is essential in the prediction of the maximum gasification system performance which can be attained for a given biomass material (Sharma, 2008). Such information is vital for designing a gasification system (Karmakar & Datta, 2011).

Thermodynamic models can provide a better understanding of gasifiers with some experimental data and operating experience. Furthermore, thermodynamic models

save time and are easy to calculate; therefore, they are commonly used for process simulation (Gómez-Barea & Leckner, 2010; Wan et al., 2014; Wan, 2016).

Thermodynamic equilibrium modelling can predict the equilibrium composition of syngas through the Gibbs free energy minimization, where stoichiometric and non-stoichiometric approaches are used (Li et al., 2001; Haryanto et al., 2009). The stoichiometric technique takes into consideration the equilibrium constants of an individual set of reactions related to the change in the Gibbs free energy (Jarungthammachote & Dutta, 2007; Sharma, 2008). On the other hand, the non-stoichiometric equilibrium modelling technique considers minimising the reacting species' Gibbs free energy. The stoichiometric modelling approach requires a detailed description of all possible reactions occurring in a gasifier (Gambarotta et al., 2018). This can be very difficult when all possible chemical reactions taking place in the gasifier are unfully known (Ramos et al., 2019).

2.7.3.1 Stoichiometric modelling approach

The overall gasification reaction can be written as (Huang & Ramaswamy, 2009; Upadhyay et al., 2019):

$$\begin{aligned} CH_xO_yN_z + wH_2O + m(O_2 + 3.76N_2) \\ = n_1CO + n_2H_2 + n_3CO_2 + n_4H_2O + n_5CH_4 + n_6C_6H_6 \\ + (1-\alpha)C + (\frac{z}{2} + 3.76m)N_2 \end{aligned} \quad (2.2)$$

Global C, H, O and N mass balance:

$$\sum_i mass_{reactants} = \sum_i mass_{products} \quad (2.3)$$

Equilibrium constants

$$K_j = \prod_i (x_i)^{v_i} (\frac{P_i}{P_0})^{\Sigma_i v_i} \quad (2.4)$$

x_i represents the fraction of mole of species i within the ideal gas mixture, P_o is standard pressure (1 atm), ν is the stoichiometric number.

The constant value K was determined based on the Standard Gibbs function shown in Eqn. 2.5.

$$\ln K = -\frac{\sum_{i=1}^{N} n_i \Delta g_{f,T,i}^0}{RT} \tag{2.5}$$

Where R denotes the universal gas constant and $\Delta g_{f,T,i}^0$ stands for the standard Gibbs function of formation at a given temperature T of the gas species i.

$$\Delta \bar{g}_{f,T,i}^0 = \bar{h}_{f,i}^0 - a'TlnT - b'T^2 - \frac{c'}{2}T^3 - \frac{d'}{3}T^4 + \frac{e'}{2T} + f' + g'T \tag{2.6}$$

The enthalpy of formation of individual gas species and the coefficients a'-g' can be obtained in the literature.

The energy balance:

$$\sum_i n_i \left[\bar{h}_{f,i}^0\right]_{i,reactants} = \sum_i n_i \left[\bar{h}_{f,i}^0 + \Delta h_{T,i}^0\right]_{i,products} \tag{2.7}$$

Where $\bar{h}_{f,i}^0$ denotes the enthalpy of formation, which is taken to be zero for chemical elements at the reference state (298 K, 1 atm), and $\Delta h_{T,i}^0$ denotes the difference between the enthalpies at any given state and the reference state.

$$\Delta h_{T,i}^0 = \int_{298}^{T} C_{P,i}(T)\, dT \tag{2.9}$$

The specific heat capacity C_P (in kJ/kmolK), was determined using the empirical equation below (Jarungthammachote & Dutta, 2007).

$$C_{P,i}(T) = C_1 + C_2T + C_3T^2 + C_4T^3 \tag{2.10}$$

Where $C_1 - C_4$ represents the specific heat capacity coefficients for various gases and can be found in the literature.

2.7.3.2 Non-stoichiometric modelling approach

For a system at the state of thermodynamic equilibrium, the total Gibbs free energy (G^t) is minimized and defined by Jarungthammachote and Dutta (2008):

$$G^t = \sum_{i=1}^{N} n_i \mu_i \tag{2.11}$$

Where μ_i and n_i represent the numbers of chemical potential and moles of i_{th} species, respectively. Bearing in mind the ideal gas law, μ_i is defined by;

$$\mu_i = G_i^0 + RTln\left(\frac{f_i}{f_i^0}\right) \tag{2.12}$$

Where R, T and f_i represent the universal gas constant, temperature, and fugacity of i_{th} species, respectively. The standard thermodynamic quantity is denoted by superscript 0, therefore, f_i^0 and G_i^0 represent the species' i standard fugacity and Gibbs free energy, respectively. Taking into consideration the pressure, Eqn. (2.12) is expressed as follows:

$$\mu_i = G_i^0 + RTln\left(\frac{\emptyset P_i}{P^0}\right) \tag{2.13}$$

Where $\emptyset$ stands for coefficient of fugacity. f and P attain the same value when pressure approaches zero; at this, the real gas condition approaches the ideal gas condition. Assuming ideal gas at 1 atm, then Eqn. (2.13) can be rewritten as:

$$\mu_i = \Delta G_i^0 + RTln(y_i) \tag{2.14}$$

Where y_i stands for the gas species' i molar fraction and ΔG_i^0 denotes species' i standard Gibbs free energy of formation, and for all chemical elements ΔG_i^0 is set to zero. Substituting Eqn. (2.14) into Eqn. (2.11), we obtain:

$$G^t = \sum_{i=1}^{N} n_i \Delta G_{f,i}^0 + \sum_{i=1}^{N} n_i RTln\left(\frac{n_i}{n_{tot}}\right) \tag{2.15}$$

The main objective is to determine a set of n_i that minimizes the total system's Gibbs free energy while satisfying the elemental mass balance given by:

$$\sum_{i=1}^{N} a_{ij} n_i = A_i \tag{2.16}$$

Where a_{ij} indicates the total atoms of element j of the reacting mixture. Through the application of the Lagrange multiplier technique, the Gibbs free energy is minimised (Koukkari & Pajarre, 2006), i.e.,

$$\frac{\partial L}{\partial n_i} = \Delta G_{f,i}^0 + n_i RT ln\left(\frac{n_i}{n_{tot}}\right) + \sum_{j=1}^{k} \lambda_j a_{ij} = 0 \tag{2.17}$$

Where L and λ_j represents the Lagrange function and multiplier, respectively. Eqn. (2.17) represents n equilibrium equations of each of the species present in the system, which can be presented as a matrix of i rows, and those are solved simultaneously with Eqn. (2.16) to obtain the composition of product gas.

Some research has been done in the past exploring biomass gasification process 'modelling for Fischer Tropsch synthesis application. Buragohain et al. (2010), for instance, developed a model for various types of biomass feedstock such as bamboo dust, rice husk, and sawdust based on a non-stoichiometric equilibrium model using FactSage software. The authors investigated the influence of biomass type, equivalence ratio, gasification temperature, and gasifying agent on the H_2 and CO yield, LHV, H_2/CO ratio, and overall gasifier efficiency. They reported an optimal set of operational gasification conditions of ER of 0.2-0.4, gasification temperature of 800 – 1000 ℃, and air as the gasifying agent for FTs. Leibbrandt et al. (2013) developed a thermodynamic equilibrium model of oxygen-blown gasification of sugarcane bagasse and pyrolysis slurry from sugarcane bagasse using Aspen Plus. Sensitivity analysis was carried out to investigate how equivalence ratio, moisture

content, pressure, and gasification temperature affect the gasification efficiency and stoichiometric H_2/CO ratio. They determined optimum operating conditions to produce a stoichiometric H_2/CO syngas ratio of 2 and found out to be 5% moisture content, steam to biomass ratio of 2.25, equivalence ratio of 0.25 and gasification temperature of 1100 K.

Fernandez-Lopez et al. (2017) modelled animal waste biomass in a dual gasification system by means of Aspen Plus. The model was based on minimizing Gibbs free energy. Sensitivity analysis was performed on the effect of using steam and CO_2 as gasification agents, gasifying to biomass ratio and, gasification temperature on syngas composition and LHV of syngas. Based on the sensitivity analysis results, they established the best-operating conditions for Fischer-Tropsch synthesis, energy generation, and the net CO2 emission from an environmental perspective. The simulated results showed that steam gasification at 0.7 gasifying to biomass ratio with a gasification temperature of 850 ℃ produced syngas with an H_2/CO close to 2 hence the best operating condition for Fischer-Tropsch synthesis. Under other conditions, the syngas' LHV was maximized at 750 ℃ using CO_2 as the gasifying agent with gasifying to biomass ratio of 0.1. In either case, they noted that the lowest net CO_2 emission could not be attained at the determined best-operating conditions. Han et al. (2017) developed a comprehensive computer model of hardwood chips using Aspen Plus in a downdraft gasifier. The model was based on the minimization of Gibbs free energy by restricting the chemical equilibrium of the reactions in the reduction zone. Sensitivity analysis was performed on the effect of gasification temperature, moisture content and equivalence ratio on bio-syngas quality. They observed from the simulation results that Fischer-Tropsch synthesis (FTs) is optimized within a

temperature range of 650 ℃– 800 ℃, biomass moisture content of less than 10 % and an equivalence ratio of 0.2 – 0.3.

Pala et al. (2017) simulated steam gasification of pine sawdust, municipal solid waste, coffee bean husk, green waste, food waste, wood residue, and wood chips in Aspen Plus with subsequent adjusting of syngas' H_2/CO ratio to 2.15 by shift reaction for direct FTs application. The model was based on minimizing Gibbs free energy by the application of a restricted equilibrium approach. They investigated how gasification temperature, steam to biomass ratio, and shift reaction temperature affect syngas composition, carbon monoxide conversion, carbon dioxide conversion, and H_2/CO ratio. They observed that steam gasification of food wastes yielded syngas with a close to 2.15 H_2/CO ratio. In contrast, the remaining feedstocks required a syngas adjustment to attain an H_2/CO molar ratio close to 2.15. Faraji & Saidi (2021) developed a comprehensive steady-state equilibrium simulation model for different algal biomass for the generation of hydrogen-rich syngas through the integration of pyrolysis and air gasification processes in Aspen Plus. The authors considered a three-zone gasification process: drying, decomposition, and gasification. They investigated how temperature, gasifier pressure, and airflow rate the composition of syngas and the H_2/CO ratio. They determined optimal gasification operational conditions to maximize CO and H_2 production and found out to be gasification pressure of 1 atm, air-fuel ratio of 0.01 m^3/h, and gasification temperature of 600 ℃.

2.8 Response Surface Methodology (RSM)

RSM is a mathematical and statistical tool with a wide range of applications in engineering where simultaneous optimization of different response variables is required (Roy et al., 2020). It is a popular method for optimizing new and current modelled systems or processes (Mojaver et al., 2019; Inayat et al., 2020; Zaman &

Ghosh, 2021). RSM is extremely applied when multiple independent variables efficiently affect the response of a process. The goal is to create a regression model to characterize the system performance and optimize the system response by considering the interactions between the key factors. Analysis of variance (ANOVA) is an important tool in RSM.

Several research has been done in the past exploring biomass gasification process optimization using RSM for different applications. For instance, Singh and Tirkey (2021) developed a robust model for air gasification of Syzygium cumini in a downdraft gasifier based on Gibbs free energy minimization using Aspen Plus simulation tool. The authors considered a four-phase gasification process: drying, decomposition, gasification, and syngas filtration. The influence of ER and gasification temperature on gas composition, cold gas efficiency (CGE), and higher heating value of syngas (HHV) was studied. They further adopted central composite design in multi-objective optimization for hydrogen (H_2), CGE, and HHV using response surface methodology (RSM). Zaman et al. (2020) modelled steam gasification of rice husk in a fluidized bed gasifier using Aspen Plus simulation tool. The authors considered a two-zone gasification process: decomposition and gasification. The authors studied the effect of S/B and gasification temperature on product gas quality and gasifier CGE. They further used the thermodynamic model results as RSM input data to study the synchronized influence of S/B and gasification temperature on LHV_{Syngas} and CGE and hence establish the optimal operating condition zone. Zaman and Ghosh (2021) used a generic input-out technique to establish and optimize an Aspen Plus steam-gasification model in a fluidized bed gasifier. They conducted statistical analysis and optimization of LHV_{Syngas} and CGE considering gasification temperature and S/B for different feeds using RSM.

2.9 Research Gaps

From the brief literature survey, it was established that many of the previous simulation studies on process modelling and simulation for Fischer Tropsch synthesis applications have focused on the fundamental process. Moreover, most of the research studies employed the single-parameter optimization technique which is not efficient in determining the optimal working parameters of a process. To our knowledge, no work has considered the inclusion of a comprehensive syngas purification coupled with RSM optimization for Fischer Tropsch synthesis application from air-gasification of rice husk. Furthermore, 400 runs of Aspen Plus simulated results were used to construct an RSM design matrix, offering another mileage of the present study.

CHAPTER THREE: RESEARCH METHODOLOGY

3.1 Introduction

The chapter presents the four major steps considered in investigating the feasibility of air-gasification of rice husk for FTs application through modelling and optimization. It presents discussions on the collection, preparation and characterising of the biomass feedstock of study. Then an experimental setup of air-gasification of rice husk for the validation of the developed simulation model is designed. The chapter then explains the use of the validated simulation model in performing a sensitivity analysis to investigate the effect of operating conditions of the gasification system on the producer gas composition. Finally, the chapter discusses on the multi-objective optimization of the operating conditions of a gasification process for FTs applications using RSM.

3.2 Thermodynamic Model Development

3.2.1 Biomass sample collection, preparation and characterisation

Rice husk was sourced locally from a rice mill factory in Mwea irrigation scheme region, Kirinyaga County, Kenya. Figure 3.1 illustrates the image of the studied biomass material.

Figure 3.1 Image of rice husk

The ultimate and proximate analysis of rice husk was carried out based on the

ASTM standards.

3.2.1.1 Proximate analysis

The biomass sample was grinded and sieved to 500 μm according to ASTM standards. The analysis was replicated thrice, and the average recorded.

Moisture content: For determination of moisture content based on STM standards E 871, 1g of rice husk was weighed in a dried crucible and set in an oven fixed at a temperature between 120 ^{o}C and 150 ^{o}C for 4 h until reaching a constant weight (García et al., 2012). After the process, the sample was withdrawn from the oven and allowed to cool (Singh et al., 2017; Yusuf & Inambao, 2020). The moisture content was then determined based on Eqn. 3.1 (García et al., 2012).

$$\text{Moisture content } \% = \frac{W_0 - W}{W_{s0}} \tag{3.1}$$

Where W_0 denotes the initial weight of the sample plus crucible, W represents the resulting dry sample weight plus crucible, W_{s0} stands for the initial weight of the sample.

The total solid of rice husk was determined as per Eqn. 3.2.

$$\text{Total solid } (\%) = 100 - \text{Moisture content } (\%) \tag{3.2}$$

Ash content: The previously dried biomass sample was taken into a furnace (Model: WiseTherm) at 550 ^{o}C for 3-4 h according to ASTM E 1755 (García et al., 2012). After the process, the sample was removed from the furnace to allow it to cool. The ash content was then calculated by using Eqn. 3.3 (García et al., 2012).

$$\text{Ash content } \% = 100 - \frac{W - W_{sc}}{W_{ds0}} \tag{3.3}$$

Where W_{sc} denotes the resulting weight of the sample residue plus the weight of the crucible, W_{ds0} stands for the initial weight of the dried sample after moisture content calculation.

Volatile matter: VM was determined as a weight loss of a dried biomass sample according to ASTM E 872 (García et al., 2012). The weight loss was determined by Eqn. 3.4 (García et al., 2012), where W_a denote the initial sample weight plus crucible with top, W_v represent the resultant crucible weight with top plus sample residue, W_{s0} stands for the initial sample weight.

$$\text{Weight loss } \% = \text{A} = \frac{\text{W}_\text{a} - W_v}{\text{W}_{\text{s0}}} \quad (3.4)$$

The volatile matter was then calculated as follows (García et al., 2012):

$$\text{VM } \% = \text{A} - \text{moisture } \% \quad (3.5)$$

Fixed carbon: This was determined by the difference as shown in the following formulae (García et al., 2012; Olupot et al., 2016).

$$(\%) \text{ Fixed carbon (db)} = 100 - (\%\text{Ash (db)} + \%\text{VM (db)}) \quad (3.6)$$

3.2.1.2 Ultimate analysis

A TGA 701 Leco thermogravimetric analyzer was used to study the sample's combustion and co-combustion. The sample was combusted at temperatures ranging from 25°C to 950°C at heating rates of 10, 20, 30 and 40°C/min in the presence of oxygen. The sample's thermal combustion and co-combustion were carried out at temperatures between 25°C to 950°C and a fixed heating rate of 10°C/min under three different atmospheres (O_2, CO_2, and air) and the samples were held at 950°C until no further loss of weight was recorded. For each experiment, 80 mg of fuel was used.

Retsch SM 200 cutting mill was used to grind the sample to -212 μm. A Leco CHN 628 with add-on 628 S modules was used for CHN and Sulphur analyses based on ASTM D 5373-02 and ASTM D 4239-05, respectively.

3.2.2 Model development using Engineering Equation Solver

Equations were established to develop a numerical simulation model based on a stoichiometric thermodynamic model approach. The following assumptions were considered during the model formulation:

i. The reaction process in the gasifier is assumed to be a steady-state with a uniform pressure
ii. Char is considered to be graphitic carbon
iii. The rates of reaction in the gasifier are considered to be fast enough, and the residence time of the reactions in all gasifier's zones is assumed to be sufficient to achieve thermodynamic and chemical equilibrium
iv. The modelled biomass feedstock is assumed to consist only of carbon, hydrogen, oxygen and nitrogen
v. The gasification agent is considered to be natural air (21% Oxygen and 79% Nitrogen)
vi. The products comprise only H_2, CO, CH_4, CO_2, H_2O, and N_2 with N_2 considered inert throughout the process
vii. The involved gases follow the ideal gas law
viii. Ashes are inert

The biomass feedstock chemical formula when one carbon atom is considered is taken to be $CH_xO_yN_zS_k$. Where *x*, y, z and k are the numbers of H, O, N and S atoms, respectively, for each atom of carbon per mole present in the biomass (Upadhyay et al., 2019). These atoms are defined based on the ultimate analysis of biomass. The overall gasification reaction can be written as (Costa et al., 2015):

$$CH_xO_yN_zS_k + wH_2O + m(O_2 + 3.76N_2) = n_1CO + n_2H_2 + n_3CO_2 + n_4H_2O + n_5CH_4 + n_6C_6H_6 + (1-\alpha)C + \left(\frac{z}{2} + 3.76m\right)N_2 \quad (3.7)$$

Where *w* and *m* represent the mole of moisture and oxygen present per mole of biomass respectively. In accordance with (Azzone et al., 2012; Upadhyay et al., 2019), *w* and *m* are determined by

$$w = \sum_{i=1}^{n} X_i \left(\frac{m_{biomass} * wc_i}{m_{H_2O} * (1 - wc_i)}\right) \quad (3.8)$$

Where

$$m_{biomass} = 12 + (1 * x) + (16 * y) + (14 * z) \quad (3.9)$$

On the right-hand side of Eqn. 3.7, n_1, n_2, n_3, n_4, n_5, and n_6 are the numbers of moles of H_2, CO, CH_4, CO_2, and C_6H_6, and the expression $(1-\alpha)$ represents the particles of unconverted carbon that bypass the chemical equilibrium in the form of char. It is mathematically expressed as (Lim & Lee, 2014):

$$\alpha = 0.901 + 0.439 * \left(1 - e^{(-ER + 0.0003T)}\right) \quad (3.10)$$

As a percentage of the gasification product's total weight, tar yield is given by (Abuadala et al., 2010; Rupesh et al., 2015):

$$n_6 wt\% = 35.98e^{(-0.00298T)} \quad (3.11)$$

Eqn. 3.12 was used to determine the values of x, y, z and k from the biomass ultimate analysis (Barman et al., 2012; La Villetta et al., 2017; Upadhyay et al., 2019).

$$x = \frac{H * M_C}{C * M_H};\quad y = \frac{O * M_C}{C * M_O};\quad z = \frac{N * M_C}{C * M_N};\quad k = \frac{S * M_C}{C * M_S} \quad (3.12)$$

Where M_N, M_O, M_H, M_C and M_S represent the molecular weight of nitrogen, oxygen, hydrogen, carbon and sulphur and N, O, H, C and S denote the mass fractions of those elements of the fuel mixture.

Three elemental balance equations, two equilibrium constant equations and one enthalpy balance equation were used in developing the simulation model. From Eqn. 3.7, the elemental balance for Carbon, Hydrogen and Oxygen was obtained as follows (Zainal et al., 2001; Huang & Ramaswamy, 2009):

Carbon balance:

$$n_1 + n_3 + n_5 + 6n_6 - \alpha = 0 \tag{3.13}$$

Hydrogen balance:

$$2n_2 + 2n_4 + 4n_5 + 6n_6 - x - 2w = 0 \tag{3.14}$$

Oxygen balance:

$$n_1 + 2n_3 + n_4 - y - w - 2m = 0 \tag{3.15}$$

Considering the drying, pyrolysis, reduction, and combustion gasification zones and assuming that the products of pyrolysis are combusted and attained equilibrium in the reduction zone, methane formation (Eqn. 3.16) and water-gas shift (Eqn. 3.17) reactions were considered (Zainal et al., 2001; Huang & Ramaswamy, 2009; Vaezi et al., 2009):

$$C + 2H_2 \leftrightarrow CH_4 \tag{3.16}$$

$$CO + H_2O \leftrightarrow CO_2 + H_2 \tag{3.17}$$

The methane formation and water-gas shift reaction's equilibrium constants are described in Eqn. 3.18 and Eqn. 3.19, respectively (Jarungthammachote & Dutta, 2007; Gautam et al., 2010; Barman et al., 2012; Itai et al., 2014; Jia et al., 2017).

$$K_1 = \frac{P_{CH_4}}{(P_{H_2})^2} = \frac{n_3 * n_T}{{n_1}^2} \tag{3.18}$$

$$K_2 = \frac{P_{CO_2} P_{H_2}}{P_{CO} P_{H_2O}} = \frac{n_4 n_1}{n_2 n_5} \tag{3.19}$$

Where K_1 and K_2 represent the equilibrium constants for methane formation and water-gas shift reactions respectively, n_T represents the total molar concentration of the synthetic gas (Gautam et al., 2010; Arafat & Jijakli, 2013; Itai et al., 2014; Aydin et al., 2017).

$$n_T = n_1 + n_2 + n_3 + n_4 + n_5 + n_6 + (\frac{z}{2} + 3.76m)N_2 \tag{3.20}$$

Based on the equilibrium state of the ideal gas mixture, the equilibrium constants K_1 and K_2 were determined using Gibbs free energy minimization as shown in Eqn. 3.21 (Jarungthammachote & Dutta, 2007; Melgar et al., 2007; Gautam et al., 2010; Itai et al., 2014; Jia et al., 2017).

$$\ln K(T) = \frac{-\Delta G_T}{\tilde{R}T} \tag{3.21}$$

$$\Delta G_T = \sum_i n_i \bar{g}^0_{f,T,i} \tag{3.22}$$

Where $\tilde{R}$ denotes the universal gas constant, 0.008314 kJ/(mol.K), ΔG_T stands for standard Gibbs function, and $\bar{g}^0_{f,T,i}$ stand for individual gas species' Gibbs function, which can be mathematically determined by Eqn. 3.23 (Jarungthammachote & Dutta, 2007; Gautam et al., 2010; Syed et al., 2011):

$$\bar{g}^0_{f,T} = \bar{h}^0_f - aTlnT - bT^2 - \frac{c}{2}T^3 - \frac{d}{3}T^4 + \frac{e}{2T} + f + gT \tag{3.23}$$

The enthalpy of formation of individual gas species and the coefficients a-g are presented in Table A-1 (Cengel & Boles, 2014) in the Appendix section.

Assuming that the gasifier is completely adiabatic, the enthalpy balance in the gasifier is expressed as (Zainal et al., 2001; Arafat & Jijakli, 2013; Khanmohammadi et al., 2016):

$$H^0_{f,wood} + w(H^0_{f,\,H_2O(l)} + H_{(Vap)}) + m\left(H^0_{f,O_2} + 3.76H^0_{f,N_2}\right)$$
$$= n_1\left(H^0_{f,CO} + \int_{298}^{T} C_{p,CO}dT\right) + n_2\left(H^0_{f,H_2} + \int_{298}^{T} C_{p,H_2}dT\right)$$
$$+ n_3\left(H^0_{f,CO_2} + \int_{298}^{T} C_{p,CO_2}dT\right)$$
$$+ n_4\left(H^0_{f,H_2O(g)} + \int_{298}^{T} C_{p,H_2O}dT\right)$$
$$+ n_5\left(H^0_{f,CH_4} + \int_{298}^{T} C_{p,CH_4}dT\right)$$
$$+ n_6\left(H^0_{f,C_6H_6} + \int_{298}^{T} C_{p,C_6H_6}dT\right) + (1-\alpha)(H^0_{f,C}$$
$$+ \int_{298}^{T} C_{p,C}dT) + (\frac{z}{2} + 3.76m)(H^0_{f,N_2} + \int_{298}^{T} C_{p,N_2}dT) \quad (3.24)$$

Eqn. 3.24 can be reduced to Eqn. 3.25 since H^0_{f,O_2}, H^0_{f,N_2}, $H^0_{f,C}$ and H^0_{f,H_2} are zero at ambient temperature.

$$H^0_{f,wood} + w(H^0_{f,\,H_2O(l)} + H_{(Vap)})$$
$$= n_1(H^0_{f,CO} + \int_{298}^{T} C_{p,CO}dT) + n_2(\int_{298}^{T} C_{p,H_2}dT) + n_3(H^0_{f,CO_2}$$
$$+ \int_{298}^{T} C_{p,CO_2}dT) + n_4(H^0_{f,H_2O(g)} + \int_{298}^{T} C_{p,H_2O}dT)$$
$$+ n_5(H^0_{f,CH_4} + \int_{298}^{T} C_{p,CH_4}dT)$$
$$+ n_6\left(H^0_{f,C_6H_6} + \int_{298}^{T} C_{p,C_6H_6}dT\right) + (1-\alpha)(\int_{298}^{T} C_{p,C}dT) + (\frac{z}{2}$$
$$+ 3.76m)(\int_{298}^{T} C_{p,N_2}dT) \quad (3.25)$$

Where $H^0_{f,wood}$, $H^0_{f,\,H_2O(l)}$, $H^0_{f,CO}$, H^0_{f,CO_2}, $H^0_{f,H_2O(g)}$, H^0_{f,CH_4} and H^0_{f,C_6H_6} represent the biomass fuel, liquid water, carbon monoxide, carbon dioxide, water vapour, methane and benzene enthalpies of formation, respectively. $H_{(Vap)}$ is the enthalpy of vaporization of water, $C_{p,CO}$, C_{p,H_2}, C_{p,CO_2}, C_{p,H_2O}, C_{p,CH_4}, C_{p,C_6H_6}, $C_{p,C}$ and C_{p,N_2} denote the products' specific heats at a constant pressure. $\int_{298}^{T} C_{p,i}dT$ denotes the

change in enthalpy of a given state with respect to the reference state. The enthalpies of formation of gas species are shown in Table A-2 (Cengel & Boles, 2014) in the Appendix section.

Determining the enthalpy of formation of biomass fuel requires the knowledge of the fuel's lower heating value (LHV) or high heating value (HHV). Applying HHV, the biomass enthalpy of formation in $(kJ/kmol)$ is given by Mendiburu et al. (2014).

$$H^0_{f,wood} = HHV(m_{biomass}) + \frac{x}{2}(H^0_{f-298})_{H_2O(l)} + (H^0_{f-298})_{CO_2} \quad (3.26)$$

The HHV of biomass fuel is determined using the following equation (Channiwala & Parikh, 2002):

$$HHV(kJ/kg) = 349.1 * \%C + 1178.3 * \%H + 100.5 * \%S - 103.4 * \%O - 15.1 * \%N - 21.1 * \%A \quad (3.27)$$

The specific heat capacity C_P (in kJ/kmolK), was determined using the empirical equation below (Jarungthammachote & Dutta, 2007).

$$\int_{298}^{T} C_{P,i}(T) = C_1T + C_2T^2 + C_3T^3 + C_4T^4 + k \quad (3.28)$$

Where k is the constant of integration and $C_1 - C_4$ represents the specific heat capacity coefficients for various gases within a wide range of temperatures, which are shown in Table A-3 (Jarungthammachote & Dutta, 2007) in the Appendix section.

The solid carbon's specific heat capacity C_P (in kJ/kmolK), was determined as per Eqn. 3.29 below (La Villetta et al., 2017).

$$C_c = 17.166 + 4.271 * \frac{T}{1000} - \frac{8.79 * 10^5}{T^2} \quad (3.29)$$

3.2.2.1 Calculation procedure

This equilibrium model was built by making a user-friendly interface using EES. In this equilibrium model, a user interface consisted of a diagram window with drawings

including a feed stream of biomass and pre-heated air, as illustrated in Figure 3.2. The user interface also contains tables with input variables (biomass ultimate analysis and gasification operating conditions), output variables (syngas composition) and a calculator. This model can be used to study how temperature, equivalence ratio, and moisture content influence the product gas composition as well as other gasification process performance parameters.

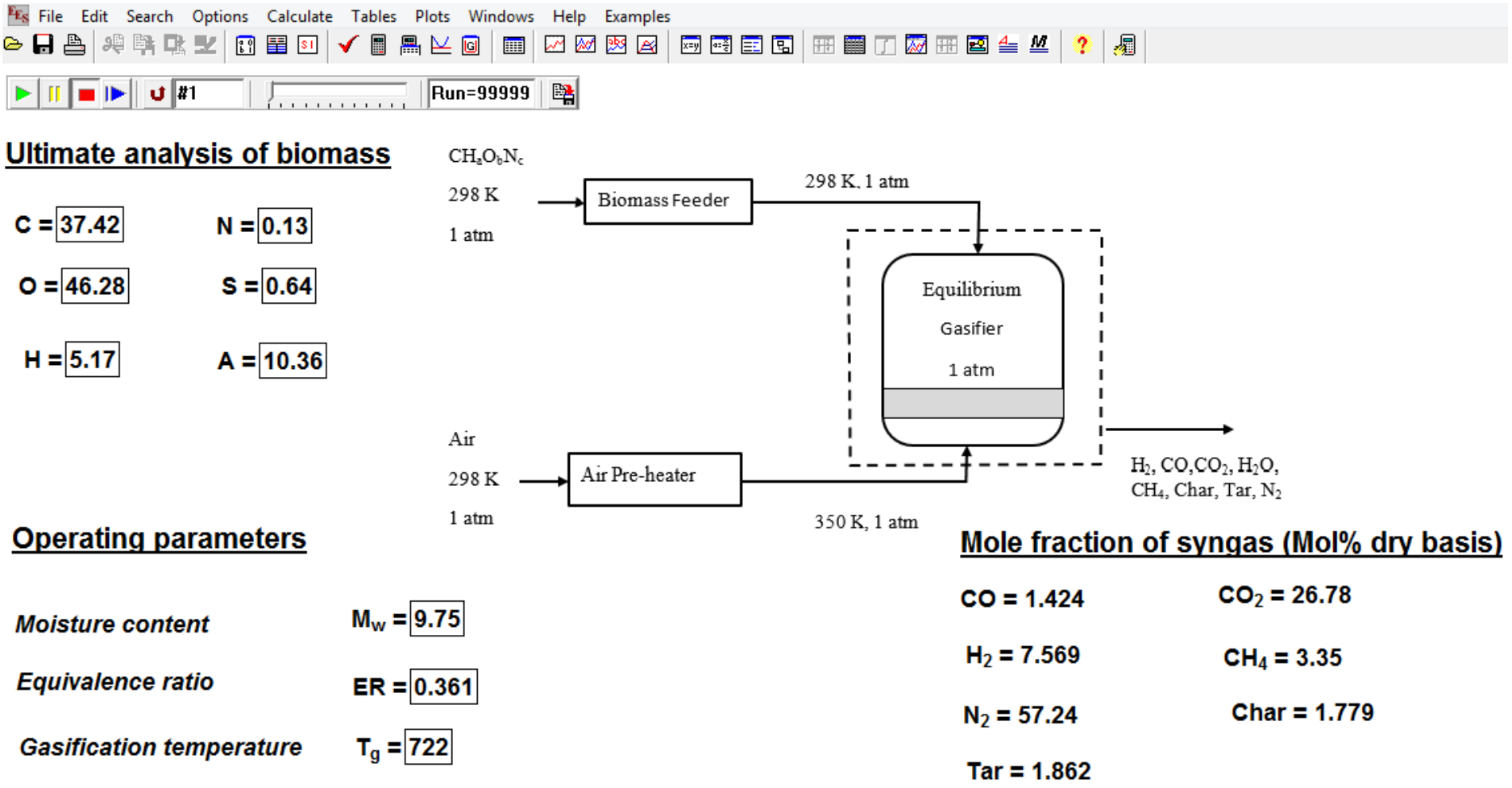

Figure 3.2 User interface for the modified thermodynamic equilibrium model

3.2.3 Model development using Aspen Plus

In this section, Aspen Plus process description, components specification, physical properties selection, streams and block specification, sensitivity analysis and parameter optimization are discussed in detail.

3.2.3.1 Model development

This study was carried out using Aspen Plus (Advanced System for Process Engineering Plus) Version 10 software. A four-zone thermodynamic equilibrium simulation model of a fixed-bed downdraft gasification system was developed using the various Aspen Plus unit operation blocks representative of different processes in biomass gasification. The four zones comprising drying, decomposition, oxidation, and gasification were created. The biomass moisture content is lowered in the drying zone before loading into the decomposition reactor. In the second zone, the pre-dried biomass is converted from nonconventional biomass to its conventional components (Char, Hydrogen, Oxygen, Nitrogen, Water, Sulfur, Chlorine, and Ash). The oxidation and gasification zones model the partial oxidation of the decomposed elements by minimizing the Gibbs free energy (Jarungthammachote & Dutta, 2008).

The standard component database in the software does not include biomass and ash. Therefore, MIXCINC was specified as the global stream class. This stream class contains three sub-streams consisting of MIXED, CISOLID, and NC. This option is recommended when simulating both conventional components (MIXED), nonconventional solids such as carbon (CISOLID), and nonconventional feed such as biomass and ash (NC). The Peng-Robison equation of state (Gagliano et al., 2017) (see Eqn. 3.30) was used as the global property method for the simulation to estimate the physical properties of the conventional components produced by the gasification process.

$$p = \frac{RT}{V - b} - \frac{a(T)}{V(V + b) + b(V - b)} \quad (3.30)$$

Where a and b represent the measure of attractive forces between the molecules and the size of the molecules respectively.

Being nonconventional components, only the biomass and ash enthalpies and densities were estimated during the simulation using the HCOALGEN and DCOALIGT models, respectively (Han et al., 2017; Safarian et al., 2022; Hussain et al., 2023).

3.2.3.2 Aspen Plus flowsheet

The resultant rice husk gasification process model flowsheet of the fixed bed gasifier is illustrated in Figure 3.3. The direction of streamflow is indicated by the solid lines. The solid black line shows the flow of energy. The dashed-dotted lines indicate the blocks that were controlled by user-programmed FORTRAN statements. Table 3.1 provides a concise description of the Aspen Plus reactor blocks with a brief description of the default ID and an assigned ID, and a short description of the function of each block used in the simulation model flowsheet. The default ID is a unit operation block name defined by the software developer, and the user creates the assigned ID.

Table 3.1 Aspen Plus simulation model reactor block description

Block ID	Default ID	Description
DRIER	RStoic	Simulate wet biomass drying by specifying the stoichiometric reaction
MOISTSEP	Sep2	Separation of excess moisture from dry biomass
DECOMP	RYield	Decompose biomass material into conventional components by defined yield distribution from the biomass ultimate and proximate analysis
OXID	RGibbs	Model oxidation of the disintegrated biomass components
REDUC	RGibbs	Simulate biomass gasification
CYCLONE	SSplit	Simulate solid separation from the hot syngas
COOLER	Heater	Cool hot syngas to 25 ^{o}C
SCRUBER	RadFrac	Remove contaminants such as particulate matter, nitrogen compounds (NH_3, HCN), and tars from the product gas
WATERSEP	Sep2	Separate moisture from the purified syngas.

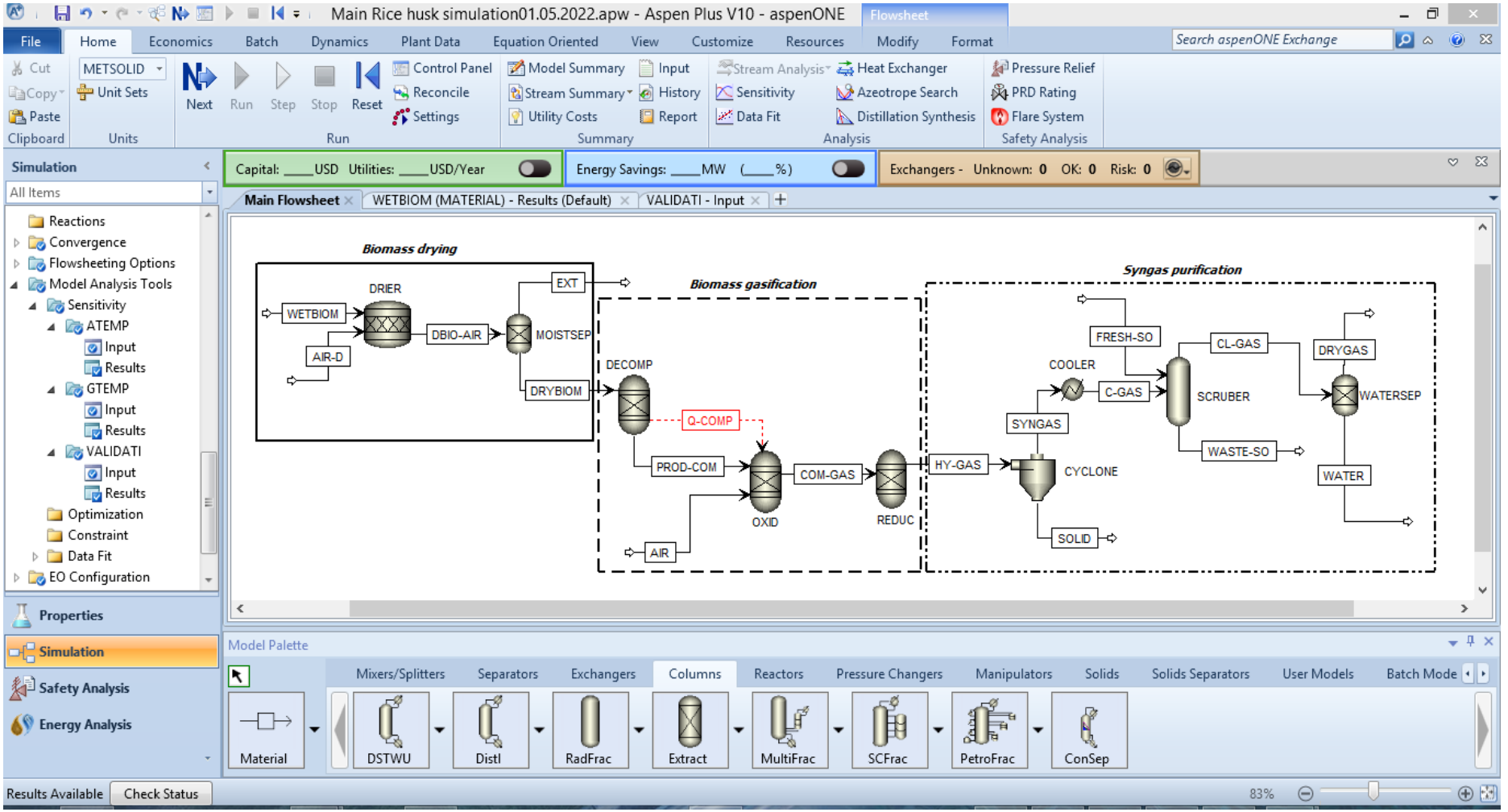

Figure 3.3 Biomass gasification process simulation flow sheet for downdraft gasifier

3.2.3.3 Model assumptions

In addition to assumptions i-iii captured in section 3.2.2, the following assumptions were made in formulating the numerical simulation model.

i. Biomass particle size is not taken into consideration
ii. Tar formation is not considered.
iii. All the gases involved obey the Peng-Robinson equation of state with the Boston-Mathias alpha function (PR-BM).

3.2.3.4 Simulation procedures

An RStoic reactor (model id: DRIER) was used to simulate biomass drying. Wet biomass is fed to the reactor as a nonconventional component. A FORTRAN statement written in the calculator block (MOISTURE) was used to control the drying process. The partially evaporated moisture was separated using a separator block Sep2 (model id: SEP) as (EXT). The dried biomass (DRYBIOM) was then fed into the next zone for decomposition. The decomposition of biomass into its elements was simulated using an RYield reactor (model id: DECOMP) which converts dry biomass (DRYBIOM) into its conventional components (Char, Hydrogen, Oxygen, Nitrogen, Water, Sulfur, Chlorine, and Ash). This is done by specifying the yield distribution via a FORTRAN statement in a calculator block (PYRYIELD) based on its determined ultimate analysis (C 37.42%; H 5.17%; O 46.28%; N 0.13%; S 0.64%; Ash 10.36%). The decomposed components were then fed into the next reactor for oxidation.

The partial oxidation of biomass was simulated in an RGibbs reactor (model id: OXID) using air as the gasification agent whose quantity was calculated in a calculator block (AIR). Due to its endothermic character, the heat of the reaction (Q-COMP) was supplied to support the reactions' thermal needs. A second RGibbs

reactor (model id: REDUC) was used to simulate the reduction zone of the gasifier. RGibbs reactor is useful when the reaction stoichiometry is unknown while the reaction temperature and pressure are known. The 'OXID' and 'REDUC' reactors create a thermochemical equilibrium composition between reactants and products. These reactors determined the final composition of the syngas through Gibbs free energy minimization by restricting chemical equilibrium-duty and temperature specification, temperature calculation approach in the oxidation zone. This was done by setting temperature and pressure as given in Table 3.2 and setting phase and, chemical equilibrium calculation in the reduction zone. The reactor unit operating and feed stream input conditions for simulation is given in Table 3.2.

Table 3.2 Reactor unit operating and feed stream input conditions for simulation

Block information		Operating conditions	
Type	Name	Temperature (℃)	Pressure (atm)
RStoic	DRIER	109.85	1
RYield	DECOMP	499.5	1
RGibbs	OXID	800	1
RGibbs	REDUC	800	1

Feed streams	Operating conditions		
	Temperature (℃)	Pressure (atm)	Flow rate (kg/hr)
WETBIOM	24.85	1	20
AIR-D	132	1	100
AIR	24.85	1	10
FRESH-SO	25	1	150

Reactions R_2-R_4 and R_7-R_8 were the governing reactions in the reduction zone to predict the syngas composition coming out of reactor 'REDUC' through the stream named 'HY-GAS'. Syngas purification and dehumidification were simulated using a series of units block consisting of a cyclone, a cooler, a scrubber, and a separator block. The block 'CYCLONE' was used to separate ash and unreacted carbon from the

product gas. The hot 'SYNGAS' was cooled to 25 ^{o}C by 'COOLER' and brought in contact with water 'FRESH-SO' in the 'SCRUBBER' to remove contaminants such as particulate matter, nitrogen compounds (NH_3, HCN), and tars. The moisture in the 'CL-GAS' stream was then condensed and separated from dry syngas by a water separator, 'WATERSEP'.

3.2.3.5 Components specification

The first step of developing the simulation model was defining the components (illustrated in Table 3.3) as well as their physical properties data. Biomass and ash were defined as nonconventional components because they cannot be characterized by an exact molecular formula. Aspen Plus simulator treats these components as pure components that do not take part in chemical equilibrium calculations but include unique models for estimating their enthalpy and density.

Table 3.3 Simulation model components definition

Component ID	**Type**	**Component name**	**Alias**
Biomass	Nonconventional	-	-
Ash	Nonconventional	-	-
H_2	Conventional	Hydrogen	H_2
H_2O	Conventional	Water	H_2O
C	Solid	Carbon-Graphite	C
CO	Conventional	Carbon-Monoxide	CO
CO_2	Conventional	Carbon-Dioxide	CO_2
S	Conventional	Sulphur	S
H_2S	Conventional	Hydrogen-Sulfide	H_2S
O_2	Conventional	Oxygen	O_2
N_2	Conventional	Nitrogen	N_2
CH_4	Conventional	Methane	CH_4
NH_3	Conventional	Ammonia	N_3H

3.2.3.6 Calculator specifications

Three calculators were used in this simulation. In each calculator module, variables were defined, and all the equations used in calculations were programmed FORTRAN subroutine as described below.

Calculator 1: MOISTURE

This calculator was used to control the biomass drying process. The required variables were defined as illustrated in Table 3.4.

Table 3.4 Variable definition for MOISTURE calculator

Variable name	**H2OWET**	**H2ODRY**	**CONVAT**
Type	Compattr-Var	Block-Var	Block-Var
Stream	WETBIOM	-	-
Substream	NC	-	-
Component	BIOMASS	-	-
Attribute	PROXANAL	-	-
Block	-	DRIER	DRIER
Variable	-	COMPATT	CONV
ID1	-	NC	1
ID2	-	BIOMASS	-
ID3	-	PROXONAL	-
Element	1	1	-

The Fortran statements was programmed as follows:

H2ODRY=10.0

CONVAT=(H2OWET-H2ODRY)/(100-H2ODRY)

The execution of this calculator block was performed before the operation of block DRIER.

Calculator 2: PYRYIELD

The pyrolysis products obtained after the decomposition of biomass were determined by a calculator block 'PYRYIELD'. The required variables were defined as shown in Tables 3.5 and 3.6.

Table 3.5 Import variable definition for PYRYIELD calculator

Variable name	**MOIST**	**ULTIM**
Type	Compattr-Var	Compattr-Var
Stream	BIOMASS	BIOMASS
Substream	NC	NC
Component	BIOMASS	BIOMASS
Attribute	PROXANAL	ULTANAL
Element	1	-

The variable WATER corresponds to the first component in the biomass proximate analysis.

Table 3.6 Export variable definition

Variable name	**Type**	**Block**	**Variable**	**ID1**	**ID2**
ASH				ASH	NC
H_2				H_2	MIXED
H_2O				H_2O	MIXED
CHAR	Block-Var	DECOMP	MASS-YIELD	C	CISOLID
O_2				O_2	MIXED
SUL				S	MIXED
N_2				N_2	MIXED
CL_2				CL_2	MIXED

The Fortran statements was programmed as follow:

FACTR = (100 - MOIST) / 100

H2O = MOIST / 100

ASH = ULTIM (1) / 100 * FACTR

CHAR = ULTIM (2) / 100 * FACTR

H2 = ULTIM (3) / 100 * FACTR

N2 = ULTIM (4) / 100 * FACTR

CL2 = ULTIM (5) / 100 * FACTR

SUL = ULTIM (6) / 100 * FACT R

O2 = ULTIM (7) / 100 * FACTR

Where FACTR represents the ultimate analysis conversion factor to wet basis, this calculator was executed before the operation of block DECOMP.

3.3 Simulation Model Validation

3.3.1 Experimental setup

Figure 3.4 illustrates the full-scale locally made pilot updraft gasifier at Jomo Kenyatta University of Agriculture and Technology (JKUAT) within the Institute of Energy and Environmental Technology used in the validation of the simulation results.

The unit comprises a 400 mm diameter and 2000 mm height reactor coupled with an electric blower (Black and Decker KTX5000 Blower 220-240 model) to provide the air needed for gasification. The gasifier was loaded with 19.6 kg of rice husks at the beginning of the experiment and manually ignited by dropping a burning piece of paper into the gasifier through the opening. The gasifier feeding door was closed after the ignition of biomass. Gasification temperature was measured and monitored at an interval of 1 minute for a period of 30 minutes by installing a K-type thermocouple connected to a data logger. Special care was taken to ensure that the thermocouples were in position after the feeding.

Figure 3.4 Schematic diagram of gasification plant at JKUAT.

The reactor's product gas purification was carried out by passing it through a series of gas-cleaning devices, consisting of a wet scrubber, a cyclone, and two filters arranged in series, as illustrated in Water was directly supplied from a water tap into the cooling and scrubbing system. The co-current water spray mixed with the gas, allowing it to cool and clean the gas. A pipe was immersed in the water tray at the bottom of the scrubber to allow excess water to overflow. Replacement of the water level in the tray was done at regular intervals. The cooled syngas then passed through a scrubber, where it was further cooled and cleaned by partially removing contaminants such as tar, char and other unwanted particles.

The producer gas was further allowed to pass through a cyclone separator to remove the unwanted particles that remained after passing through the scrubber through centrifugal action. An ash collection bin was connected to the cyclone separator to allow the collection of the separated particles. Furthermore, the gas was passed through a filter mechanism through which further cleaning of the product gas took place. The filter chamber was filled with silica to filter dust particles and dehydrate the gas. A drain is provided in the fabric filter for water removal or tar collection in

the filtering chamber.

3.3.2 Syngas sampling and analysis

3.3.2.1 Syngas sampling

Figure 3.5 (a) and (b) illustrate how the gas samples were collected for analysis at JKUAT and ILRI respectively.

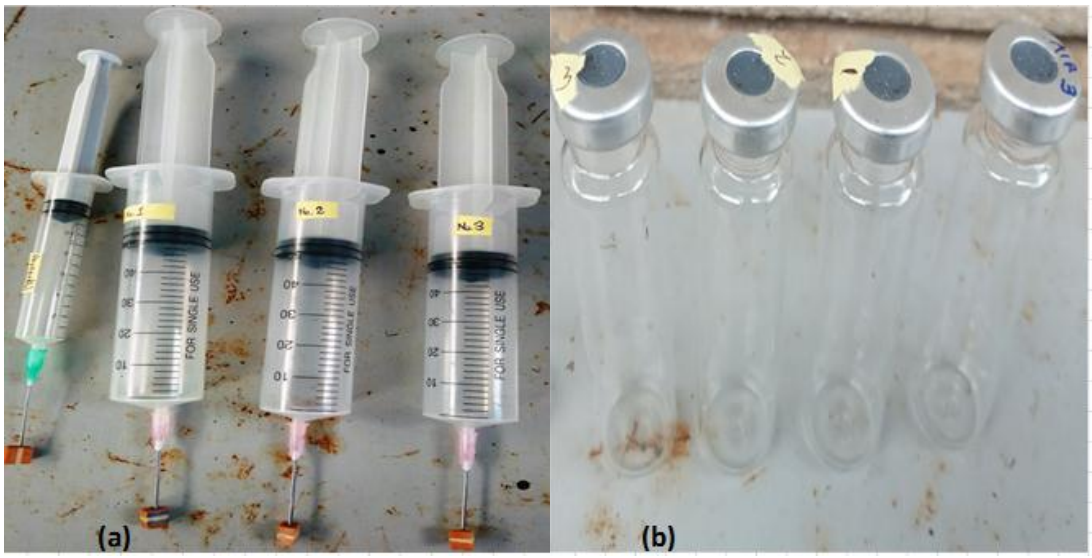

Figure 3.5 (a). Producer gas and air samples for analysis at JKUAT, (b). Producer gas and air samples for analysis at ILRI

Three samples of the producer gas corresponding to different gasification temperatures were collected in air tight syringes and self-sealing rubber septum for analysis.

3.3.2.2 Syngas analysis for N_2 and CO_2

Analysis of gas samples (N_2 and CO_2) was performed using gas chromatography with a thermal conductivity detector (GC – TCD) model (GC-8A, Shimadzu Corp., Kyoto, Japan) (see Figure 3.6 (a)) at JKUAT within the Food Science Department. Portions of 1 ml syngas samples from the headspace gas were taken using an airtight syringe and injected into gas chromatographs. The gas chromatograph was fitted with a

Poropak N column, and standard gas was injected for comparison with the sample using retention times. The column initial and final temperatures were maintained at 120 ^{o}C with the det/injecting temperature set at 150 ^{o}C. Helium gas of 99.9 % purity was used as the carrier gas. The GC was calibrated using CO_2 standard and air for CO_2 and N_2 calibration curves. Based on the retention time (0.79 for N_2 and 1.37 for CO_2), the syngas composition was estimated by comparing the peak areas of standard gas and gas samples.

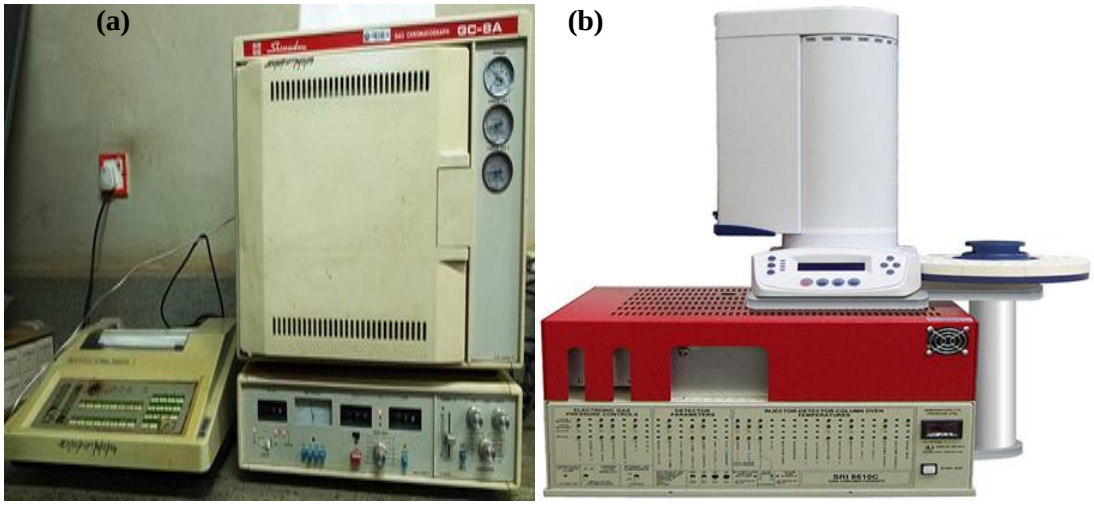

Figure 3.6 (a) GC-TCD (JKUAT) and (b) GC - ECD and FID (ILRI)

3.3.2.3 Syngas analysis for CH_4

Analysis of gas samples (CH_4) was performed using an SRI 8610C Gas chromatograph equipped with a Flame Ionization Detector (FID) for CH_4 detection (see Figure 3.6 (b)). Two 9-Inch Supelco chromatographic columns packed with a Hayesep-D polymer as the stationary phase are separately (on two different channels) used to separate both ECD and FID eluents. N_2 gas of 99.99% purity generated on Claind HC N_2 generator and H_2 gas of 99.99% purity generated on an H2-FID Schmidlin hydrogen generator is used as the carrier gas and FID combustion gas, respectively. In contrast, air from an in-built air compressor is used to support H_2 combustion in the FID. A premixed CO_2 in N_2 gases in the ratio 5:95 is used as the

ECD make-up gas for an improved signal-to-noise ratio. An optimized isocratic column oven temperature program starting at 70^{o}C, holding and maintaining it for four minutes at 70 ^{o}C is used to elute CH_4 with approximately five minutes run per sample. A constant carrier gas flow rate of between 20 and 28 ml/minute, H_2 at 20 to 25 ml/minute, air at 6 ml/minute and ECD make-up gas at 2 ml/minute are maintained throughout the temperature program while both the temperature of the detector are set at 350^{o}C. 3 ml and 1.5 ml aliquots of sample and standard gases are injected in splitless mode with the help of sample loops into the ECD and FID channels, respectively. The GC is calibrated using the CH_4 standard. The composition of CH_4 was predicted by comparing the peak areas of the calibration gas and gas samples.

Within the same range of parameters and feedstock, Njogu et al. (2015) illustrated that a mean of 1.4 % of the product gas accounts for other gases such as oxygen, sulphur etc. From their analysis, it can be proven that the concentration of CO and CO_2 relate as expressed in Eqn. (3.30),

$$\mathrm{CO} = 1.1\mathrm{CO_2} \tag{3.30}$$

By difference, the concentration of H_2 was determined by:

$$\mathrm{H_2} = 100 - (\mathrm{CO}+\mathrm{CO_2} + \mathrm{CH_4} + \mathrm{N_2} + \text{others}) \tag{3.31}$$

The Aspen Plus simulated results were further validated using a set of two published experimental results obtained at similar conditions as the simulation's operation limit. The first validation was carried out with the test results of Jayah et al. (2003). In this validation, nine runs of test results obtained from air gasification of rubber wood in a downdraft gasifier at 900 ^{o}C and 1 atm were used. Secondly, test results by Striūgas et al. (2014) were used in the comparison. In this comparison, a single run of test results obtained from air gasification of rape straw in a downdraft gasifier operated at 1000

^{o}C was used. The proximate and ultimate analysis of rubber wood and rape straw is shown in Table 3.7.

Table 3.7 Proximate and ultimate analysis of rice husk, rubber wood, and rape straw.

	Rubber wood (Jayah et al., 2003)	Rape straw (Striūgas et al., 2014)
Ultimate analysis (wt%, dry)		
C	50.60	39.60
H	6.50	5.60
N	0.20	0.78
S	0.0	0.08
O	42.0	48.54
Proximate analysis (wt%, dry)		
Moisture content	14.0-18.5	14.9
Volatile matter	80.1	62.50
Fixed carbon	19.2	17.20
Ash	0.7	5.40

The variation between the present simulation results and the experimental results was measured by the statistical parameter of root mean square error (RMSE) as expressed in Eqn. (3.32) (George et al., 2016; La Villetta et al., 2017; Upadhyay et al., 2019).

$$RMSE = \sqrt{\frac{\sum(X_e - X_p)^2}{N}} \tag{3.32}$$

Where X_e and X_p represent the experimental result and the calculated result of the product gas from the established thermodynamic model, respectively, and *N* denotes the total number of data sets. According to Beckham et al. (2023), RMSE values ranges between 0 to 20. The lower the RMSE value, the better the model on predicting results (Beckham et al., 2023; Nagahawatte et al., 2023).

3.4 Sensitivity Analysis Procedure

The sensitivity analysis was performed by varying temperature, ER, and MC in the ranges 350 ^{o}C to 1050 ^{o}C, 0.06 to 0.42, and 10% to 30%, respectively, and its effect

on the syngas composition (1), LHV_{Syngas} (2), and H_2/CO molar ratio (3) using the developed model studied. This was achieved by varying one parameter while the others were kept constant.

3.5 Parameter Optimization for Fischer-Tropsch Synthesis

3.5.1 Analysis of variance (ANOVA)

Furthermore, RSM was used for statistical analysis. The goal was to create a regression model to characterize the system performance and optimize the system response by considering the interactions between the key factors. The gasification temperature, ER, and MC in the ranges of 350 ℃ to 1050℃, 0.06 to 0.42, and 10% to 30%, respectively, were determined as the three input parameters for the investigation. In this study, simulation results obtained in Aspen Plus were used as input in Minitab to create a design matrix, as shown in Table B-4 in the appendix section. The objective response regression models were created by performing an Analysis of variance (ANOVA) at a 95 % confidence level, thus evaluating the model's quality and the significance of the parameters and their interactions.

The interaction between the independent variable and response is established by a polynomial quadratic equation as shown in Eqn. (3.33) (Mojaver et al., 2019).

$$y = \beta_0 + \sum_{i=1}^{n} \beta_i x_i + \sum_{i=1}^{n} \beta_{ii} {x_i}^2 + \sum_{i=1}^{n-1} \sum_{j=1}^{n} \beta_{ij} x_i x_j + \in \quad (3.33)$$

Where y stands for output response; x denotes the decision parameter; βi are coefficients; n represents the number of factors; and $\in$ is the statistical error.

The regression model's accuracy was computed by R^2_{adj} a parameter obtained by the ANOVA tool and determined as follows (Mojaver et al., 2019):

$$R_{adj}^2 = 1 - \left(\frac{\frac{SS_R}{(n-p)}}{\frac{SS_T}{(n-1)}} \right) = 1 - \frac{(1-R^2)(n-1)}{1-p} \quad (3.34)$$

Where the sum of squares of the residual (SS_R) and the total sum of squares (SS_T) are calculated as per Eqn. (3.35) and (3.36), respectively.

$$SS_R = \sum_{i=1}^{n} (y_i - y_j)^2 \quad (3.35)$$

$$SS_T = \sum_{i=1}^{n} {y_i}^2 - \frac{\sum_{i=1}^{n} y_i^2}{n} \quad (3.36)$$

Where y_i and y_j stand for the observations and fitted observations.

The P-value is among the model's most crucial parameter; if its magnitude exceeds 0.05, the P-value is often considered insignificant (Roy et al., 2020). R^2 is computed using Eqn. (3.37) (Mojaver et al., 2019).

$$R^2 = 1 - \frac{SS_R}{SS_T} \quad (3.37)$$

3.5.2 Multi-objective optimization

Multi-objective optimization of air gasification of rice husk was carried out using RSM. Three objective responses, including H_2, CO and H_2/CO were considered for the multi-objective optimization. In addition, the three operating parameters (gasification temperature, ER, and MC) in the sensitivity analysis section were used as decision variables. The main aim is to determine the optimized zone of the operating condition for Fischer-Tropsch synthesis. In this regard, the combined effect of the decision variable is explored.

CHAPTER FOUR: RESULTS AND DISCUSSION

4.1 Introduction

The chapter begins with a description of rice husk as the model biomass feedstock. The verification of the developed models' accuracy is then performed based on a designed experimental setup of air-gasification of rice husk. It is then followed by a parametric study to investigate the effect of operating conditions of the gasification system on the producer gas composition. Finally, a multi-objective optimization of the operating conditions of a gasification process for FTs applications using RSM is performed. A detailed discussion of the model outputs is explained.

4.2 Thermodynamic Model Development

Table 4.1 presents the physical and chemical properties of the rice husk used in this study as a modelled feedstock.

Table 4.1 Rice husk's ultimate and proximate analysis.

Ultimate analysis	(%)	Proximate analysis	(% d.b)
C	37.42	Volatile matter	72.82
H	5.17	Fixed carbon	16.82
O	46.28	Ash	10.36
N	0.13		
S	0.64		
Ash	10.36		

It can be observed from Table 4.1 that rice husk had a relatively high volatile matter (VM) of 72.82%. This is similar to the value of 72.8% reported by Janewit et al. (2008) and relatively close to the value of 73% reported by Güleç et al. (2022). The high VM content causes the rice husk to be devolatilized fast (Kipngetich et al., 2023), hence it is a suitable fuel for pyrolysis and gasification. Moreover, rice husk ignites easily due to its high VM. This makes it possible to gasify the rice husk at

relatively lower temperatures (Olupot et al., 2016) since the thermochemical reactions require less heat.

The ash content of the rice husk was found to be 10.36%. This value is relatively close to the value of 11.7% and 11.36% reported by Tuan et al. (2022) and Park et al. (2021) respectively. According to Olupot et al. (2016) and Wakatuntu et al. (2023), biomass feedstock with ash content of 5% and below does not cause slagging in the conversion systems at temperatures above 1000 ^{o}C. This means the rice husk of our study with an ash content of 10.36% is prone to cause slagging in the gasification system if the temperature is not kept below 1000 ^{o}C. With the gasification system of the study operating at a temperature ranging from 350 ^{o}C to 1050 ^{o}C, the effect of slagging is not of major concern.

It can also be observed from Table 4.1 that rice husk had a fixed carbon of 16.82%. This value conforms to the range of 14.77% and 17.75% reported by Olupot et al. (2016) and is very close to the value of 16.96% reported by Park et al. (2021). FC generates char which is utilized in the thermal cracking of tar (Olupot et al., 2016) so a feedstock with high FC is preferred for gasification process.

From the analysis, rice husk was found to have a carbon content of 37.42%, hydrogen content of 5.17%, nitrogen content of 0.13%, sulphur content of 0.64% and oxygen content of 46.28%. Except for sulphur and nitrogen contents, the remaining rice husk composition was observed to be close to the results reported by Silva et al. (2021) for carbon content, by Homchat & Ramphueiphad (2022) for hydrogen content and by Janewit et al. (2008) for oxygen content. The relatively low sulphur and nitrogen contents of the rice husk are of great benefit since minimal risks of NOx and SOx are expected during the thermochemical conversion of rice husk. Making it suitable to be

used as a biomass fuel (Olupot et al., 2016; Tripathi et al., 2016; Ogwang et al., 2021; Homchat & Ramphueiphad, 2022). Figure 3.2 and 3.3 illustrate the user interface of EES model and Aspen Plus model respectively.

4.3 Model Validation

4.3.1 Temperature profile inside the gasifier

Figure 4.1 (a) and (b) demonstrate the updraft gasifier reactor and temperature profile of the rice husk gasification process at different zones inside the gasifier over time respectively. The maximum oxidation zone temperature (T_1) was observed to be 493 ^{o}C at 7 minutes. Both the reduction and pyrolysis zone temperatures were relatively stable and low. The observed results are not directly comparable with published literature data as the size, dimension and materials used in fabricating the reactor, and the type of biomass used were different.

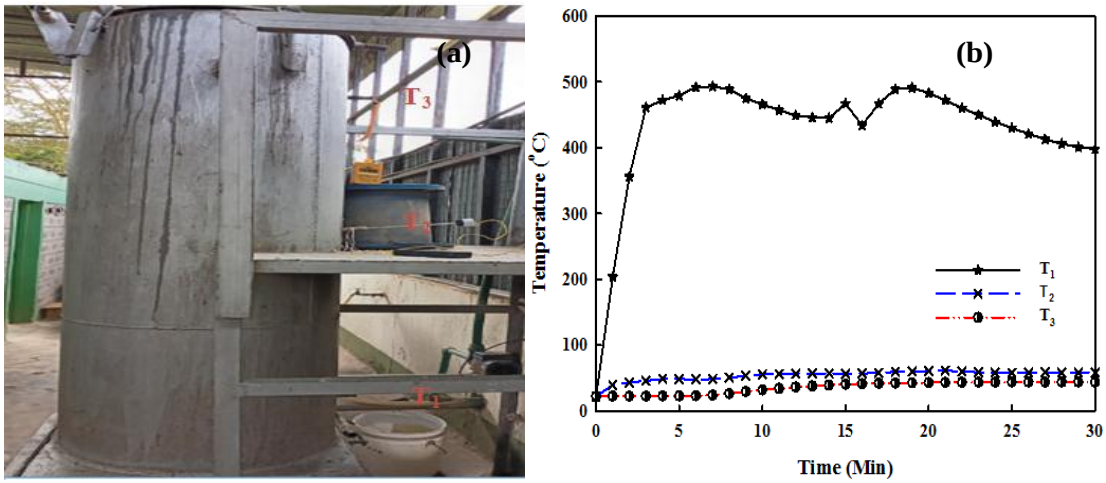

Figure 4.1 Gasification temperature profile

4.3.2 Experimental results

Table 4.2 shows the average syngas composition at different gasification temperatures and ER obtained from the air gasification of rice husk at the three chosen residence times at a constant MC of 9.75%.

Table 4.2 Syngas composition

Measured parameters	**Units**	**Run 1**	**Run 2**	**Run 3**
Time	Minutes	12	15	30
ER		0.361	0.357	0.370
Gasification temperature	^{o}C	449	467	398
CH_4	% vol.	1.44±0.05	1.29±0.06	1.61±0.08
CO	% vol.	13.59±1.05	13.20±1	13.97±1.1
CO_2	% vol.	12.35±0.05	12.00±0.05	12.70±0.06
H_2	% vol.	7.32±0.05	9.31±0.05	4.94±0.05
N_2	% vol.	63.76±4.8	62.95±5.1	65.38±5

4.3.3 Comparison between simulated and experimental results

The simulated and experimental results were compared as shown in Figure 4.2. It is evident from Figure 4.2 that the Aspen Plus model results agree with the experimental results except for CO and CO_2.

The average RMSE values for syngas were found to be 7.78 and 8.99 for Aspen Plus and EES, respectively. The RMSE was observed to reduce with temperature enhancement. The rates of reactions are slower at low temperatures, causing the reactions to take longer to attain a state of equilibrium (Aydin et al., 2017), resulting in a decrease in the equilibrium models' performance. Aydin et al. (2017) also observed a similar trend in their semi-empirical model study of various wood-based biomass feedstock in a downdraft gasifier. Although the model predicted CH_4, H_2, and N_2 concentration to a good degree of accuracy, it underestimated CO and overestimated CO_2 concentration by a large margin. It is reasoned that the bed temperature was insufficient for achieving the equilibrium state, leading to underestimating CO and overestimating CO_2 concentration.

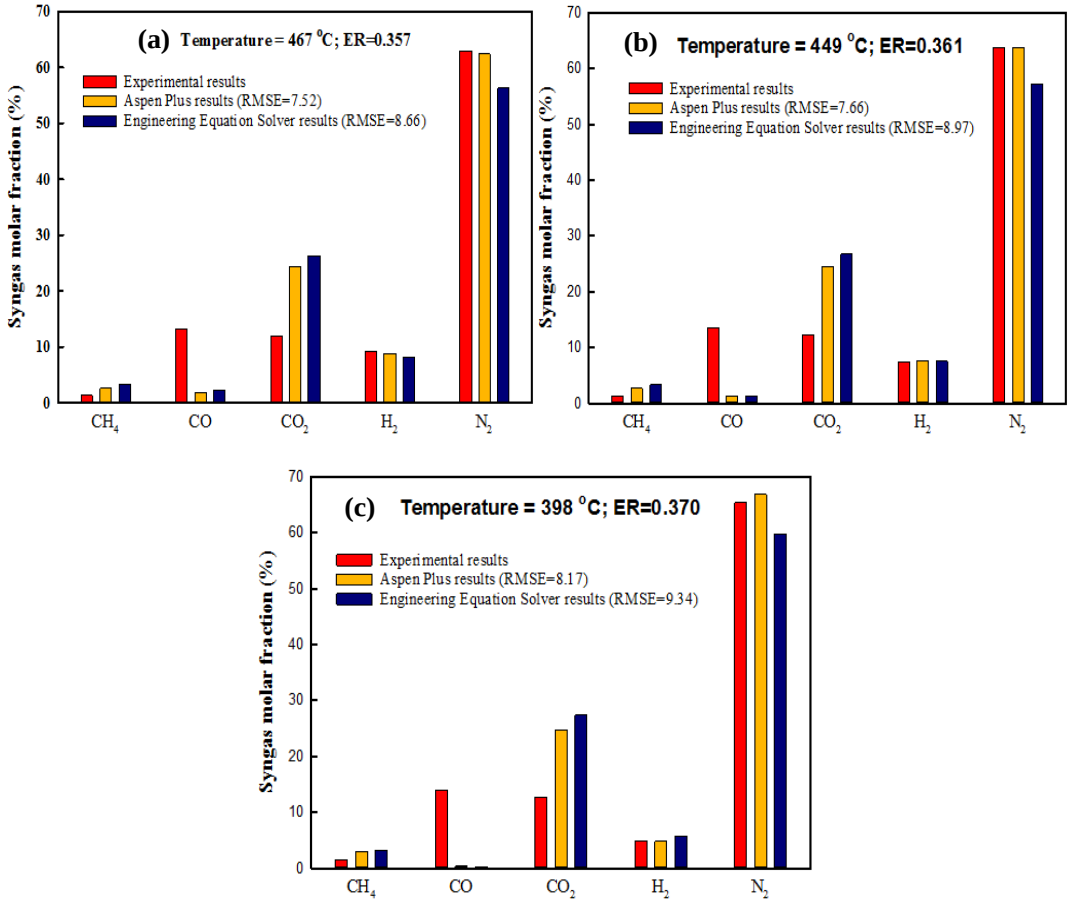

Figure 4.2 Comparison of simulated results with experimental results

The second comparison between the simulated results and the test results of Jayah et al. (2003) and Striūgas et al. (2014) is illustrated in Table 4.3. The observed RMSEs of 2.498 and 2.381 are within the acceptable range since the simulation model neglects the gasification systems' kinetics and fluid dynamics. The numerical simulation model yielded nearly 100 % of CH_4, which is an underestimated value compared to the experimental value. Due to short residence time, actual gasifiers cannot achieve thermodynamic equilibrium resulting in under-forecasting CH_4 (Zaman et al., 2020).

Table 4.3 Comparison between the experimental and simulated results

Run No	Parameters		Experiment (Jayah et al., 2003)					Aspen Plus					RMSE
	MC (%)	A/F	CO (%)	H_2 (%)	CO_2 (%)	CH_4 (%)	N_2 (%)	CO (%)	H_2 (%)	CO_2 (%)	CH_4 (%)	N_2 (%)	
1	18.5	2.03	19.600	17.200	9.900	1.400	51.900	20.744	18.897	10.199	0.004	50.155	1.362
2	16.0	2.20	20.200	18.300	9.700	1.100	50.700	19.650	17.900	10.709	0.003	51.738	0.867
3	14.7	2.37	19.400	17.200	9.700	1.100	52.600	18.346	16.712	11.317	0.002	53.623	1.097
4	16.0	1.96	18.400	17.000	10.600	1.300	52.700	18.760	17.010	11.130	0.002	53.030	0.664
5	15.2	2.12	19.700	13.200	10.800	1.300	55.000	20.665	18.824	10.236	0.004	50.271	3.374
6	14.0	2.29	18.900	12.500	8.500	1.200	59.100	19.286	17.568	10.879	0.003	52.264	3.991
7	14.7	1.86	19.100	15.500	11.400	1.100	52.900	23.574	21.474	8.881	0.008	46.064	4.690
8	13.8	2.04	22.100	12.700	10.500	1.300	53.400	21.845	19.900	9.686	0.005	48.564	3.940
9	12.5	2.36	19.100	13.000	10.700	1.200	56.00	19.003	17.311	11.011	0.003	52.673	2.498
												Average	2.498
	MC	ER	Experiment (Striūgas et al., 2014)					Aspen Plus					
1	14.9	0.29	14.590	14.430	11.800	4.040	54.960	16.874	13.448	14.186	0.003	55.492	2.381

This error analysis indicates a reliable numerical simulation model in its predictive capacity.

4.4 Sensitivity Analysis

After validation, the Aspen Plus model described above was used to simulate air gasification of rice husk at different values of reactor temperature, equivalence ratio and moisture content. Their impact on syngas composition, the lower heating value of the syngas and the hydrogen to carbon monoxide ratio are discussed below.

4.4.1 Effect of temperature

The reactor temperature affects both the amount and the composition of the syngas generated by influencing all the chemical reactions occurring during gasification. Figure 4.3 demonstrates how gasification temperature influences syngas composition.

From Figure 4.3, it can be deduced that enhancing the reactor temperature favours the formation of high CO content syngas. The composition of H_2 increased with temperature rise from 350 ℃ to 750 ℃ and then decreased with a further increase in temperature. On the other hand, the composition of CH_4 and CO_2 decreased continuously with an increase in temperature. These results have similar trends with simulation results (Han et al., 2017; Tavares et al., 2018; Li et al., 2021). The H_2, CH_4, and CO results agree with the experimental results (Son et al., 2011).

These trends in the concentrations may be accounted for by the nature of reactions R_8, R_3, and R_2, being endothermic. With an increase in temperature, these reactions' equilibrium shifts towards product formation according to Le Chatelier's Principle, thereby increasing the concentration of CO and H_2 in the syngas. Higher temperatures hinder methanation (R_4) and water-gas shift (R_7) reactions leading to the formation of syngas with a lower concentration of CO_2, CH_4, and H_2.

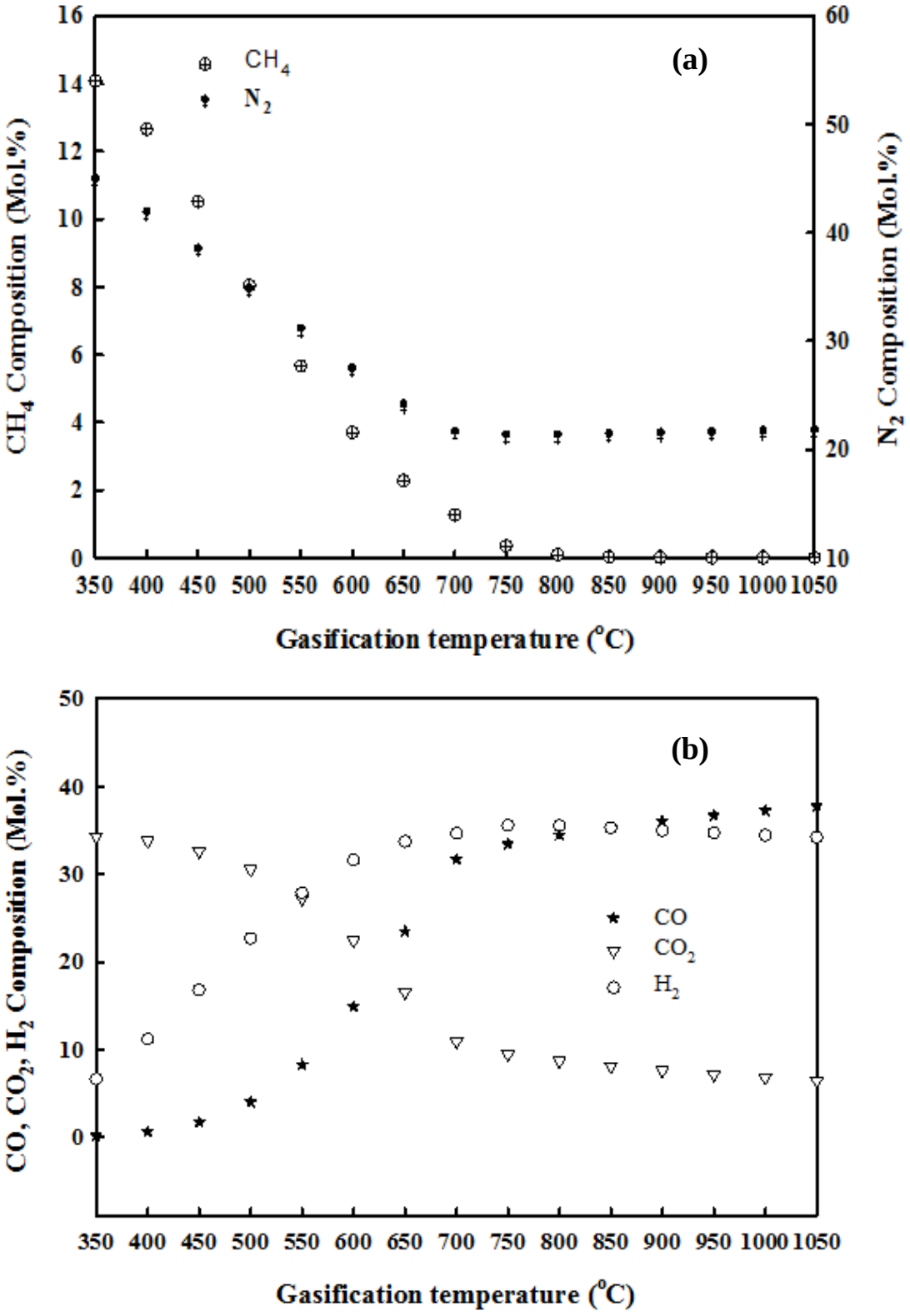

Figure 4.3 The effect of gasification temperature on the composition of syngas.

The H_2 fluctuation might be a result of the combined effect of reactions taking place in the gasifier. According to Franco et al. (2003), R_7 is a key reaction that determines

the final syngas composition during the gasification of biomass. This is due to its ability to react with CO and steam to produce H_2 and CO_2. At lower temperatures, R_7 prevailed in yielding H_2 but was hindered by a temperature increase beyond 750 $^{\circ}$C. Methanation reaction (R_4) consumes less H_2 at high temperatures. The other contributing reactions, R_8 and $R_{3,}$ are endothermic. These reactions contribute to the increase in the concentration of H_2 from 350 ℃ to 750 ℃, beyond which the reactions are limited by a lack of reactants like CH_4 and steam, leading to the decrease in the concentration of H_2 (Han et al., 2017).

Figures 4.4 illustrate the influence of varying gasification temperatures on LHV_{Syngas} and the H_2/CO ratio. The LHV_{Syngas} was observed to increase with an increase in temperature. Similar trends were reported in the simulation study (Han et al., 2017). This is because high temperature promotes the generation of combustible gases like H_2 and CO, which results in increasing the LHV_{Syngas} (Lahijani & Zainal, 2011). An opposite trend is observed for H_2/CO ratio. Similar behaviour was observed in the simulation study (Han et al., 2017).

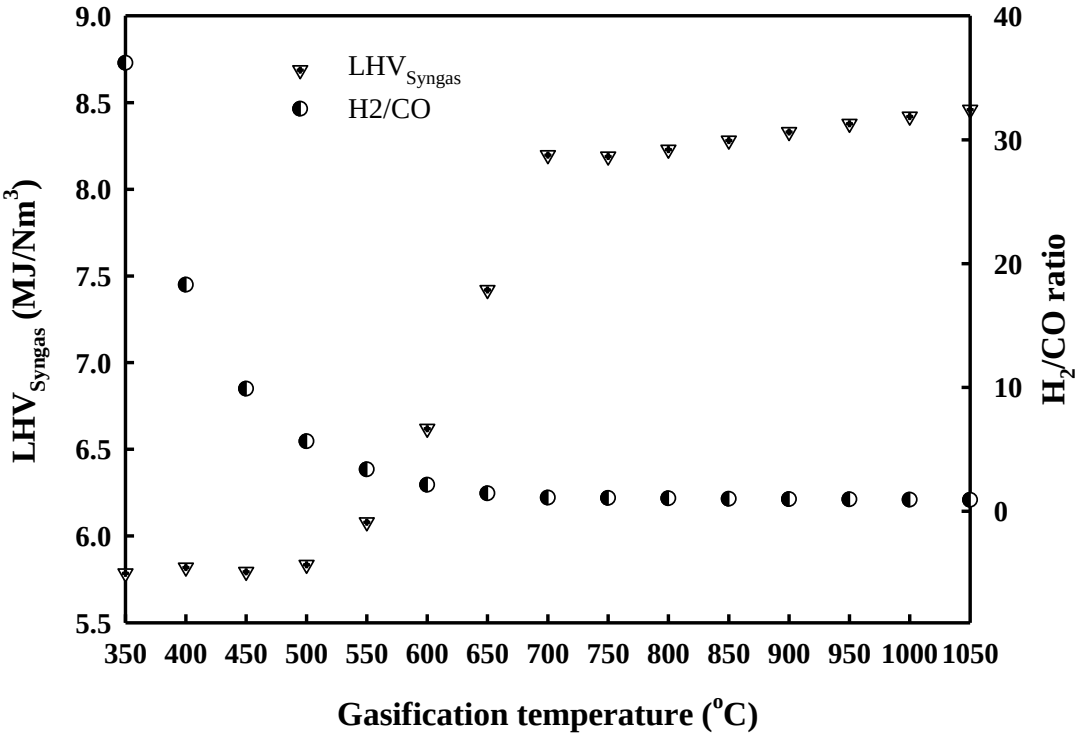

Figure 4.4 The impact of gasification temperature on LHV_{Syngas} and H_2/CO molar ratio

4.4.2 Effect of moisture content

The impact of varying biomass MC on the syngas composition is demonstrated in Figure 4.5. It can be observed in Figure 4.5 that the composition of H_2, CH_4, and CO decreased continuously with an increase in MC from 10% to 30%. An opposite trend was observed for CO_2. Similar behaviour in the variation of syngas composition with respect to changing moisture content is observed in various simulation studies (Mountouris et al., 2006; Gagliano et al., 2016; Diyoke et al., 2018).

Wet biomass reduces the oxidation zone temperature as extra energy is needed to dry the biomass (Kaushal et al., 2011; Zang et al., 2019). At the same time, increasing the MC also enhances the auto-generation of steam, which is a reactant in the char and volatile decomposition (Diyoke et al., 2018). At low biomass MC, oxidation zone temperature is high. This shifts the equilibrium of R_3 towards the formation of H_2 and

CO. As MC increases, the reduction zone temperature reduces, thereby shifting the R_3 reaction's equilibrium towards the reactants' formation. This accounts for the rise in CO_2 concentration and the decrease in the concentration of H_2 and CO with an increase in the MC of biomass.

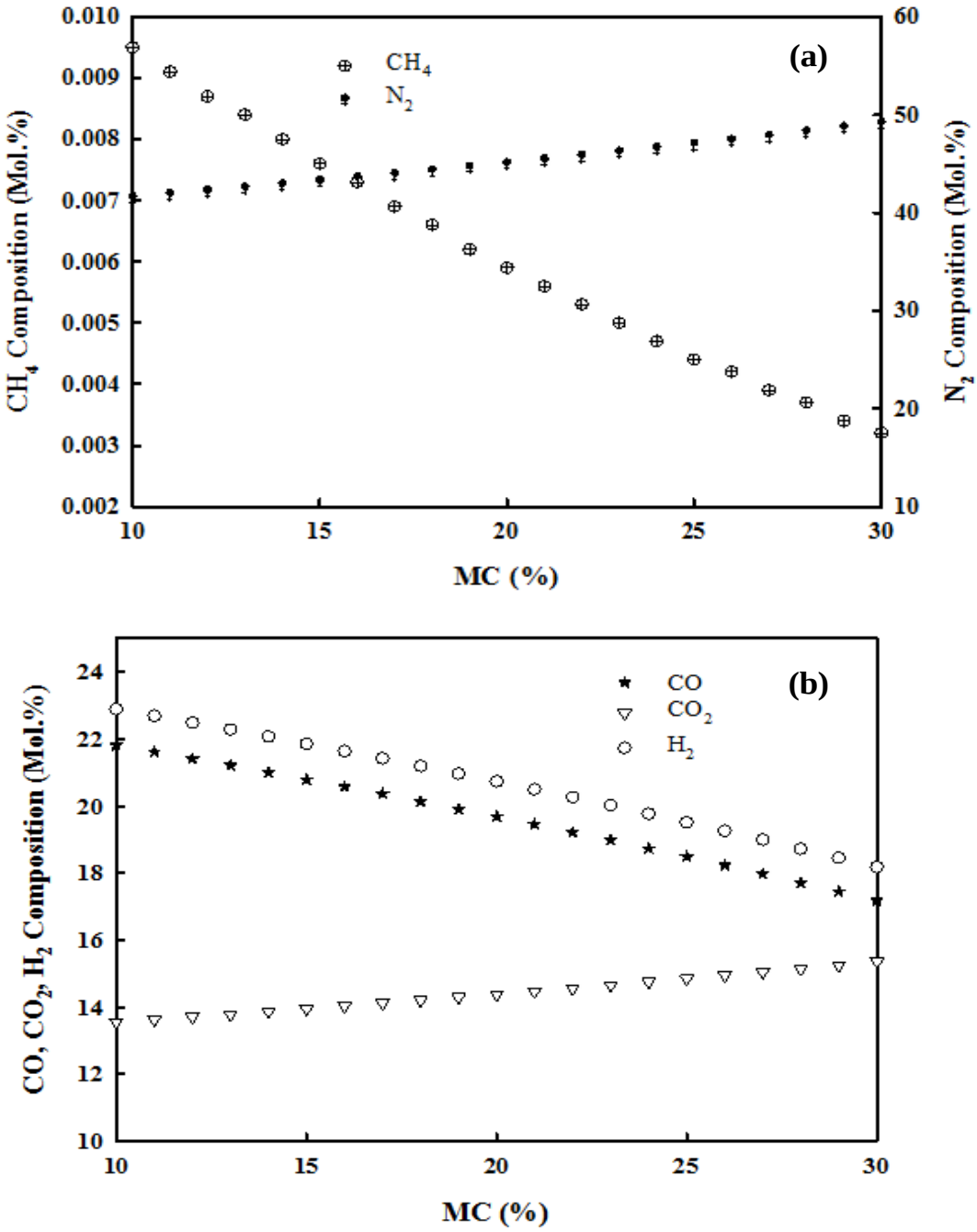

Figure 4.5 The impact of moisture content on syngas composition.

Figures 4.6 illustrate the impact of varying MC on LHV_{Syngas} and the H_2/CO molar ratio. As expected, enhancing MC lead to a continuous decline in the LHV_{Syngas}. This is attributed to the consistent reduction in the concentration of CO, CH_4, and H_2, as shown in Figure 4.6. These results have similar variations to simulation results obtained by Diyoke et al. (2018). Hence, drying fuel feed to low MC is essential in producing high-value performance parameters. H_2/CO ratio was observed to increase with increasing MC. Similar behaviour was observed in the simulation study (Han et al., 2017).

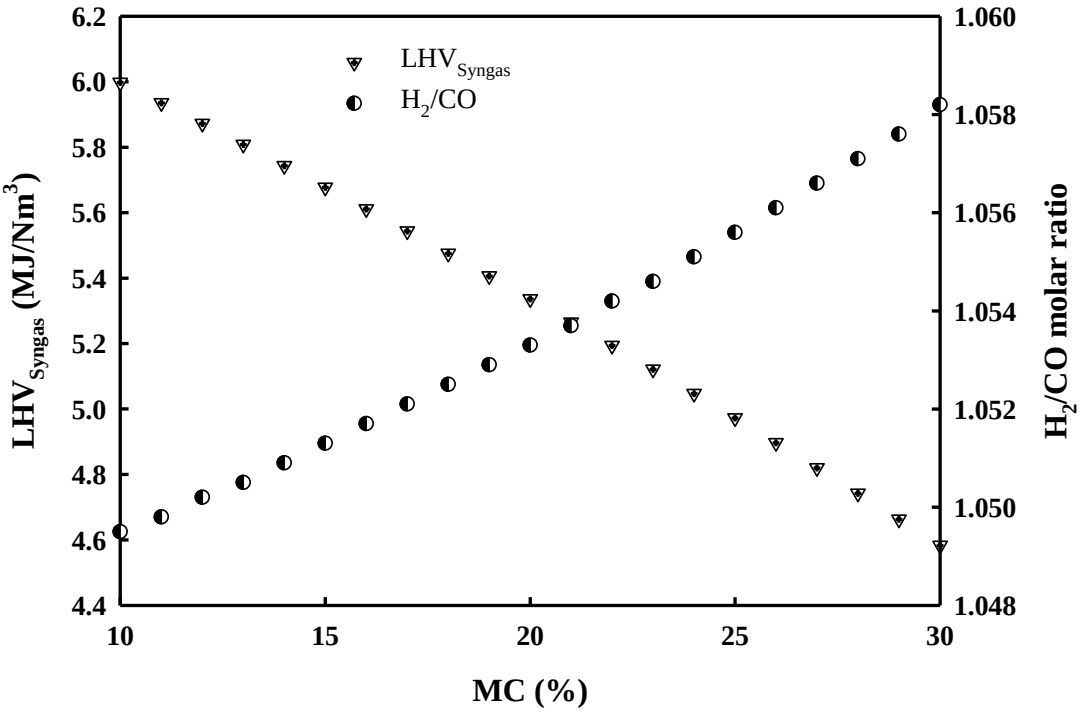

Figure 4.6 The impact of biomass moisture content on LHV_{Syngas} and H_2/CO molar

4.4.3 Effect of equivalence ratio

The influence of varying equivalence ratios on the composition of syngas is demonstrated in Figure 4.7. It was observed from this figure that the hydrogen, methane and carbon monoxide composition reduced with increasing ER. An opposite trend was observed for carbon dioxide and nitrogen.

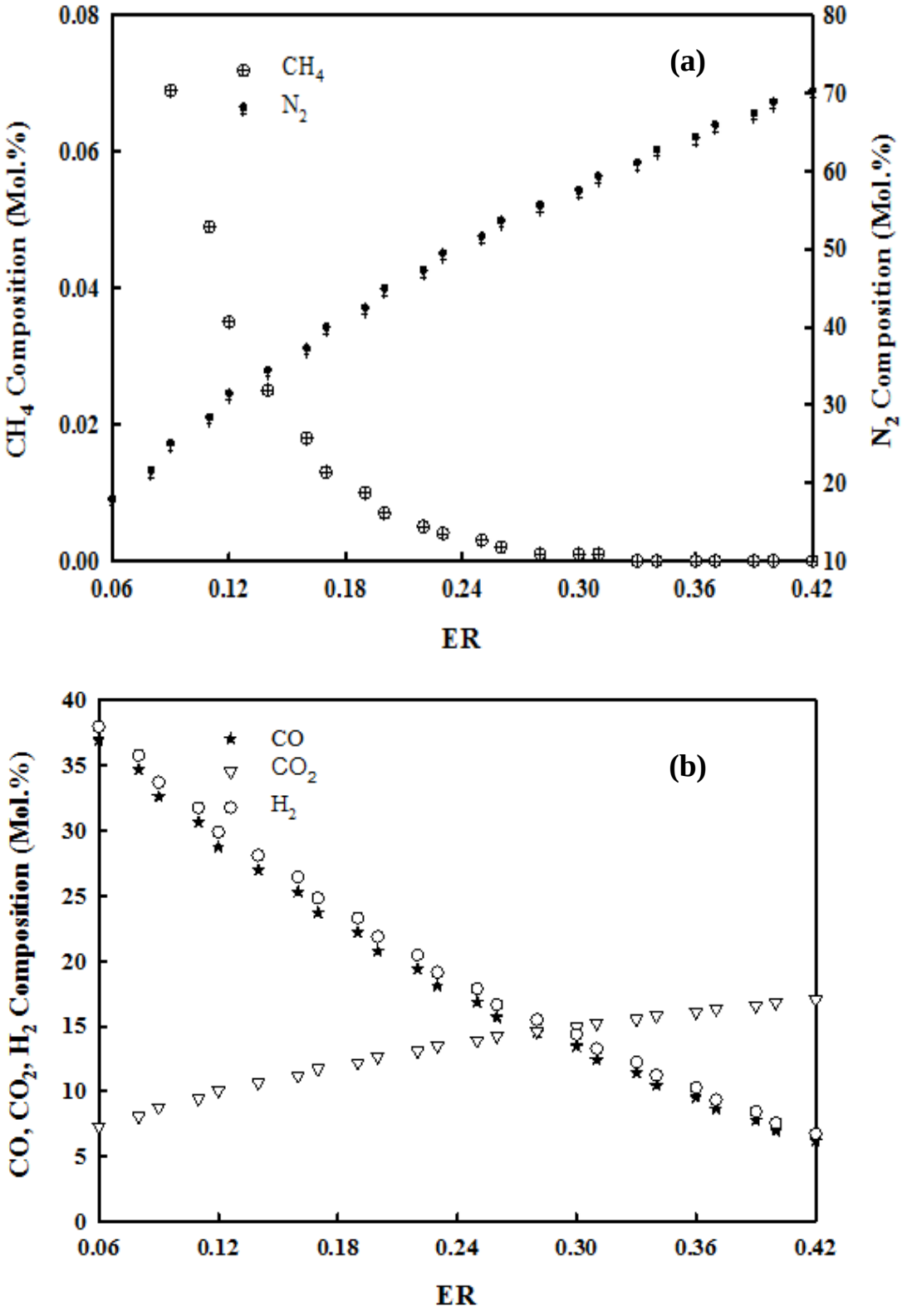

Figure 4.7 The effect of equivalence ratio on syngas composition

As the ER increases, the process shifts towards complete combustion, leading to a rise in the concentration of carbon dioxide and a decline in carbon monoxide, hydrogen

and methane concentration. Similar behaviour in the variation of syngas composition with respect to ER was observed in the studies (Nikoo & Mahinpey, 2008; Doherty et al., 2009; Rupesh et al., 2016; Diyoke et al., 2018; Lan et al., 2018).

Figures 4.8 illustrate how ER influence the LHV_{Syngas} and the H_2/CO ratio. ER enhancement leads to a decrease in the LHV_{Syngas}. An opposite trend is observed for H_2/CO molar ratio. The decline in LHV_{Syngas} with respect to increasing ER is attributed to the nitrogen's dilution of syngas which in turn results in lowering the energy content of syngas (Gómez-Barea & Leckner, 2010; Lahijani & Zainal, 2011). Similar trends were also reported in simulation studies by Favas et al. (2017) and experimental results of Lahijani & Zainal (2011); Jamin et al. (2020). An opposite trend is observed for H_2/CO ratio. Han et al. (2017) reported a similar trend in their simulation study.

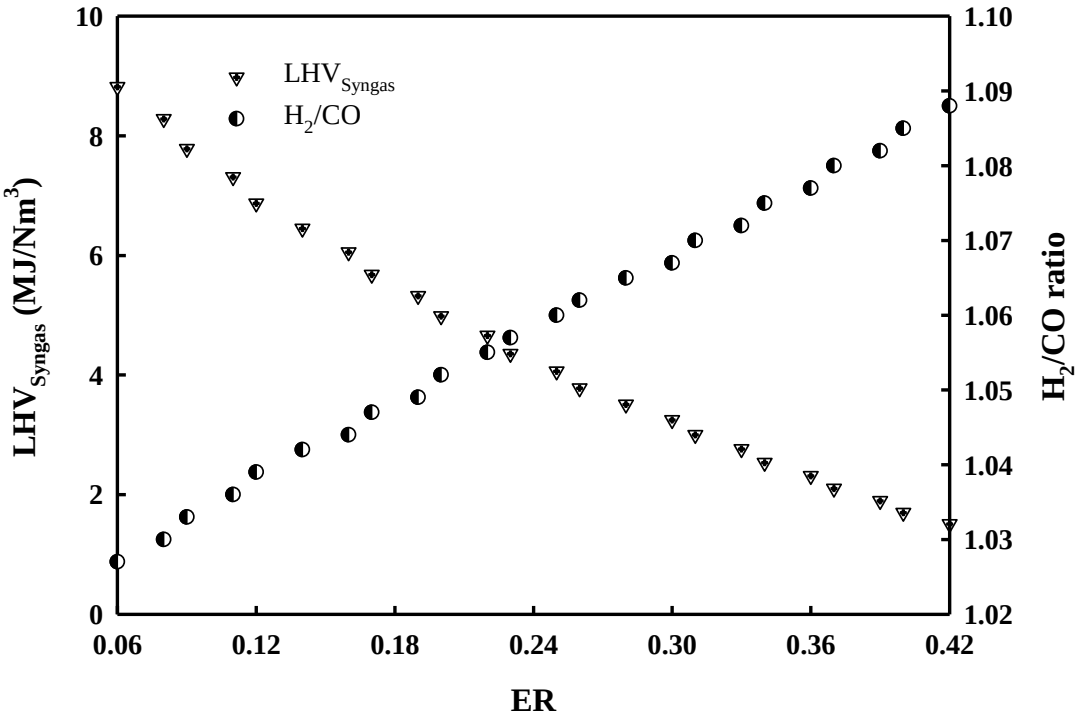

Figure 4.8 The effect of equivalence ratio on LHV_{Syngas} and H_2/CO molar

4.5 Parameter Optimization for Fischer-Tropsch Synthesis

Identifying the combination of the critical parameters (gasification temperature, moisture content and equivalence ratio) that optimises Fischer-Tropsch synthesis is one of the objectives of this study. The response surface optimisation technique is the ideal method for determining the best combination of the operating parameters.

4.5.1 Analysis of variance (ANOVA)

The RSM model ANOVA regression analysis for $LHV_{Syngas,}$ H_2, CO, and H_2/CO ratio, respectively, is shown in Table 4.4. It can be deduced from the ANOVA results shown in Table 4.4 that linear, square, and 2-way interaction regression model terms for $LHV_{Syngas,}$ H_2, CO, and H_2/CO molar are significant, except MC in the square term for H_2, CO, and H_2/CO regression models, ER in the square term for CO, and H_2/CO regression models, 2–way term of Temp*MC and ER*MC for all regression models and MC in the linear term for H_2/CO molar ratio regression model. From Table 4.4, the R^2 values of the regression models were observed to be 98.47% for LHV_{Syngas}, 98.93% for H_2, 96.94% for CO and 89.91% for H_2/CO molar ratio. The Adj-R^2 values for $LHV_{Syngas,}$ H_2, CO, and H_2/CO molar ratio were 98.28%, 98.80%, 96.56%, and 88.64%, respectively, satisfactorily close to the corresponding R^2 values. This result indicates a minimal likelihood of including an insignificant term in the model. Therefore, the regression models can determine the response variables with a high accuracy level.

Table 4.4 ANOVA results for $LHV_{Syngas,}$ H_2, CO, and H_2/CO molar.

		LHV		**H_2**		**CO**		**H_2/CO**	
Constant	**DF**	**Adj SS**	**P-value**	**Adj SS**	**P-value**	**Adj SS**	**P-value**	**Adj SS**	**P-value**
Model	9	167.559	0.000	2763.80	0.000	6560.26	0.000	34.7714	0.000
Linear	3	157.851	0.000	2551.99	0.000	5340.38	0.000	23.2763	0.000
Temp	1	23.054	0.000	101.47	0.000	3916.42	0.000	22.5819	0.000
ER	1	134.873	0.000	2430.63	0.000	1496.71	0.000	0.5072	0.003
MC	1	1.689	0.000	31.02	0.000	17.98	0.015	0.0173	0.573
Square	3	7.602	0.000	180.97	0.000	796.62	0.000	9.0954	0.000
Temp × Temp	1	6.987	0.000	167.30	0.000	794.64	0.000	9.0707	0.000
ER × ER	1	0.620	0.000	13.77	0.000	1.84	0.426	0.0183	0.563
MC × MC	1	0.002	0.830	0.04	0.763	0.05	0.892	0.0010	0.893
2-Way interaction	3	2.284	0.000	41.59	0.000	335.72	0.000	0.9353	0.001
Temp × ER	1	2.102	0.000	38.36	0.000	322.87	0.000	0.8807	0.000
Temp × MC	1	0.041	0.289	0.79	0.171	5.37	0.176	0.0329	0.438
ER × MC	1	0.092	0.114	1.56	0.056	2.48	0.356	0.0046	0.771
Error	72	2.596		29.82		207.02		3.9037	
Total	81	170.155		2793.62		6767.28		38.6751	
Coefficient of determination									
R^2		98.47%		98.93%		96.94%		80.20%	
Adj-R^2		98.28%		98.80%		96.56%		79.86%	
Pred-R^2		98.04%		98.57%		96.01%		79.13%	

The regression equations for $LHV_{Syngas,}$ H_2, CO, and H_2/CO molar ratio in the uncoded unit obtained from the ANOVA results are depicted in Eqns. (4.1) - (4.4), respectively.

$$\begin{aligned} LHV_{Syngas}\ (MJ/Nm^3) &= -6.14 + 0.03755\ Temp - 18.22\ ER + 0.0287\ MC \\ &- 0.000020\ Temp^2 + 54.8\ ER^2 - 0.00038\ MC^2 \\ &- 0.02580\ Temp * ER - 0.000042\ Temp * MC \\ &- 0.172\ ER * MC \end{aligned} \quad (4.1)$$

$$\begin{aligned} H_2\ (Mol.\%) &= -25.42 + 0.17009\ Temp - 83.4\ ER + 0.128\ MC \\ &- 0.000097\ Temp^2 + 258.5\ ER^2 - 0.00183\ MC^2 \\ &- 0.1102\ Temp * ER - 0.000184\ Temp * MC - 0.706\ ER \\ &* MC \end{aligned} \quad (4.2)$$

$$\begin{aligned} CO\ (Mol.\%) &= -153.93 + 0.4160\ Temp + 140.7\ ER + 0.417\ MC \\ &- 0.000211\ Temp^2 + 94\ ER^2 - 0.0022\ MC^2 \\ &- 0.3198\ Temp * ER - 0.000479\ Temp * MC - 0.891\ ER \\ &* MC \end{aligned} \quad (4.3)$$

$$\begin{aligned} {H_2}/{CO}\ \text{Molar ratio} &= 19.17 - 0.04049\ Temp - 17.03\ ER - 0.0453\ MC \\ &+ 0.000023\ Temp^2 + 9.4\ ER^2 + 0.00030\ MC^2 \\ &+ 0.01670\ Temp * ER + 0.000038\ Temp * MC + 0.038\ ER \\ &* MC \end{aligned} \quad (4.4)$$

Figure 4.9 further presents the Pareto chart of the standardized impact of reactor temperature, ER and MC on the $LHV_{Syngas,}$ H_2, CO, and H_2/CO molar ratio. The influence of two-way interaction coded AC, BC, and CC was found to be insignificant on all the response variables. It can be further observed that the influence of two-way interaction coded BB is insignificant on CO and H_2/CO ratio. Furthermore, the linear term C was observed to be insignificant on H_2/CO molar ratio.

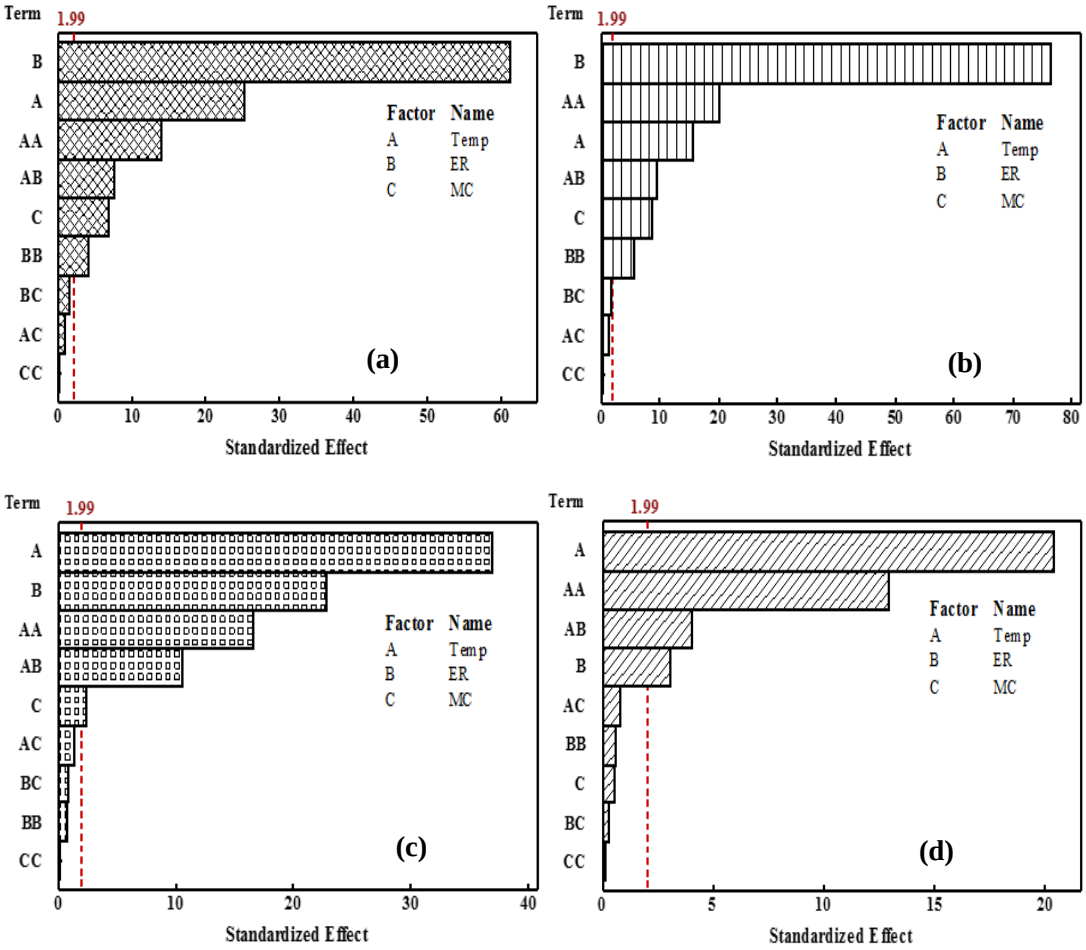

Figure 4.9 Pareto chart of the standardized effects for (a) LHV_{Syngas}, (b) H_2, (c) CO, and (d) H_2/CO molar ratio

4.5.2 Effect of parameter interaction

To visualise the effect of the interactions between the key parameters, a 2D contour and a 3D surface plots of the response variables are studied. On a 2D contour plot, one parameter is kept constant since it is not possible to display the effect of three parameters on the same plot.

4.5.2.1 The impact of operating parameters interaction on CO yield

Figure 4.10 shows the impact of temperature and moisture content interaction at different values of equivalence ratio on CO output. A higher reactor temperature and low moisture content of biomass feedstock were observed to favour the production of

CO for all ER. A low yield of CO was observed at lower temperatures and higher moisture content for all ER.

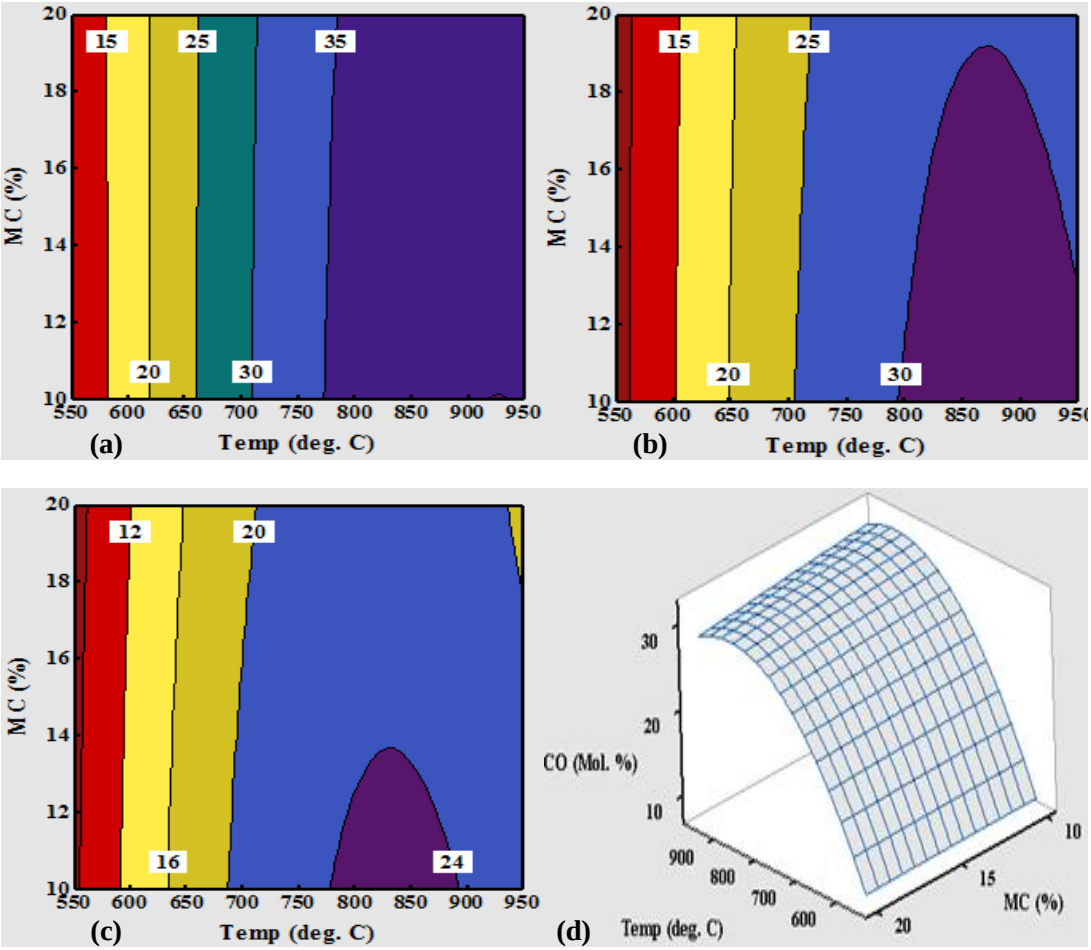

Figure 4.10 The impact of temperature and moisture content interaction on CO yield: (a) contour plot at 0.06, (b) contour plot at 0.12, (c) contour plot at 0.18, and (d) 3D surface plot at 0.12 ER.

At lower ER, the endothermic reactions R_6 and R_7 are favoured leading to the consumption of carbon dioxide and char to form more hydrogen and carbon monoxide (Doherty et al., 2009; Diyoke et al., 2018). As ER increases, gasification temperature reduces; hence less char is consumed, thereby producing less carbon monoxide and hydrogen. This accounts for the reduction in the carbon monoxide concentration in the product gas as ER increases.

Figure 4.11 demonstrates the interaction effects of temperature and equivalence ratio at various moisture content values on the CO output.

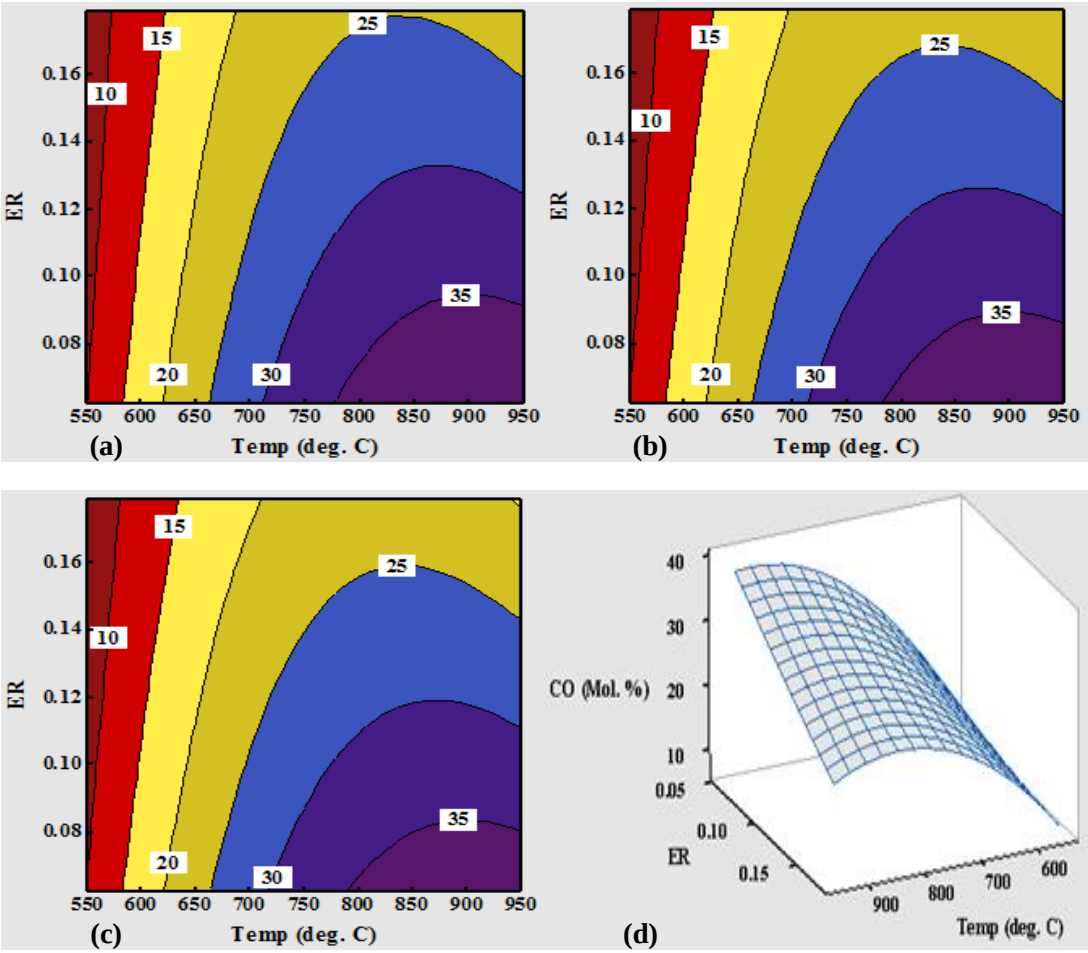

Figure 4.11 The influence of temperature and equivalence ratio interaction on CO yield: (a) contour plot at 10%, (b) contour plot at 15%, (c) contour plot at 20%, and (d) 3D surface plot at 15% MC of biomass feedstock.

It is observed that CO is maximised at a lower moisture content of biomass feedstock. A rise in moisture content leads to a decline in CO yield. This trend is in agreement with that observed by (Guangul et al., 2014). At low biomass moisture content, oxidation zone temperature is high and nearly constant. This shifts the equilibrium of reactions R_6 and R_7 towards the formation of carbon monoxide and hydrogen. With moisture content enhancement, the reduction zone temperature reduces, thereby shifting the equilibrium of reactions R_6 and R_7 towards the formation of the reactants.

This accounts for the decline in carbon monoxide concentration with increasing biomass moisture content.

4.5.2.2 The influence of operating parameters interaction on H_2 yield

Figure 4.12 demonstrates the interaction effects of temperature and moisture content at various ER values on the H_2 output. It is observed that H_2 is maximised at a lower moisture content of biomass feedstock and higher temperature for all equivalence ratios.

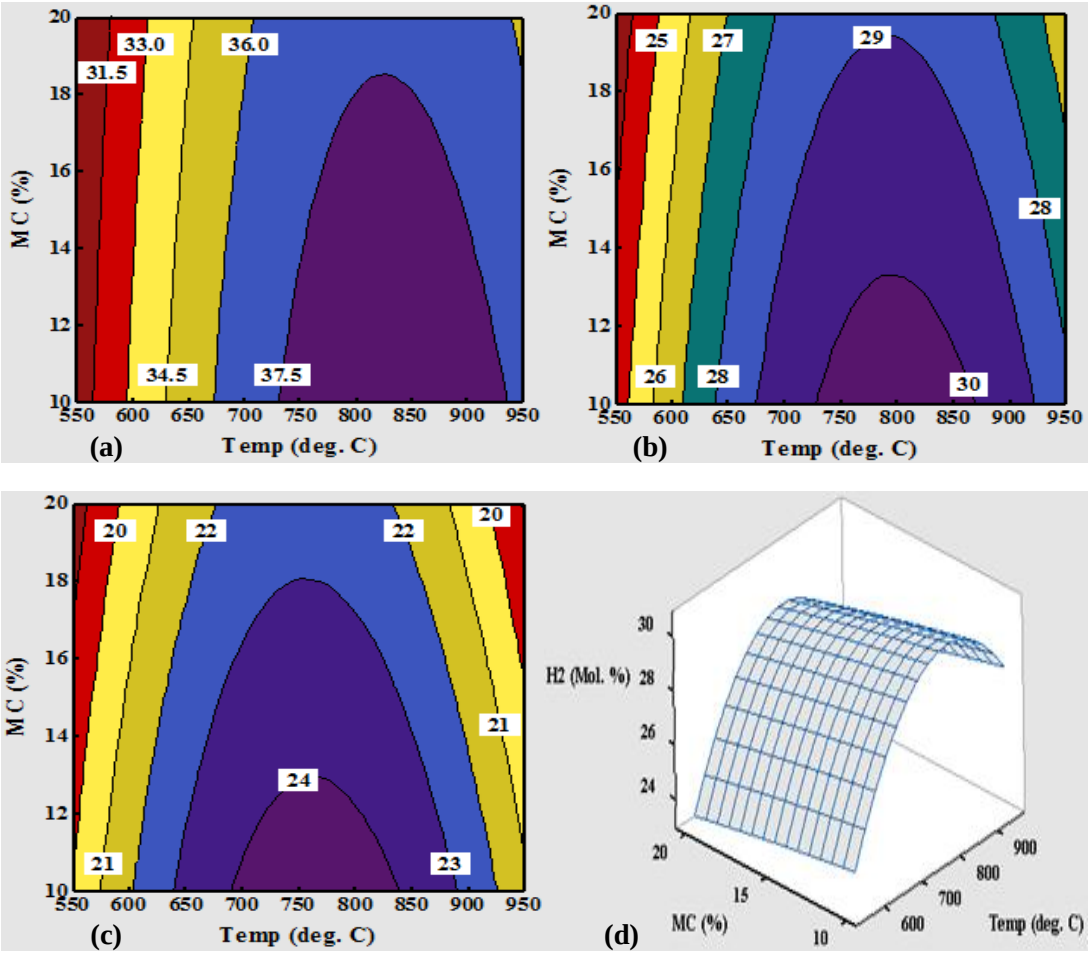

Figure 4.12 The influence of temperature and moisture content interaction on H_2 yield: (a) contour plot at 0.06, (b) contour plot at 0.12, (c) contour plot at 0.18, and (d) 3D surface plot at 0.12 ER.

However, at ER of 0.06, the H_2 yield was maximum compared to ER of 0.12 and 0.18. This trend is in agreement with that observed by (Guangul et al., 2014). At lower ER,

the endothermic reaction R_6 is favoured leading to the consumption of char to form more hydrogen and carbon monoxide (Doherty et al., 2009; Diyoke et al., 2018). As ER increases, gasification temperature reduces; hence less char is consumed, and H_2 is converted into H_2O, thereby reducing the concentration of hydrogen in the syngas (Guangul et al., 2014).

Figure 4.13 demonstrates how equivalence ratio and temperature interaction at different moisture content values affect the H_2 output. The H_2 yield in the syngas decreased slightly with increasing moisture content. An optimal H_2 yield was observed at 10 % moisture content. This behaviour is in agreement with results observed by Guangul et al. (2014). At low biomass moisture content, oxidation zone temperature is high and nearly constant. This shifts the equilibrium of reactions R_6 and R_7 towards the formation of carbon monoxide and hydrogen. The reduction zone temperature reduces with increasing moisture content, thereby shifting the equilibrium of reaction R_6 towards the formation of the reactants. This accounts for the reduction in hydrogen concentration with moisture content enhancement.

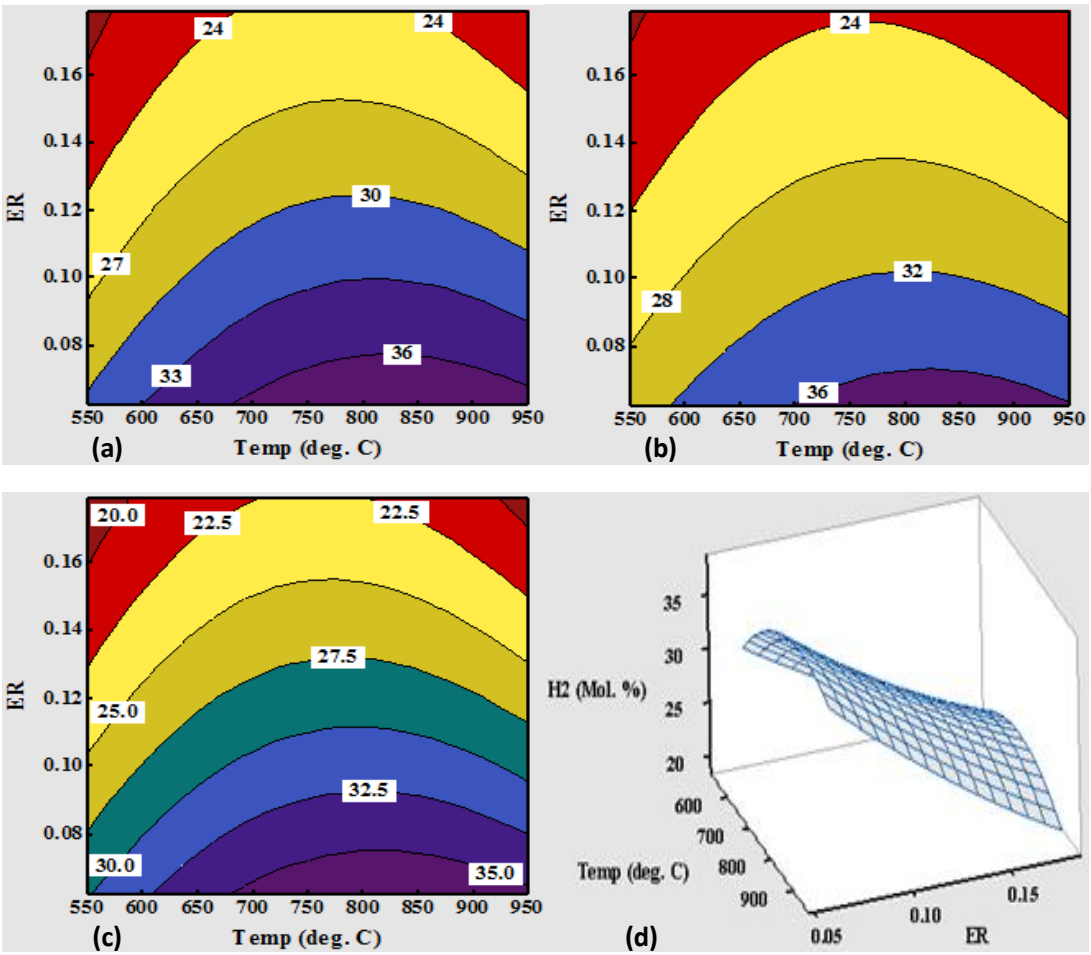

Figure 4.13 The influence of temperature and equivalence ratio interaction on H_2 yield: (a) contour plot at 10%, (b) contour plot at 15%, (c) contour plot at 20%, and (d) 3D surface plot at 15% MC of biomass feedstock.

4.5.2.3 The interaction effect of operating parameters on H_2/CO ratio

Figure 4.14 demonstrates the effect of interacting moisture content and temperature at different values of equivalence ratio on the H_2/CO ratio. An optimal H_2/CO ratio was observed at a lower equivalence ratio. Although a high H_2/CO ratio was observed in the region of higher moisture content, a very low H_2 and CO yields were observed in this region. The H_2/CO ratio reduces with equivalence ratio enhancement. This trend is in agreement with that observed by Guangul et al. (2014).

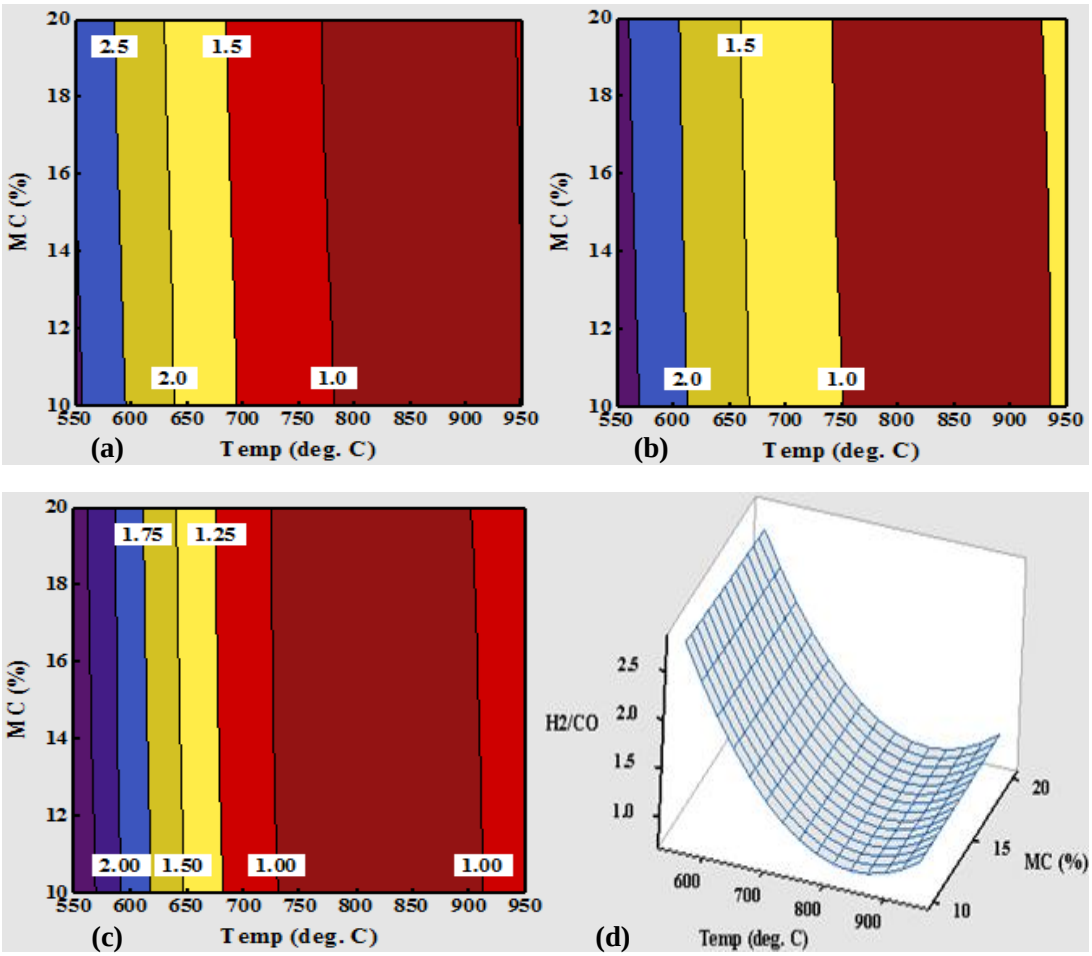

Figure 4.14 The impact of temperature and moisture content interaction on H_2/CO ratio: (a) contour plot at 0.06, (b) contour plot at 0.12, (c) contour plot at 0.18, and (d) 3D surface plot at 0.12 ER.

Figure 4.15 demonstrates the interaction effects of temperature and equivalence ratio at various moisture content values on H_2/CO ratio. A maximum H_2/CO ratio was observed at lower moisture content. The H_2/CO ratio increases with increasing moisture content. This trend is in agreement with that observed by Guangul et al. (2014).

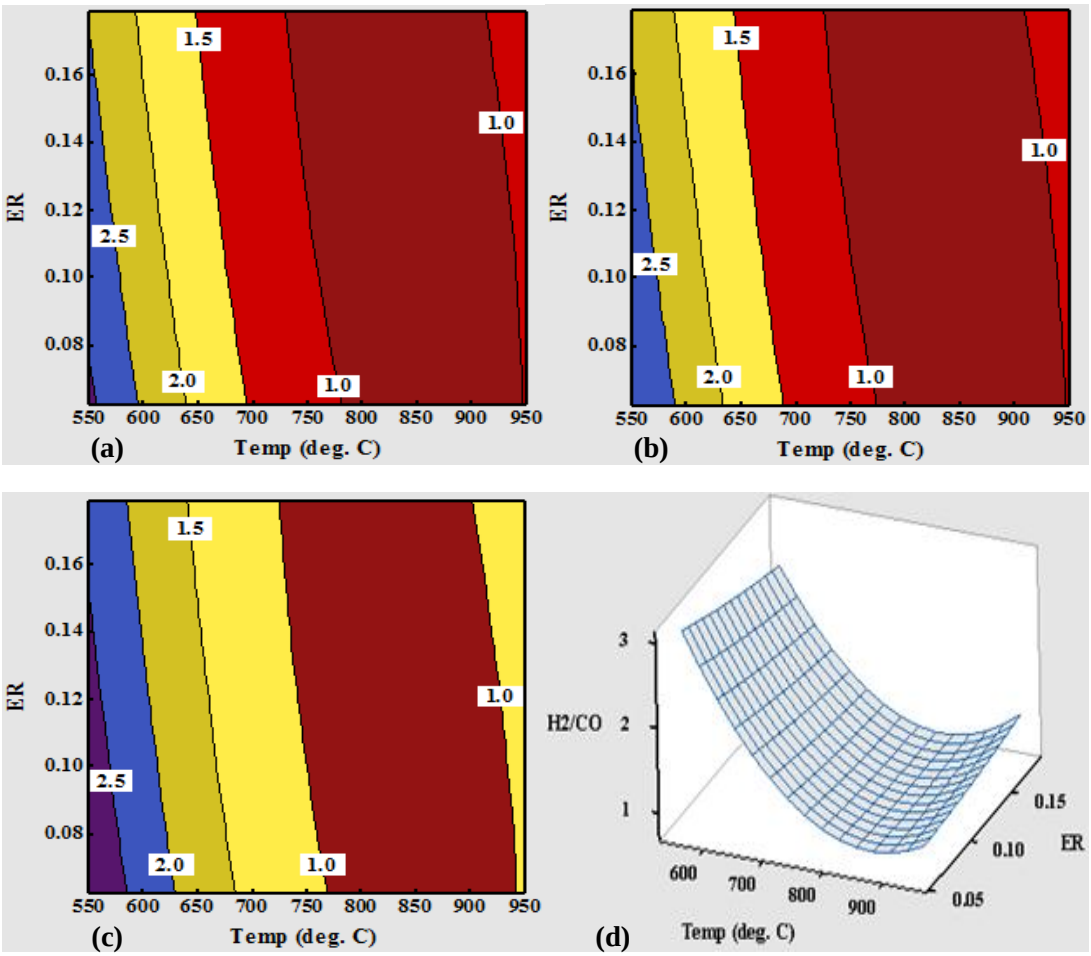

Figure 4.15 The impact of temperature and equivalence ratio interaction on H_2/CO ratio: (a) contour plot at 10%, (b) contour plot at 15%, (c) contour plot at 20%, and (d) 3D surface plot at 15% MC of biomass feedstock.

4.5.3 Multi-objective optimization for FT synthesis

Identifying the combination of the key parameters (gasification temperature, moisture content of biomass and equivalence ratio) that optimises Fischer-Tropsch synthesis is one of the objectives of this study. The response surface optimisation technique is the ideal method for determining the best operating parameters combination. Here, the goal is to identify the optimal zone or range of the operational condition for Fischer-Tropsch synthesis. By using Response Surface Method, an optimization of the parameters is achieved. Figure 4.16 shows the optimized zone represented by the

white region. Any chosen point in the optimal zone represents the optimum working point.

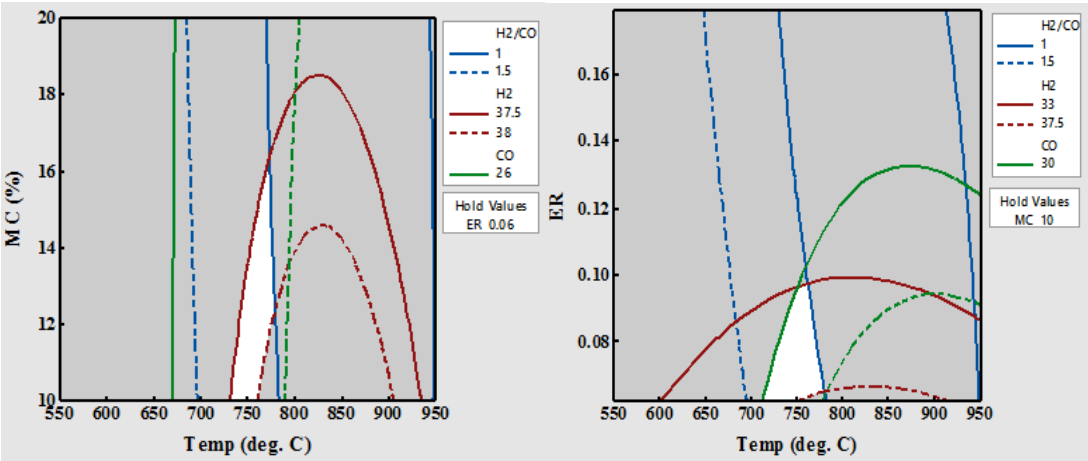

Figure 4.16 The synchronized effect of gasification temperature, MC and ER.

It can be observed from Figure 4.16, that the optimal conditions for Fischer-Tropsch synthesis ranges from 720 ^{o}C and 780 ^{o}C of gasification temperature, 0.06 and 0.095 of ER, and 10% and 16% of MC.

CHAPTER FIVE: CONCLUSIONS AND RECOMMENDATIONS

5.1. Conclusion

In this work, two numerical simulation models of air-gasification of rice husks integrated with syngas purification and RSM using Engineering Equation Solver and Aspen Plus were developed. The key conclusions drawn from this study can be summarized as follow:

Rice husk was found to be a suitable feedstock for gasification process due to its high volatile matter of 72.82%, low sulphur of 0.64% and low nitrogen contents of 0.13%. Hence, two user-friendly numerical simulation models are developed based on rice husk feedstock.

The Aspen Plus model with an average RMSE of 7.78 exhibited high accuracy in predicting the behaviour of fixed-bed gasifiers than the Engineering Equation Solver model with an average RMSE of 8.99. Furthermore, with an average RMSE of 2.498 for rubber wood biomass and 2.381 for rape straw biomass, the Aspen Plus simulation model exhibited high sensitivity in simulating other biomass feedstock.

The model exhibited high sensitivity in evaluating the influence of gasification temperature, ER and MC on the product gas quality which agrees with results reported by other authors. Gasification temperature and ER were found to be the most sensitive parameters, with a high temperature and low ER favouring CO and H_2 yield and LHV_{Syngas}.

The regression models for lower heating value, H_2, CO and H_2/CO ratio generated from the ANOVA tool were found to have high R^2 values of 98.47%, 98.93%, 96.94% and 89.91% with corresponding Adj-R^2 values of 98.28%, 98.80%, 96.56%, and

88.64%, respectively. The optimal conditions for Fischer-Tropsch synthesis were found to be a gasification temperature range of 720 ^{o}C and 780 ^{o}C, ER range between 0.06 and 0.095, and MC range between 10% and 16%.

5.2 Recommendations

The following research ideas can be used to enhance further and supplement the findings of this work. One of the key aspects that the present model did not consider and could further be developed in the future is integrating the present model with reaction kinetics and hydrodynamics to enhance its accuracy. Secondly, coupling the proposed system with a tar reforming sub-model with subsequent syngas H_2/CO ratio adjustment could enhance the system's performance.

5.3 Contribution to Knowledge

A new approach for an improved simulation model based on the previously developed simulation model by other authors is implemented in this study. The aim of the model is to simulate and perform a multi-objective optimization of gasification system's operating conditions to predict the feasibility of FTs application from air-gasification of biomass. The modifications introduced include:

1. Integrating syngas purification sub-model to remove impurities and moisture from the product gas.
2. Integrating the simulation model with RSM optimization technique to avoid the limitation of a single-parameter optimization technique (considered in many of the previously developed models) in determining the optimal working parameters of a gasification process.
3. Constructing an RSM design matrix using 400 runs of Aspen Plus simulated results for purposes of increasing the accuracy of the developed model.

REFERENCES

Abuadala, A., Dincer, I., & Naterer, G. F. (2010). Exergy analysis of hydrogen production from biomass gasification. *International Journal of Hydrogen Energy*, *35*(10), 4981–4990. https://doi.org/10.1016/j.ijhydene.2009.08.025

Ahmad, A. A., Zawawi, N. A., Kasim, F. H., Inayat, A., & Khasri, A. (2016). Assessing the gasification performance of biomass: A review on biomass gasification process conditions, optimization and economic evaluation. *Renewable and Sustainable Energy Reviews*, *53*, 1333–1347. https://doi.org/10.1016/j.rser.2015.09.030

Ahmed, T. Y., Ahmad, M. M., Yusup, S., Inayat, A., & Khan, Z. (2012). Mathematical and computational approaches for design of biomass gasification for hydrogen production: A review. *Renewable and Sustainable Energy Reviews*, *16*(4), 2304–2315.

Ail, S. S., & Dasappa, S. (2016). Biomass to liquid transportation fuel via Fischer Tropsch synthesis – Technology review and current scenario. *Renewable and Sustainable Energy Reviews*, *58*(C), 267–286.

Albina, D. O. (2006). Emissions from multiple-spouted and spout-fluid fluidized beds using rice husks as fuel. *Renewable Energy*, *31*(13), 2152–2163. https://doi.org/10.1016/j.renene.2006.02.013

Al-Rahbi, A. S., Onwudili, J. A., & Williams, P. T. (2016). Thermal decomposition and gasification of biomass pyrolysis gases using a hot bed of waste derived pyrolysis char. *Bioresource Technology*, *204*, 71–79. https://doi.org/10.1016/j.biortech.2015.12.016

Altafini, C. R., Wander, P. R., & Barreto, R. M. (2003). Prediction of the working parameters of a wood waste gasifier through an equilibrium model. *Energy Conversion and Management*, *44*(17), 2763–2777.

Alvarez, J., Lopez, G., Amutio, M., Bilbao, J., & Olazar, M. (2014). Upgrading the rice husk char obtained by flash pyrolysis for the production of amorphous silica and high quality activated carbon. *Bioresource Technology*, *170*, 132–137. https://doi.org/10.1016/j.biortech.2014.07.073

Amick, J. A. (1982). Purification of Rice Hulls as a Source of Solar Grade Silicon for Solar Cells. *Journal of The Electrochemical Society*, *129*(4), 864. https://doi.org/10.1149/1.2123989

Arafat, H. A., & Jijakli, K. (2013). Modeling and comparative assessment of municipal solid waste gasification for energy production. *Waste Management (New York, N.Y.)*, *33*(8), 1704–1713. https://doi.org/10.1016/j.wasman.2013.04.008

Asadullah, M. (2014). Barriers of commercial power generation using biomass gasification gas: A review. *Renewable and Sustainable Energy Reviews*, *29*(C), 201–215.

Aydin, E. S., Yucel, O., & Sadikoglu, H. (2017). Development of a semi-empirical equilibrium model for downdraft gasification systems. *Energy*, *130*, 86–98. https://doi.org/10.1016/j.energy.2017.04.132

Azzone, E., Morini, M., & Pinelli, M. (2012). Development of an equilibrium model for the simulation of thermochemical gasification and application to agricultural residues. *Renewable Energy*.

Bahng, M.-K., Mukarakate, C., Robichaud, D. J., & Nimlos, M. R. (2009). Current technologies for analysis of biomass thermochemical processing: A review. *Analytica Chimica Acta*, *651*(2), 117–138. https://doi.org/10.1016/j.aca.2009.08.016

Bakar, R. A., Yahya, R., & Gan, S. N. (2016). Production of High Purity Amorphous Silica from Rice Husk. *Procedia Chemistry*, *19*, 189–195. https://doi.org/10.1016/j.proche.2016.03.092

Balat, M. (2005). Use of biomass sources for energy in Turkey and a view to biomass potential. *Biomass and Bioenergy*, *29*(1), 32–41. https://doi.org/10.1016/j.biombioe.2005.02.004

Barman, N. S., Ghosh, S., & De, S. (2012). Gasification of biomass in a fixed bed downdraft gasifier—A realistic model including tar. *Bioresource Technology*, *107*, 505–511. https://doi.org/10.1016/j.biortech.2011.12.124

Bassyouni, M., ul Hasan, S. W., Abdel-Aziz, M. H., Abdel-hamid, S. M.-S., Naveed, S., Hussain, A., & Ani, F. N. (2014). Date palm waste gasification in downdraft gasifier and simulation using ASPEN HYSYS. *Energy Conversion and Management*, *88*, 693–699. https://doi.org/10.1016/j.enconman.2014.08.061

Basu, P. (2013). *Biomass Gasification: Practical Design and Theory*. Academic Press.

Beckham, N. R., Akeh, L. J., Mitaart, G. N. P., & Moniaga, J. V. (2023). Determining factors that affect student performance using various machine learning methods. *Procedia Computer Science*, *216*, 597–603. https://doi.org/10.1016/j.procs.2022.12.174

Begum, S., Rasul, M. G., & Akbar, D. (2014). A Numerical Investigation of Municipal Solid Waste Gasification Using Aspen Plus. *Procedia Engineering*, *90*, 710–717. https://doi.org/10.1016/j.proeng.2014.11.800

Bondioli, F., Barbieri, L., Ferrari, A. M., & Manfredini, T. (2010). Characterization of Rice Husk Ash and Its Recycling as Quartz Substitute for the Production of Ceramic Glazes. *Journal of the American Ceramic Society*, *93*(1), 121–126. https://doi.org/10.1111/j.1551-2916.2009.03337.x

Brammer, J. G., & Bridgwater, A. V. (2002). The influence of feedstock drying on the performance and economics of a biomass gasifier–engine CHP system. *Biomass and Bioenergy*, *22*(4), 271–281. https://doi.org/10.1016/S0961-9534(02)00003-X

Bridgwater, A. V. (2003). Renewable fuels and chemicals by thermal processing of biomass. *Chemical Engineering Journal*, *91*(2–3), 87–102. https://doi.org/10.1016/S1385-8947(02)00142-0

Broer, K. M., & Brown, R. C. (2015). The role of char and tar in determining the gas-phase partitioning of nitrogen during biomass gasification. *Applied Energy*, *158*, 474–483.

Budiman, H., Nuryatini, & Zuas, O. (2015). Comparison between GC-TCD and GC-FID for the determination of propane in gas mixture. *Procedia Chemistry*, *16*, 465–472. https://doi.org/10.1016/j.proche.2015.12.080

Buragohain, B., Mahanta, P., & Moholkar, V. S. (2010). Thermodynamic optimization of biomass gasification for decentralized power generation and Fischer–Tropsch synthesis. *Energy*, *35*(6), 2557–2579. https://doi.org/10.1016/j.energy.2010.03.003

Cengel, Y., & Boles, M. (2014). *Thermodynamics: An Engineering Approach* (8th edition). McGraw-Hill Education.

Chang, A. C. C., Chang, H.-F., Lin, F.-J., Lin, K.-H., & Chen, C.-H. (2011). Biomass gasification for hydrogen production. *International Journal of Hydrogen Energy*, *36*(21), 14252–14260. https://doi.org/10.1016/j.ijhydene.2011.05.105

Chiodini, A., Bua, L., Carnelli, L., Zwart, R., Vreugdenhil, B., & Vocciante, M. (2017). Enhancements in Biomass-to-Liquid processes: Gasification aiming at high hydrogen/carbon monoxide ratios for direct Fischer-Tropsch synthesis applications. *Biomass and Bioenergy*, *106*, 104–114. https://doi.org/10.1016/j.biombioe.2017.08.022

Converti, A., Oliveira, R. P. S., Torres, B. R., Lodi, A., & Zilli, M. (2009). Biogas production and valorization by means of a two-step biological process. *Bioresource Technology*, *100*(23), 5771–5776. https://doi.org/10.1016/j.biortech.2009.05.072

Couto, N., Rouboa, A., Silva, V., Monteiro, E., & Bouziane, K. (2013). Influence of the Biomass Gasification Processes on the Final Composition of Syngas. *Energy Procedia*, *36*, 596–606. https://doi.org/10.1016/j.egypro.2013.07.068

Couto, N., Silva, V., Monteiro, E., Brito, P. S. D., & Rouboa, A. (2015). Modeling of fluidized bed gasification: Assessment of zero-dimensional and CFD approaches. *Journal of Thermal Science*, *24*(4), 378–385. https://doi.org/10.1007/s11630-015-0798-7

Coyle, E. D., & Simmons, R. A. (Eds.). (2014). *Understanding the global energy crisis*. Purdue University Press.

Damartzis, T., & Zabaniotou, A. (2011). Thermochemical conversion of biomass to second generation biofuels through integrated process design—A review. *Renewable and Sustainable Energy Reviews*, *15*(1), 366–378. https://doi.org/10.1016/j.rser.2010.08.003

Dasappa, S., Paul, P., Mukunda, H., N K S, R., Gururaja Rao, S., & H V, S. (2004). Biomass gasification technology—A route to meet energy needs. *Current Science*, *87*.

Davis, S. J., & Caldeira, K. (2010). Consumption-based accounting of CO2 emissions. *Proceedings of the National Academy of Sciences*, *107*(12), 5687–5692. https://doi.org/10.1073/pnas.0906974107

Dayton, D. C., & Foust, T. D. (2020). Chapter Five—Analytical Methods in Thermochemical Conversion. In D. C. Dayton & T. D. Foust (Eds.), *Analytical*

Methods for Biomass Characterization and Conversion (pp. 75–88). Elsevier. https://doi.org/10.1016/B978-0-12-815605-6.00005-6

Demirbas, A. (2004). Combustion characteristics of different biomass fuels. *Progress in Energy and Combustion Science*, *30*(2), 219–230. https://doi.org/10.1016/j.pecs.2003.10.004

Demirbas, A. (2008). Importance of biomass energy sources for Turkey. *Energy Policy*, *36*(2), 834–842. https://doi.org/10.1016/j.enpol.2007.11.005

Diyoke, C., Gao, N., Aneke, M., Wang, M., & Wu, C. (2018). Modelling of down-draft gasification of biomass – An integrated pyrolysis, combustion and reduction process. *Applied Thermal Engineering*, *142*, 444–456. https://doi.org/10.1016/j.applthermaleng.2018.06.079

Doherty, W., Reynolds, A., & Kennedy, D. (2009). The effect of air preheating in a biomass CFB gasifier using ASPEN Plus simulation. *Biomass and Bioenergy*, *33*(9), 1158–1167. https://doi.org/10.1016/j.biombioe.2009.05.004

Đurišić-Mladenović, N., Škrbić, B. D., & Zabaniotou, A. (2016). Chemometric interpretation of different biomass gasification processes based on the syngas quality: Assessment of crude glycerol co-gasification with lignocellulosic biomass. *Renewable and Sustainable Energy Reviews*, *59*, 649–661. https://doi.org/10.1016/j.rser.2016.01.002

Elakiya M., Saranya S., Saravana Kumar C., Gouthaman J., & Kirubakaran, V. (2016). Performance evaluation of groundnut shell in a downdraft gasifier. *2016 International Conference on Energy Efficient Technologies for Sustainability (ICEETS)*, 116–121. https://doi.org/10.1109/ICEETS.2016.7582910

Faraji, M., & Saidi, M. (2021). Hydrogen-rich syngas production via integrated configuration of pyrolysis and air gasification processes of various algal biomass: Process simulation and evaluation using Aspen Plus software. *International Journal of Hydrogen Energy*, *46*(36), 18844–18856. https://doi.org/10.1016/j.ijhydene.2021.03.047

Favas, J., Monteiro, E., & Rouboa, A. (2017). Hydrogen production using plasma gasification with steam injection. *International Journal of Hydrogen Energy*, *42*(16), 10997–11005. https://doi.org/10.1016/j.ijhydene.2017.03.109

Fernandez-Lopez, M., Pedroche, J., Valverde, J. L., & Sanchez-Silva, L. (2017). Simulation of the gasification of animal wastes in a dual gasifier using Aspen Plus®. *Energy Conversion and Management*, *140*, 211–217. https://doi.org/10.1016/j.enconman.2017.03.008

Franco, C., Pinto, F., Gulyurtlu, I., & Cabrita, I. (2003). The study of reactions influencing the biomass steam gasification process☆. *Fuel*, *82*(7), 835–842. https://doi.org/10.1016/S0016-2361(02)00313-7

Gagliano, A., Nocera, F., Bruno, M., & Cardillo, G. (2017). Development of an Equilibrium-based Model of Gasification of Biomass by Aspen Plus. *Energy Procedia*, *111*, 1010–1019. https://doi.org/10.1016/j.egypro.2017.03.264

Gagliano, A., Nocera, F., Patania, F., Bruno, M., & Castaldo, D. G. (2016). A robust numerical model for characterizing the syngas composition in a downdraft

gasification process. *Comptes Rendus Chimie*, *19*(4), 441–449. https://doi.org/10.1016/j.crci.2015.09.019

Gai, C., & Dong, Y. (2012). Experimental study on non-woody biomass gasification in a downdraft gasifier. *International Journal of Hydrogen Energy*, *37*(6), 4935–4944. https://doi.org/10.1016/j.ijhydene.2011.12.031

Gambarotta, A., Morini, M., & Zubani, A. (2018). A non-stoichiometric equilibrium model for the simulation of the biomass gasification process. *Applied Energy*, *227*, 119–127. https://doi.org/10.1016/j.apenergy.2017.07.135

García, R., Pizarro, C., Lavín, A. G., & Bueno, J. L. (2012). Characterization of Spanish biomass wastes for energy use. *Bioresource Technology*, *103*(1), 249–258. https://doi.org/10.1016/j.biortech.2011.10.004

Gautam, G., Adhikari, S., & Bhavnani, S. (2010). Estimation of Biomass Synthesis Gas Composition using Equilibrium Modeling. *Energy & Fuels*, *24*(4), 2692–2698. https://doi.org/10.1021/ef901477c

George, J., Arun, P., & Muraleedharan, C. (2016). Stoichiometric Equilibrium Model Based Assessment of Hydrogen Generation through Biomass Gasification. *Procedia Technology*, *25*, 982–989. https://doi.org/10.1016/j.protcy.2016.08.194

Gómez-Barea, A., & Leckner, B. (2010). Modeling of biomass gasification in fluidized bed. *Progress in Energy and Combustion Science*, *36*(4), 444–509. https://doi.org/10.1016/j.pecs.2009.12.002

Government of Kenya. (2009). *National Rice Development Strategic Plan (2008-2018)*. Mnistry of Agriculture.

Granada, E., Eguía, P., Vilan, J. A., Comesaña, J. A., & Comesaña, R. (2012). FTIR quantitative analysis technique for gases. Application in a biomass thermochemical process. *Renewable Energy*, *41*, 416–421. https://doi.org/10.1016/j.renene.2011.11.020

Guangul, F. M., Sulaiman, S. A., & Ramli, A. (2014). Study of the effects of operating factors on the resulting producer gas of oil palm fronds gasification with a single throat downdraft gasifier. *Renewable Energy*, *72*, 271–283. https://doi.org/10.1016/j.renene.2014.07.022

Güleç, F., Pekaslan, D., Williams, O., & Lester, E. (2022). Predictability of higher heating value of biomass feedstocks via proximate and ultimate analyses – A comprehensive study of artificial neural network applications. *Fuel*, *320*, 123944. https://doi.org/10.1016/j.fuel.2022.123944

Gunnarsson, C. C., & Petersen, C. M. (2007). Water hyacinths as a resource in agriculture and energy production: A literature review. *Waste Management*, *27*(1), 117–129. https://doi.org/10.1016/j.wasman.2005.12.011

Han, J., & Kim, H. (2008). The reduction and control technology of tar during biomass gasification/pyrolysis: An overview. *Renewable and Sustainable Energy Reviews*, *12*(2), 397–416. https://doi.org/10.1016/j.rser.2006.07.015

Han, J., Liang, Y., Hu, J., Qin, L., Street, J., Lu, Y., & Yu, F. (2017). Modeling downdraft biomass gasification process by restricting chemical reaction

equilibrium with Aspen Plus. *Energy Conversion and Management*, *153*, 641–648. https://doi.org/10.1016/j.enconman.2017.10.030

Harvey, D. (2000). *Modern analytical chemistry*. McGraw-Hill.

Haryanto, A., Fernando, S. D., Pordesimo, L. O., & Adhikari, S. (2009). Upgrading of syngas derived from biomass gasification: A thermodynamic analysis. *Biomass and Bioenergy*, *33*(5), 882–889. https://doi.org/10.1016/j.biombioe.2009.01.010

Heidenreich, S., & Foscolo, P. U. (2015). New concepts in biomass gasification. *Progress in Energy and Combustion Science*, *46*, 72–95. https://doi.org/10.1016/j.pecs.2014.06.002

Higman, C., & Burgt, M. van der. (2003). *Gasification*. Gulf Professional.

Homchat, K., & Ramphueiphad, S. (2022). The continuous carbonisation of rice husk on the gasifier for high yield charcoal production. *Results in Engineering*, *15*, 100495. https://doi.org/10.1016/j.rineng.2022.100495

Hu, J., Yu, F., & Lu, Y. (2012). Application of Fischer–Tropsch Synthesis in Biomass to Liquid Conversion. *Catalysts*, *2*(2), Article 2. https://doi.org/10.3390/catal2020303

Huang, H. J., & Ramaswamy, S. (2009). Modeling biomass gasification using thermodynamic equilibrium approach. *Applied Biochemistry and Biotechnology*, *154*(1–3), 14–25. https://doi.org/10.1007/s12010-008-8483-x

Hunt, L. P., Dismukes, J. P., Amick, J. A., Schei, A., & Larsen, K. (1984). Rice Hulls as a Raw Material for Producing Silicon. *Journal of The Electrochemical Society*, *131*(7), 1683. https://doi.org/10.1149/1.2115937

Hussain, M., Zabiri, H., Uddin, F., Yusup, S., & Tufa, L. D. (2023). Pilot-scale biomass gasification system for hydrogen production from palm kernel shell (part A): Steady-state simulation. *Biomass Conversion and Biorefinery*, *13*(5), 3849–3862. https://doi.org/10.1007/s13399-021-01474-1

IEA. (2014). *Key World Energy Statistics*. Chirat.

Inayat, M., Sulaiman, S. A., Shahbaz, M., & Bhayo, B. A. (2020). Application of response surface methodology in catalytic co-gasification of palm wastes for bioenergy conversion using mineral catalysts. *Biomass and Bioenergy*, *132*, 105418. https://doi.org/10.1016/j.biombioe.2019.105418

Ismagilov, Z. R., Shikina, N. V., Andrievskaya, I. P., Rudina, N. A., Mansurov, Z. A., Burkitbaev, M. M., Biisenbaev, M. A., & Kurmanbekov, A. A. (2009). Preparation of carbonized rice husk monoliths and modification of the porous structure by SiO2 leaching. *Catalysis Today*, *Supplement*(147), S58–S65. https://doi.org/10.1016/j.cattod.2009.07.043

Itai, Y., Santos, R., Branquinho, M., Malico, I., Ghesti, G. F., & Brasil, A. M. (2014). Numerical and experimental assessment of a downdraft gasifier for electric power in Amazon using açaí seed (Euterpe oleracea Mart.) as a fuel. *Renewable Energy*, *66*, 662–669.

Jain, A. K., & Goss, J. R. (2000). Determination of reactor scaling factors for throatless rice husk gasifier. *Biomass and Bioenergy*, *18*(3), 249–256.

Jamin Nur Ashikin, Saleh Suriyati, & Abdul Samad Noor Asma Fazli. (2020). Influences of Gasification Temperature and Equivalence Ratio on Fluidized Bed Gasification of Raw and Torrefied Wood Wastes. *Chemical Engineering Transactions*, *80*, 127–132. https://doi.org/10.3303/CET2080022

Janewit, W., Worasuwannarak, N., & Pipatmanomai, S. (2008). Product yields and characteristics of rice husk, rice straw and corncob during fast pyrolysis in a drop-tube/fixed-bed reactor. *Songklanakarin Journal of Science and Technology*, *30*.

Jangsawang, W., Laohalidanond, K., & Kerdsuwan, S. (2015). Optimum Equivalence Ratio of Biomass Gasification Process Based on Thermodynamic Equilibrium Model. *Energy Procedia*, *79*, 520–527. https://doi.org/10.1016/j.egypro.2015.11.528

Jarungthammachote, S., & Dutta, A. (2007). Thermodynamic equilibrium model and second law analysis of a downdraft waste gasifier. *Energy*, *32*(9), 1660–1669. https://doi.org/10.1016/j.energy.2007.01.010

Jarungthammachote, S., & Dutta, A. (2008). Equilibrium modeling of gasification: Gibbs free energy minimization approach and its application to spouted bed and spout-fluid bed gasifiers. *Energy Conversion and Management*, *49*(6), 1345–1356. https://doi.org/10.1016/j.enconman.2008.01.006

Jayah, T. H., Aye, L., Fuller, R. J., & Stewart, D. F. (2003). Computer simulation of a downdraft wood gasifier for tea drying. *Biomass and Bioenergy*, *25*(4), 459–469. https://doi.org/10.1016/S0961-9534(03)00037-0

Jenkins, B. M., Baxter, L. L., Miles, T. R., & Miles, T. R. (1998). Combustion properties of biomass. *Fuel Processing Technology*, *54*(1), 17–46. https://doi.org/10.1016/S0378-3820(97)00059-3

Jia, J., Xu, L., Abudula, A., & Sun, B. (2017). Effects of operating parameters on performance of a downdraft gasifier in steady and transient state. *Energy Conversion and Management*. https://agris.fao.org/agris-search/search.do?recordID=US201800123845

Kaewluan, S., & Pipatmanomai, S. (2011). Potential of synthesis gas production from rubber wood chip gasification in a bubbling fluidised bed gasifier. *Energy Conversion and Management*, *52*(1), 75–84. https://doi.org/10.1016/j.enconman.2010.06.044

Kalogirou, S. A. (2001). Artificial neural networks in renewable energy systems applications: A review. *Renewable and Sustainable Energy Reviews*, *5*(4), 373–401. https://doi.org/10.1016/S1364-0321(01)00006-5

Karmakar, M. K., & Datta, A. B. (2011). Generation of hydrogen rich gas through fluidized bed gasification of biomass. *Bioresource Technology*, *102*(2), 1907–1913. https://doi.org/10.1016/j.biortech.2010.08.015

Kate, G. U., & Chaurasia, A. S. (2018). Gasification of rice husk in two-stage gasifier to produce syngas, silica and activated carbon. *Energy Sources, Part A: Recovery, Utilization, and Environmental Effects*, *40*(4), 466–471. https://doi.org/10.1080/15567036.2017.1423418

Kaushal, P., Proell, T., & Hofbauer, H. (2011). Application of a detailed mathematical model to the gasifier unit of the dual fluidized bed gasification plant. *Biomass and Bioenergy*, *35*(7), 2491–2498. https://doi.org/10.1016/j.biombioe.2011.01.025

Khanmohammadi, S., Atashkari, K., & Kouhikamali, R. (2016). Modeling and Assessment of a Biomass Gasification Integrated System for Multigeneration Purpose. *International Journal of Chemical Engineering*, *2016*, e2639241. https://doi.org/10.1155/2016/2639241

Kipngetich, P., Kiplimo, R., Tanui, J. K., & Chisale, P. (2023). Effects of carbonization on the combustion of rice husks briquettes in a fixed bed. *Cleaner Engineering and Technology*, *13*, 100608. https://doi.org/10.1016/j.clet.2023.100608

Koukkari, P., & Pajarre, R. (2006). Introducing mechanistic kinetics to the Lagrangian Gibbs energy calculation. *Computers & Chemical Engineering*, *30*(6–7), 1189–1196. https://doi.org/10.1016/j.compchemeng.2006.03.001

Kraussler, M., Binder, M., & Hofbauer, H. (2016). 2250-h long term operation of a water gas shift pilot plant processing tar-rich product gas from an industrial scale dual fluidized bed biomass steam gasification plant. *International Journal of Hydrogen Energy*, *41*(15), 6247–6258. https://doi.org/10.1016/j.ijhydene.2016.02.137

Kumar, A., & Samadder, S. R. (2017). A review on technological options of waste to energy for effective management of municipal solid waste. *Waste Management*, *69*, 407–422. https://doi.org/10.1016/j.wasman.2017.08.046

Kuo, P.-C., Wu, W., & Chen, W.-H. (2014). Gasification performances of raw and torrefied biomass in a downdraft fixed bed gasifier using thermodynamic analysis. *Fuel*, *117*, 1231–1241. https://doi.org/10.1016/j.fuel.2013.07.125

La Villetta, M., Costa, M., & Massarotti, N. (2017). Modelling approaches to biomass gasification: A review with emphasis on the stoichiometric method. *Renewable and Sustainable Energy Reviews*, *74*, 71–88. https://doi.org/10.1016/j.rser.2017.02.027

Lahijani, P., & Zainal, Z. A. (2011). Gasification of palm empty fruit bunch in a bubbling fluidized bed: A performance and agglomeration study. *Bioresource Technology*, *102*(2), 2068–2076. https://doi.org/10.1016/j.biortech.2010.09.101

Lan, W., Chen, G., Zhu, X., Wang, X., Liu, C., & Xu, B. (2018). Biomass gasification-gas turbine combustion for power generation system model based on ASPEN PLUS. *Science of The Total Environment*, *628–629*, 1278–1286. https://doi.org/10.1016/j.scitotenv.2018.02.159

Leibbrandt, N. H., Aboyade, A. O., Knoetze, J. H., & Görgens, J. F. (2013). Process efficiency of biofuel production via gasification and Fischer–Tropsch synthesis. *Fuel*, *109*, 484–492. https://doi.org/10.1016/j.fuel.2013.03.013

Li, J., Xu, K., Yao, X., & Chen, S. (2021). Prediction and optimization of syngas production from steam gasification: Numerical study of operating conditions and biomass composition. *Energy Conversion and Management*, *236*, 114077. https://doi.org/10.1016/j.enconman.2021.114077

Li, S., Zheng, H., Zheng, Y., Tian, J., Jing, T., Chang, J.-S., & Ho, S.-H. (2019). Recent advances in hydrogen production by thermo-catalytic conversion of biomass. *International Journal of Hydrogen Energy*, *44*(28), 14266–14278. https://doi.org/10.1016/j.ijhydene.2019.03.018

Li, X., Grace, J. R., Watkinson, A. P., Lim, C. J., & Ergüdenler, A. (2001). Equilibrium modeling of gasification: A free energy minimization approach and its application to a circulating fluidized bed coal gasifier. *Fuel*, *80*(2), 195–207. https://doi.org/10.1016/S0016-2361(00)00074-0

Mahishi, M. R., & Goswami, D. Y. (2007). Thermodynamic optimization of biomass gasifier for hydrogen production. *International Journal of Hydrogen Energy*, *32*(16), 3831–3840. https://doi.org/10.1016/j.ijhydene.2007.05.018

Martín, M., & Grossmann, I. E. (2011). Process Optimization of FT-Diesel Production from Lignocellulosic Switchgrass. *Industrial & Engineering Chemistry Research*, *50*(23), 13485–13499. https://doi.org/10.1021/ie201261t

Mathieu, P., & Dubuisson, R. (2002). Performance analysis of a biomass gasifier. *Energy Conversion and Management*, *43*(9), 1291–1299. https://doi.org/10.1016/S0196-8904(02)00015-8

McKendry, P. (2002). Energy production from biomass (part 3): Gasification technologies. *Bioresource Technology*, *83*(1), 55–63. https://doi.org/10.1016/S0960-8524(01)00120-1

Melgar, A., Perez, J. F., Laget, H., & Horillo, A. (2007). Thermochemical equilibrium modelling of a gasifying process. *Energy Conversion and Management*, *48*(1), 59–67. https://doi.org/10.1016/j.enconman.2006.05.004

Mendiburu, A. Z., Carvalho, J. A., & Coronado, C. J. R. (2014). Thermochemical equilibrium modeling of biomass downdraft gasifier: Stoichiometric models. *Energy*, *66*, 189–201. https://doi.org/10.1016/j.energy.2013.11.022

Michela Costa, Maurizio La Villetta, & Nicola Massarotti. (2015). Optimal tuning of a thermo-chemical equilibrium model for downdraft biomass gasifiers. *Chemical Engineering Transactions*, *43*, 439–444. https://doi.org/10.3303/CET1543074

Mojaver, P., Khalilarya, S., & Chitsaz, A. (2019). Multi-objective optimization using response surface methodology and exergy analysis of a novel integrated biomass gasification, solid oxide fuel cell and high-temperature sodium heat pipe system. *Applied Thermal Engineering*, *156*, 627–639. https://doi.org/10.1016/j.applthermaleng.2019.04.104

Motta, I. L., Miranda, N. T., Maciel Filho, R., & Wolf Maciel, M. R. (2018). Biomass gasification in fluidized beds: A review of biomass moisture content and operating pressure effects. *Renewable and Sustainable Energy Reviews*, *94*(C), 998–1023.

Mountouris, A., Voutsas, E., & Tassios, D. (2006). Solid waste plasma gasification: Equilibrium model development and exergy analysis. *Energy Conversion and Management*, *47*(13), 1723–1737. https://doi.org/10.1016/j.enconman.2005.10.015

Nagahawatte, N. D., Paskaranandavadivel, N., Bear, L. R., Avci, R., & Cheng, L. K. (2023). A novel framework for the removal of pacing artifacts from bio-electrical recordings. *Computers in Biology and Medicine*, *155*, 106673. https://doi.org/10.1016/j.compbiomed.2023.106673

Natarajan, E., Nordin, A., & Rao, A. N. (1998). Overview of combustion and gasification of rice husk in fluidized bed reactors. *Biomass and Bioenergy*, *14*, 533–546.

Nikoo, M. B., & Mahinpey, N. (2008). Simulation of biomass gasification in fluidized bed reactor using ASPEN PLUS. *Biomass and Bioenergy*, *32*(12), 1245–1254. https://doi.org/10.1016/j.biombioe.2008.02.020

Njogu, P., Kinyua, R., Muthoni, P., & Nemoto, Y. (2015). Thermal Gasification of Rice Husks from Rice Growing Areas in Mwea, Embu County, Kenya. *Smart Grid and Renewable Energy*, *06*(05), 113–119. https://doi.org/10.4236/sgre.2015.65010

Ogwang, G., Olupot, P. W., Kasedde, H., Menya, E., Storz, H., & Kiros, Y. (2021). Experimental evaluation of rice husk ash for applications in geopolymer mortars. *Journal of Bioresources and Bioproducts*, *6*(2), 160–167. https://doi.org/10.1016/j.jobab.2021.02.008

Olupot, P. W., Candia, A., Menya, E., & Walozi, R. (2016). Characterization of rice husk varieties in Uganda for biofuels and their techno-economic feasibility in gasification. *Chemical Engineering Research and Design*, *107*, 63–72. https://doi.org/10.1016/j.cherd.2015.11.010

Pala, L. P. R., Wang, Q., Kolb, G., & Hessel, V. (2017). Steam gasification of biomass with subsequent syngas adjustment using shift reaction for syngas production: An Aspen Plus model. *Renewable Energy*, *101*, 484–492. https://doi.org/10.1016/j.renene.2016.08.069

Panwar, N. L., Kothari, R., & Tyagi, V. V. (2012). Thermo chemical conversion of biomass – Eco friendly energy routes. *Renewable and Sustainable Energy Reviews*, *16*(4), 1801–1816.

Park, S. J., Son, S. H., Kook, J. W., Ra, H. W., Yoon, S. J., Mun, T.-Y., Moon, J. H., Yoon, S. M., Kim, J. H., Kim, Y. K., Lee, J. G., Lee, D.-Y., & Seo, M. W. (2021). Gasification operational characteristics of 20-tons-Per-Day rice husk fluidized-bed reactor. *Renewable Energy*, *169*, 788–798. https://doi.org/10.1016/j.renene.2021.01.045

Pereira, E. G., da Silva, J. N., de Oliveira, J. L., & Machado, C. S. (2012). Sustainable energy: A review of gasification technologies. *Renewable and Sustainable Energy Reviews*, *16*(7), 4753–4762. https://doi.org/10.1016/j.rser.2012.04.023

Plis, P., & Wilk, R. K. (2011). Theoretical and experimental investigation of biomass gasification process in a fixed bed gasifier. *Energy*, *36*(6), 3838–3845. https://doi.org/10.1016/j.energy.2010.08.039

Puig-Arnavat, M., Bruno, J. C., & Coronas, A. (2010). Review and analysis of biomass gasification models. *Renewable and Sustainable Energy Reviews*, *14*(9), 2841–2851. https://doi.org/10.1016/j.rser.2010.07.030

Raheem, A., Zhao, M., Dastyar, W., Channa, A. Q., Ji, G., & Zhang, Y. (2019). Parametric gasification process of sugarcane bagasse for syngas production. *International Journal of Hydrogen Energy*, *44*(31), 16234–16247. https://doi.org/10.1016/j.ijhydene.2019.04.127

Ramirez, J. A., & Rainey, T. J. (2019). Comparative techno-economic analysis of biofuel production through gasification, thermal liquefaction and pyrolysis of sugarcane bagasse. *Journal of Cleaner Production*, *229*, 513–527. https://doi.org/10.1016/j.jclepro.2019.05.017

Ramos, A., Monteiro, E., & Rouboa, A. (2019). Numerical approaches and comprehensive models for gasification process: A review. *Renewable and Sustainable Energy Reviews*, *110*, 188–206. https://doi.org/10.1016/j.rser.2019.04.048

Ratnadhariya, J. K., & Channiwala, S. A. (2009). Three zone equilibrium and kinetic free modeling of biomass gasifier – a novel approach. *Renewable Energy*, *34*(4), 1050–1058. https://doi.org/10.1016/j.renene.2008.08.001

Reed, T., & Das, A. (1988). *Handbook of Biomass Downdraft Gasifier Engine Systems*. Solar Energy Research Institute.

Roy, D., Samanta, S., & Ghosh, S. (2019). Techno-economic and environmental analyses of a biomass based system employing solid oxide fuel cell, externally fired gas turbine and organic Rankine cycle. *Journal of Cleaner Production*, *225*, 36–57. https://doi.org/10.1016/j.jclepro.2019.03.261

Roy, D., Samanta, S., & Ghosh, S. (2020). Performance optimization through response surface methodology of an integrated biomass gasification based combined heat and power plant employing solid oxide fuel cell and externally fired gas turbine. *Energy Conversion and Management*, *222*, 113182. https://doi.org/10.1016/j.enconman.2020.113182

Rupesh, S., Muraleedharan, C., & Arun, P. (2015). A comparative study on gaseous fuel generation capability of biomass materials by thermo-chemical gasification using stoichiometric quasi-steady-state model. *International Journal of Energy and Environmental Engineering*, *6*(4), 375–384. https://doi.org/10.1007/s40095-015-0182-0

Rupesh, S., Muraleedharan, C., & Arun, P. (2016). ASPEN plus modelling of air–steam gasification of biomass with sorbent enabled CO2 capture. *Resource-Efficient Technologies*, *2*(2), 94–103. https://doi.org/10.1016/j.reffit.2016.07.002

Safarian, S., Unnthorsson, R., & Richter, C. (2022). Hydrogen production via biomass gasification: Simulation and performance analysis under different gasifying agents. *Biofuels*, *13*(6), 717–726. https://doi.org/10.1080/17597269.2021.1894781

Sansaniwal, S. K., Pal, K., Rosen, M. A., & Tyagi, S. K. (2017). Recent advances in the development of biomass gasification technology: A comprehensive review. *Renewable and Sustainable Energy Reviews*, *72*, 363–384. https://doi.org/10.1016/j.rser.2017.01.038

Schuster, G., Löffler, G., Weigl, K., & Hofbauer, H. (2001). Biomass steam gasification—An extensive parametric modeling study. *Bioresource Technology*, *77*(1), 71–79. https://doi.org/10.1016/s0960-8524(00)00115-2

Sharma, A. Kr. (2008). Equilibrium and kinetic modeling of char reduction reactions in a downdraft biomass gasifier: A comparison. *Solar Energy*, *82*(10), 918–928. https://doi.org/10.1016/j.solener.2008.03.004

Silva, L. A., Santos, I. F. S. D., Machado, G. D. O., Tiago Filho, G. L., & Barros, R. M. (2021). Rice husk energy production in Brazil: An economic and energy extensive analysis. *Journal of Cleaner Production*, *290*, 125188. https://doi.org/10.1016/j.jclepro.2020.125188

Singh, D. K., & Tirkey, J. V. (2021). Modeling and multi-objective optimization of variable air gasification performance parameters using Syzygium cumini biomass by integrating ASPEN Plus with Response surface methodology (RSM). *International Journal of Hydrogen Energy*, *46*(36), 18816–18831. https://doi.org/10.1016/j.ijhydene.2021.03.054

Singh, Y. D., Mahanta, P., & Bora, U. (2017). Comprehensive characterization of lignocellulosic biomass through proximate, ultimate and compositional analysis for bioenergy production. *Renewable Energy*, *103*, 490–500. https://doi.org/10.1016/j.renene.2016.11.039

Snavely, K., & Subramaniam, B. (1998). Thermal Conductivity Detector Analysis of Hydrogen Using Helium Carrier Gas and HayeSep® D Columns. *Journal of Chromatographic Science*, *36*(4), 191–196. https://doi.org/10.1093/chromsci/36.4.191

Son, Y.-I., Yoon, S. J., Kim, Y. K., & Lee, J.-G. (2011). Gasification and power generation characteristics of woody biomass utilizing a downdraft gasifier. *Biomass and Bioenergy*, *35*(10), 4215–4220. https://doi.org/10.1016/j.biombioe.2011.07.008

Striūgas, N., Zakarauskas, K., Džiugys, A., Navakas, R., & Paulauskas, R. (2014). An evaluation of performance of automatically operated multi-fuel downdraft gasifier for energy production. *Applied Thermal Engineering*, *73*(1), 1151–1159. https://doi.org/10.1016/j.applthermaleng.2014.09.007

Syed, S., Janajreh, I., & Ghenai, C. (2011). Thermodynamics Equilibrium Analysis within the Entrained Flow Gasifier Environment. *International Journal of Thermal and Environmental Engineering*, *4*(1), 47–54. https://doi.org/10.5383/ijtee.04.01.007

Tavares, R., Monteiro, E., Tabet, F., & Rouboa, A. (2020). Numerical investigation of optimum operating conditions for syngas and hydrogen production from biomass gasification using Aspen Plus. *Renewable Energy*, *146*, 1309–1314. https://doi.org/10.1016/j.renene.2019.07.051

Tavares, R., Ramos, A., & Rouboa, A. (2018). Microplastics thermal treatment by polyethylene terephthalate-biomass gasification. *Energy Conversion and Management*, *162*, 118–131. https://doi.org/10.1016/j.enconman.2018.02.001

Tripathi, M., Sahu, J. N., & Ganesan, P. (2016). Effect of process parameters on production of biochar from biomass waste through pyrolysis: A review.

Renewable and Sustainable Energy Reviews, *55*, 467–481. https://doi.org/10.1016/j.rser.2015.10.122

Tuan, P. D., Minh Quan, L., Nhi, V. T., Huong, H. M., Phung, L. T. K., & Feng, D. (2022). Enrichment of hydrogen in product gas from a pilot-scale rice husk updraft gasification system. *Carbon Resources Conversion*, *5*(3), 231–239. https://doi.org/10.1016/j.crcon.2022.07.003

Upadhyay, D. S., Sakhiya, A. K., Panchal, K., Patel, A. H., & Patel, R. N. (2019). Effect of equivalence ratio on the performance of the downdraft gasifier – An experimental and modelling approach. *Energy*, *168*, 833–846. https://doi.org/10.1016/j.energy.2018.11.133

Vaezi, M., Passandideh-Fard, M., Moghiman, M., & Charmchi, M. (2009). *Modeling Biomass Gasification: A New Approach to Utilize Renewable Sources of Energy*. 927–935. https://doi.org/10.1115/IMECE2008-68707

Veziroglu, T. (2008). 21st Century's Energy: Hydrogen Energy System. *Undefined*. https://www.semanticscholar.org/paper/21st-Century%27s-Energy%3A-Hydrogen-Energy-System-Veziroglu/d793cd7031b5a56622749d7e9fecbe00d076b1b2

Virmond, E., De Sena, R. F., Albrecht, W., Althoff, C. A., Moreira, R. F. P. M., & José, H. J. (2012). Characterisation of agroindustrial solid residues as biofuels and potential application in thermochemical processes. *Waste Management*, *32*(10), 1952–1961. https://doi.org/10.1016/j.wasman.2012.05.014

Wakatuntu, J., Olupot, P. W., Jjagwe, J., Menya, E., & Okure, M. (2023). Optimization of pyrolysis conditions for production of rice husk-based bio-oil as an energy carrier. *Results in Engineering*, *17*, 100947. https://doi.org/10.1016/j.rineng.2023.100947

Wan, W. (2016). An innovative system by integrating the gasification unit with the supercritical water unit to produce clean syngas: Effects of operating parameters. *International Journal of Hydrogen Energy*, *41*(33), 14573–14582. https://doi.org/10.1016/j.ijhydene.2016.04.237

Wan, W., Dai, Z., Yu, G., & Wang, F. (2014). System simulation of two kinds of petcoke gasification process for hydrogen. *International Journal of Energy Research*, *38*(9), 1162–1170. https://doi.org/10.1002/er.3129

Willard, H. H., Merritt, L. L., Dean, J. A., & Settle, F. A. (1986). *Instrumental methods of analysis.*

Wittayakun, J., Khemthong, P., & Prayoonpokarach, S. (2008). Synthesis and characterization of zeolite NaY from rice husk silica. *Korean Journal of Chemical Engineering*, *25*(4), 861–864. https://doi.org/10.1007/s11814-008-0142-y

Wu, C., Yin, X., Ma, L., Zhou, Z., & Chen, H. (2008). Design and Operation of A 5.5 MWe Biomass Integrated Gasification Combined Cycle Demonstration Plant. *Energy & Fuels*, *22*(6), 4259–4264. https://doi.org/10.1021/ef8004042

Xiang, X., Gong, G., Shi, Y., Cai, Y., & Wang, C. (2018). Thermodynamic modeling and analysis of a serial composite process for biomass and coal co-gasification.

Renewable and Sustainable Energy Reviews, *82*, 2768–2778. https://doi.org/10.1016/j.rser.2017.10.008

Yoon, S. J., Son, Y.-I., Kim, Y.-K., & Lee, J.-G. (2012). Gasification and power generation characteristics of rice husk and rice husk pellet using a downdraft fixed-bed gasifier. *Renewable Energy*, *42*, 163–167. https://doi.org/10.1016/j.renene.2011.08.028

Younger, P. L. (2015). *Energy*. http://www.credoreference.com/book/hoddertxec

Yusuf, A. A., & Inambao, F. L. (2020). Characterization of Ugandan biomass wastes as the potential candidates towards bioenergy production. *Renewable and Sustainable Energy Reviews*, *117*, 109477. https://doi.org/10.1016/j.rser.2019.109477

Zainal, Z. A., Ali, R., Lean, C. H., & Seetharamu, K. N. (2001). Prediction of performance of a downdraft gasifier using equilibrium modeling for different biomass materials. *Energy Conversion and Management*, *42*. https://doi.org/10.1016/S0196-8904(00)00078-9

Zaman, S. A., & Ghosh, S. (2021). A generic input–output approach in developing and optimizing an Aspen plus steam-gasification model for biomass. *Bioresource Technology*, *337*, 125412. https://doi.org/10.1016/j.biortech.2021.125412

Zaman, S. A., Roy, D., & Ghosh, S. (2020). Process modeling and optimization for biomass steam-gasification employing response surface methodology. *Biomass and Bioenergy*, *143*, 105847. https://doi.org/10.1016/j.biombioe.2020.105847

Zang, G., Jia, J., Shi, Y., Sharma, T., & Ratner, A. (2019). Modeling and economic analysis of waste tire gasification in fluidized and fixed bed gasifiers. *Waste Management*, *89*, 201–211. https://doi.org/10.1016/j.wasman.2019.03.070

Zhao, Y., Sun, S., Tian, H., Qian, J., Su, F., & Ling, F. (2009). Characteristics of rice husk gasification in an entrained flow reactor. *Bioresource Technology*, *100*(23), 6040–6044. https://doi.org/10.1016/j.biortech.2009.06.030

Zheng, J.-L., Zhu, X.-F., Guo, Q.-X., & Zhu, Q.-S. (2006). Thermal conversion of rice husks and sawdust to liquid fuel. *Waste Management (New York, N.Y.)*, *26*(12), 1430–1435. https://doi.org/10.1016/j.wasman.2005.10.011

Zhong, L.-D., Mei, W.-H., & Zhu-Hong. (2009). Kinetic model establishment and verification of the biomass gasification on fluidized bed. *2009 International Conference on Machine Learning and Cybernetics*, *4*, 2112–2117. https://doi.org/10.1109/ICMLC.2009.5212211

Zinla, D., Gbaha, P., Koffi, P. M. E., & Koua, B. K. (2021). Characterization of rice, coffee and cocoa crops residues as fuel of thermal power plant in Côte d'Ivoire. *Fuel*, *283*, 119250. https://doi.org/10.1016/j.fuel.2020.119250

Appendix A.1: Model development

Table A.1 The values of $\bar{h}_f^0$ (kJ/mol) and coeffients for $\bar{g}_{f,T}^0$ (kJ/mol).

Gas species	$\mathbf{CH_4}$	**CO**	$\mathbf{CO_2}$	$\mathbf{H_2O}$
$\bar{h}_{f,298}^0$	-74.850	-110.530	-393.520	-241.820
A	$-0.462 * 10^{-3}$	$5.619 * 10^{-3}$	$-0.195 * 10^{-3}$	$-8.950 * 10^{-3}$
B	$0.113 * 10^{-6}$	$-0.119 * 10^{-6}$	$0.312 * 10^{-6}$	$-3.672 * 10^{-6}$
C	$0.132 * 10^{-9}$	$6.383 * 10^{-9}$	$-0.245 * 10^{-9}$	$5.209 * 10^{-9}$
D	$-6.647 * 10^{-12}$	$-1.846 * 10^{-12}$	$6.946 * 10^{-12}$	$-1.478 * 10^{-12}$
E	$-4.891 * 10^{2}$	$-4.891 * 10^{2}$	$-4.891 * 10^{2}$	0.0
F	14.110	0.868	5.270	2.868
g	-0.2234	-0.0613	-0.1207	-0.0172

Table A.2 Enthalpy of formation in kJ/kmol at 25℃ and 1 atm.

Chemical species	**Formula**	**Phase**	$\Delta \boldsymbol{H_{298}^0}$
Carbon monoxide	CO	g	-110530
Hydrogen	H_2	g	0
Carbon dioxide	CO_2	g	-393520
Water	H_2O	g	-241820
Water	H_2O	l	-285830
Methane	CH_4	g	-74850
Oxygen	O_2	g	0
Nitrogen	N_2	g	0
Benzene	C_6H_6	g	82930

Table A.3 Coefficients for different gases' specific heat capacity.

Gas species	$\boldsymbol{C_1}$	$\boldsymbol{C_2}$	$\boldsymbol{C_3}$	$\boldsymbol{C_4}$
Methane	19.89	$5.202*10^{-2}$	$1.269*10^{-5}$	$-11.01*10^{-9}$
Nitrogen	28.90	$-0.1571*10^{-2}$	$0.8081*10^{-5}$	$-2.873*10^{-9}$
Carbon Monoxide	28.16	$0.1675*10^{-2}$	$0.5372*10^{-5}$	$-2.222*10^{-9}$
Water vapor	32.24	$0.1923*10^{-2}$	$1.055*10^{-5}$	$-3.595*10^{-9}$
Hydrogen	29.11	$-0.1916*10^{-2}$	$0.4003*10^{-5}$	$-0.8704*10^{-9}$
Carbon dioxide	22.26	$5.981*10^{-2}$	$-3.501*10^{-5}$	$-7.469*10^{-9}$
Benzene	-36.22	$48.475*10^{-2}$	$-31.57*10^{-5}$	$77.62*10^{-9}$

Appendix A.2: EES model simulation code

{Setting constants}

R=0.008314 {Universal gas constant in kJ/mol.K}

T_g=449 {Gasification temperature in K}

T_0=298 {Ambient temperature in K}

M_w=16 {Moisture content of biomass fuel}

ER=0.1 {Equivalence ratio}

{Enthalpy of formation in kJ/mol for the individual ideal gas species at reference point (T_0=298 K and 1 atm)}

h_fco=-110.530; h_fco2=-393.520; h_fh2o=-241.820; h_fch4=-74.850; h_fc6h6=82.930

{Coeficients for Gibbs free energy change for individual ideal gas species}

a1_co=5.619*10^(-3); a2_co=-1.190*10^(-5); a3_co=6.383*10^(-9); a4_co=-1.846*10^(-12); a5_co=-4.891*10^(2); a6_co=8.684*10^(-1); a7_co=-6.131*10^(-2)

a1_co2=-1.949*10^(-2); a2_co2=3.122*10^(-5); a3_co2=-2.448*10^(-8); a4_co2=6.946*10^(-12); a5_co2=-4.891*10^(2); a6_co2=5.270; a7_co2=-1.207*10^(-1)

a1_h2o=-8.95*10^(-3); a2_h2o=-3.67*10^(-6);a3_h2o=5.209*10^(-9); a4_h2o=-1.478*10^(-12); a5_h2o=0; a6_h2o=2.868; a7_h2o=-1.722*10^(-2)

a1_ch4=-4.62*10^(-2); a2_ch4=1.13*10^(-5); a3_ch4=1.319*10^(-8); a4_ch4=-6.647*10^(-12);a5_ch4=-4.891*10^(2); a6_ch4=14.11;a7_ch4=-2.234*10^(-1)

{Gibbs change of individual species}

dg_fco=h_fco- a1_co*T_g*ln(T_g)- a2_co*(T_g^2)-(a3_co/2)*(T_g^3)-(a4_co/3)*(T_g^4)+ a5_co/(2*T_g)+a6_co+a7_co*T_g

dg_fco2=h_fco2-a1_co2*T_g*ln(T_g)-a2_co2*(T_g^2)(a3_co2/2)*(T_g^3)(a4_co2/3)*(T_g^4)+a5_co2/(2*T_g)+a6_co2+a7_co2*T_g

dg_fh2o=h_fh2o-a1_h2o*T_g*ln(T_g)-a2_h2o*(T_g^2)-(a3_h2o/2)*(T_g^3)-(a4_h2o/3)*(T_g^4)+a5_h2o/(2*T_g)+a6_h2o+a7_h2o*T_g

dg_fch4=h_fch4-a1_ch4*T_g*ln(T_g)-a2_ch4*(T_g^2)-(a3_ch4/2)*(T_g^3)-(a4_ch4/3)*(T_g^4)+a5_ch4/(2*T_g)+a6_ch4+a7_ch4*T_g

{Calculating Equilibrium constants for methane formation and water-gas shift reaction}

```
K_1=exp(-(dg_fch4)/(R*T_g))
k_2=exp(-(dg_fco2-dg_fco-dg_fh2o)/(R*T_g))
{Ultimate analysis of biomass fuel in %}
C=37.42
H=5.17
O=46.28
N=0.13
S=0.64
A=10.36
{Molecular masses of C, H, O and N}
MC=12.001
MH=1.0079
MO=15.999
MN=14.007
{Composition of biomass fuel per mole of Carbon}
x=(H*MC)/(C*MH)
y=(O*MC)/(C*MO)
Z=(N*MC)/(C*MN)
{Moisture content of biomass fuel}
w=(M_bio*M_w)/(18*(100-M_w))
M_bio=MC+(MH*x)+(MO*y)+(MN*z)
m=ER*(1+x/4-y/2)
{Mass balance Equations}
n_CO+n_CO2+n_CH4+6*n_Tar+(1-a_c)-1=0        {Carbon balance}
a_c=0.901+0.439*(1-exp(-ER+0.0003*T_g))     {Carbon conversion factor}
2*n_H2+2*n_H2O+4*n_CH4+6*n_Tar-x-2*w=0      { Hydrogen balance}
n_CO+2*n_CO2+n_H2O-y-w-2*m=0                {Oxygen balance}
n_Tar=(35.98*exp(-0.00298*T_g))/100         {Weight of tar}
n_N2=3.76*m                                 {Nitrogen balance}
n_Char=1-a_c
{Equilibrium constant equations}
{Equilibrium contant for water-gas shift reaction}
K_1*n_CO*n_H2O-n_CO2*n_H2=0
 {Equilibrium contant for methane formation}
```

k_2*n_H2^2-(n_CH4*(n_CO+n_H2+n_CO2+n_H2O+n_CH4+n_Tar+n_N2))=0

{Finding enthalpy of formation of biomass fuel}

HHV=349.1*C+1178.3*H+100.5*S-103.4*O-15.1*N-21.1*A

HHV_mol=HHV *M_bio

H_fH2O_l=-285830

H_Vap=2260*18

dH_wood=HHV_mol+(x/2*H_fH2O_l)+(h_fco2*1000)

LHV=HHV-2260*((9*H)/100+M_w/100)

{Mole fraction of syngas (Mol% dry basis)}

n_gwco=n_CO/(1-n_H2O); n_gwco2=n_CO2/(1-n_H2O); n_gwch4=n_CH4/(1-n_H2O); n_gwh2=n_H2/(1-n_H2O); n_gwn2=n_N2/(1-n_H2O); n_gwc=n_Char/(1-n_H2O); n_gwTar=n_Tar/(1-n_H2O)

n_gt=n_gwco+n_gwco2+n_gwch4+n_gwh2+n_gwn2 +n_gwc+n_gwTar

CO=(n_gwco/n_gt)*100; CO_2=(n_gwco2/n_gt)*100; CH_4=(n_gwch4/n_gt)*100; H_2=(n_gwh2/n_gt)*100; N_2=(n_gwn2/n_gt)*100; Char=(n_gwc/n_gt)*100; Tar=(n_gwTar/n_gt)*100

Appendix B: Effect of operating conditions on the composition of syngas

Table B.1 Effect of temperature on the composition of syngas.

Temperature	CH_4	CO	CO_2	H_2	N_2	LHV_{Syngas}	H_2/CO
350	14.093	0.183	34.306	6.626	44.793	5.785	36.208
400	12.661	0.612	33.789	11.189	41.749	5.819	18.288
450	10.520	1.698	32.624	16.791	38.367	5.794	9.891
500	8.045	4.021	30.542	22.662	34.730	5.834	5.635
550	5.666	8.274	27.214	27.853	30.993	6.079	3.366
600	3.702	14.900	22.435	31.619	27.344	6.619	2.122
650	2.280	23.479	16.509	33.720	24.013	7.420	1.436
700	1.262	31.700	10.892	34.669	21.476	8.197	1.094
750	0.353	33.446	9.448	35.574	21.180	8.189	1.064
800	0.098	34.505	8.656	35.556	21.186	8.229	1.030
850	0.029	35.328	8.076	35.294	21.272	8.281	0.999
900	0.010	36.041	7.586	34.991	21.372	8.331	0.971
950	0.003	36.678	7.151	34.699	21.468	8.378	0.946
1000	0.001	37.251	6.761	34.429	21.557	8.420	0.924
1050	0.001	37.769	6.410	34.183	21.638	8.459	0.905

Table B.2 Effect of biomass moisture content on the composition of syngas.

MC	CH_4	CO	CO_2	H_2	N_2	LHV_{Syngas}	H_2/CO
10	0.01	21.82	13.55	22.90	41.50	6.00	1.05
11	0.01	21.62	13.62	22.70	41.83	5.94	1.05
12	0.01	21.42	13.70	22.49	42.15	5.87	1.05
13	0.01	21.21	13.78	22.29	42.48	5.81	1.05
14	0.01	21.01	13.86	22.08	42.82	5.74	1.05
15	0.01	20.80	13.94	21.86	43.17	5.68	1.05
16	0.01	20.58	14.03	21.65	43.51	5.61	1.05
17	0.01	20.36	14.11	21.42	43.87	5.54	1.05
18	0.01	20.14	14.20	21.20	44.23	5.48	1.05
19	0.01	19.92	14.29	20.97	44.60	5.41	1.05
20	0.01	19.69	14.38	20.74	44.97	5.34	1.05
21	0.01	19.46	14.47	20.50	45.35	5.27	1.05
22	0.01	19.22	14.56	20.26	45.73	5.19	1.05
23	0.01	18.98	14.65	20.02	46.13	5.12	1.05
24	0.00	18.74	14.75	19.77	46.52	5.05	1.06
25	0.00	18.49	14.84	19.52	46.93	4.97	1.06
26	0.00	18.24	14.94	19.26	47.34	4.90	1.06
27	0.00	17.98	15.04	19.00	47.76	4.82	1.06
28	0.00	17.72	15.14	18.73	48.19	4.74	1.06
29	0.00	17.45	15.25	18.46	48.63	4.66	1.06
30	0.00	17.18	15.35	18.18	49.07	4.58	1.06

Table B.3 Effect of equivalence ratio on the composition of syngas.

ER	CH_4	CO	CO_2	H_2	N_2	LHV_{Syngas}	H_2/CO
0.06	0.142	36.971	7.292	37.976	17.619	8.818	1.027
0.08	0.098	34.731	8.058	35.788	21.324	8.283	1.030
0.09	0.069	32.623	8.774	33.715	24.818	7.783	1.033
0.11	0.049	30.638	9.444	31.751	28.119	7.313	1.036
0.12	0.035	28.764	10.070	29.888	31.244	6.870	1.039
0.14	0.025	26.992	10.656	28.119	34.208	6.452	1.042
0.16	0.018	25.315	11.205	26.437	37.024	6.056	1.044
0.17	0.013	23.724	11.722	24.837	39.704	5.681	1.047
0.19	0.010	22.213	12.207	23.313	42.257	5.324	1.049
0.20	0.007	20.777	12.664	21.858	44.694	4.985	1.052
0.22	0.005	19.410	13.095	20.469	47.021	4.662	1.055
0.23	0.004	18.106	13.502	19.140	49.248	4.353	1.057
0.25	0.003	16.863	13.887	17.868	51.380	4.059	1.060
0.26	0.002	15.675	14.251	16.649	53.423	3.777	1.062
0.28	0.001	14.539	14.597	15.479	55.384	3.507	1.065
0.30	0.001	13.452	14.924	14.355	57.268	3.248	1.067
0.31	0.001	12.410	15.236	13.275	59.079	3.000	1.070
0.33	0.000	11.411	15.532	12.235	60.822	2.762	1.072
0.34	0.000	10.453	15.813	11.234	62.500	2.532	1.075
0.36	0.000	9.532	16.081	10.269	64.118	2.312	1.077
0.37	0.000	8.647	16.337	9.337	65.679	2.100	1.080
0.39	0.000	7.796	16.581	8.438	67.185	1.895	1.082
0.40	0.000	6.977	16.814	7.569	68.641	1.698	1.085
0.42	0.000	6.187	17.036	6.729	70.048	1.508	1.088

Table B.4 Design matrix with Aspen Plus simulated results

Temperature	ER	MC	StdOrder	RunOrder	Blocks	PtType	CO	H_2	LHV_{Syngas}	H_2/CO
550	0.06	10	1	1	1	1	8.49	29.92	6.60	3.53
550	0.06	15	2	2	1	1	8.43	29.40	6.47	3.49
550	0.06	20	3	3	1	1	8.38	28.85	6.33	3.44
550	0.07	10	4	4	1	1	8.38	28.85	6.33	3.44
550	0.12	10	5	5	1	1	7.80	23.14	4.94	2.97
550	0.12	15	6	6	1	1	7.75	22.55	4.80	2.91
550	0.12	20	7	7	1	1	7.69	21.92	4.65	2.85
550	0.18	10	8	8	1	1	7.45	19.38	4.08	2.60
550	0.18	15	9	9	1	1	7.39	18.80	3.96	2.54
550	0.18	20	10	10	1	1	7.33	18.19	3.82	2.48
600	0.06	10	11	11	1	1	15.22	33.82	7.07	2.22
600	0.06	15	12	12	1	1	15.14	33.27	6.96	2.20
600	0.06	20	13	13	1	1	15.05	32.68	6.84	2.17
600	0.12	10	14	14	1	1	14.18	26.52	5.61	1.87
600	0.12	15	15	15	1	1	14.09	25.87	5.49	1.84
600	0.12	20	16	16	1	1	13.99	25.17	5.35	1.80
600	0.18	10	17	17	1	1	13.61	22.37	4.83	1.64
600	0.18	15	18	18	1	1	13.53	21.71	4.71	1.61
600	0.18	20	19	19	1	1	13.43	21.03	4.59	1.57
650	0.06	10	20	20	1	1	23.91	35.92	7.81	1.50
650	0.06	15	21	21	1	1	23.80	35.37	7.72	1.49
650	0.06	20	22	22	1	1	23.68	34.78	7.61	1.47
650	0.12	10	23	23	1	1	22.49	28.54	6.51	1.27
650	0.12	15	24	24	1	1	22.36	27.87	6.40	1.25
650	0.12	20	25	25	1	1	21.96	27.20	6.23	1.24
650	0.18	10	26	26	1	1	18.59	24.31	5.25	1.31
650	0.18	15	27	27	1	1	17.74	23.53	5.01	1.33

650	0.18	20	28	28	1	1	16.81	22.64	4.75	1.35
700	0.06	10	29	29	1	1	32.87	36.62	8.65	1.11
700	0.06	15	30	30	1	1	32.74	36.10	8.56	1.10
700	0.06	20	31	31	1	1	32.60	35.53	8.47	1.09
700	0.12	10	32	32	1	1	26.01	29.86	6.69	1.15
700	0.12	15	33	33	1	1	25.20	29.13	6.49	1.16
700	0.12	20	34	34	1	1	24.31	28.32	6.26	1.17
700	0.18	10	35	35	1	1	20.43	24.64	5.30	1.21
700	0.18	15	36	36	1	1	19.46	23.69	5.07	1.22
700	0.18	20	37	37	1	1	18.42	22.65	4.81	1.23
750	0.06	10	38	38	1	1	35.70	37.61	8.75	1.05
750	0.06	15	39	39	1	1	35.16	37.13	8.61	1.06
750	0.06	20	40	40	1	1	34.56	36.58	8.46	1.06
750	0.12	10	41	41	1	1	27.43	29.93	6.74	1.09
750	0.12	15	42	42	1	1	26.58	29.11	6.54	1.10
750	0.12	20	43	43	1	1	25.66	28.21	6.32	1.10
750	0.18	10	44	44	1	1	21.63	24.24	5.36	1.12
750	0.18	15	45	45	1	1	20.63	23.24	5.13	1.13
750	0.18	20	46	46	1	1	19.55	22.15	4.87	1.13
800	0.06	10	47	47	1	1	36.78	37.78	8.77	1.03
800	0.06	15	48	48	1	1	36.23	37.24	8.64	1.03
800	0.06	20	49	49	1	1	35.62	36.65	8.50	1.03
800	0.12	10	50	50	1	1	28.47	29.58	6.80	1.04
800	0.12	15	51	51	1	1	27.61	28.72	6.60	1.04
800	0.12	20	52	52	1	1	26.68	27.79	6.38	1.04
800	0.18	10	53	53	1	1	22.62	23.71	5.42	1.05
800	0.18	15	54	54	1	1	21.61	22.69	5.18	1.05
800	0.18	20	55	55	1	1	20.51	21.58	4.92	1.05
850	0.06	10	56	56	1	1	37.57	37.60	8.82	1.00
850	0.06	15	57	57	1	1	37.03	37.04	8.69	1.00

850	0.06	20	58	58	1	1	36.43	36.43	8.54	1.00
850	0.12	10	59	59	1	1	29.34	29.15	6.86	0.99
850	0.12	15	60	60	1	1	28.49	28.28	6.65	0.99
850	0.12	20	61	61	1	1	27.56	27.33	6.43	0.99
850	0.18	10	62	62	1	1	23.49	23.18	5.47	0.99
850	0.18	15	63	63	1	1	22.48	22.15	5.23	0.99
850	0.18	20	64	64	1	1	21.38	21.03	4.97	0.98
900	0.06	10	65	65	1	1	38.24	37.34	8.86	0.98
900	0.06	15	66	66	1	1	37.71	36.78	8.74	0.98
900	0.06	20	67	67	1	1	37.13	36.15	8.59	0.97
900	0.12	10	68	68	1	1	30.13	28.74	6.91	0.95
900	0.12	15	69	69	1	1	29.28	27.85	6.70	0.95
900	0.12	20	70	70	1	1	28.35	26.89	6.48	0.95
900	0.18	10	71	71	1	1	24.29	22.69	5.52	0.93
900	0.18	15	72	72	1	1	23.27	21.65	5.28	0.93
900	0.18	20	73	73	1	1	22.16	20.53	5.01	0.93
950	0.06	10	74	74	1	1	38.84	37.09	8.91	0.95
950	0.06	15	75	75	1	1	38.32	36.51	8.78	0.95
950	0.06	20	76	76	1	1	37.74	35.88	8.64	0.95
950	0.12	10	77	77	1	1	30.83	28.35	6.95	0.92
950	0.12	15	78	78	1	1	29.99	27.46	6.75	0.92
950	0.12	20	79	79	1	1	29.07	26.48	6.53	0.91
950	0.18	10	80	80	1	1	25.01	22.25	5.56	0.89
950	0.18	15	81	81	1	1	23.99	21.20	5.32	0.88
950	0.18	20	82	82	1	1	22.87	20.07	5.05	0.88

Appendix C: Gass Chromatograph calibration

Appendix C.1 CH_4 Calibration Curve

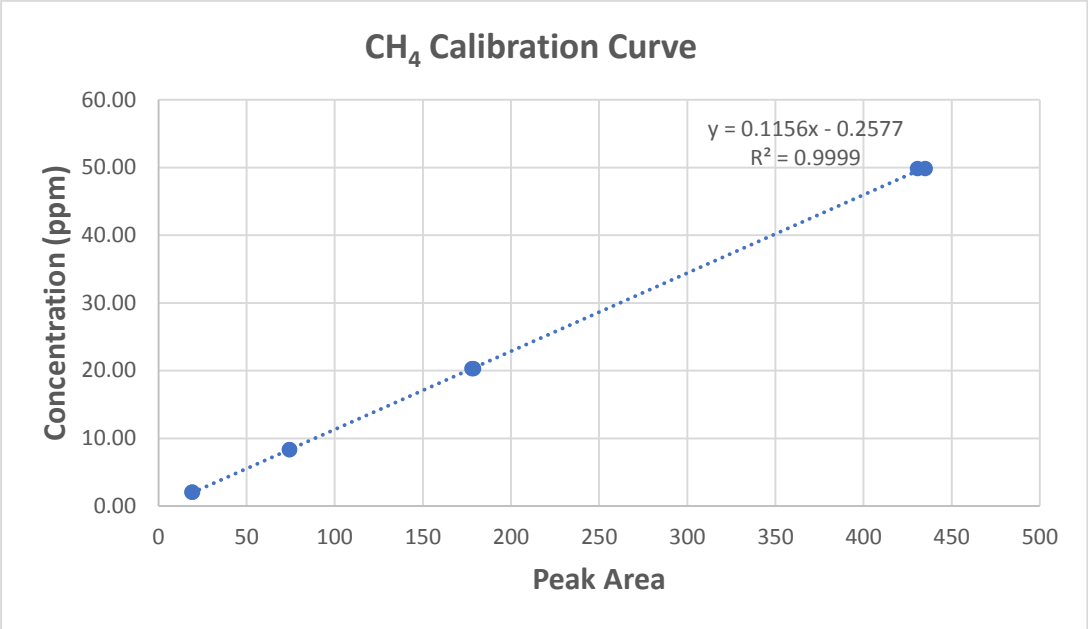

Appendix C.2 CO_2 Calibration Curve

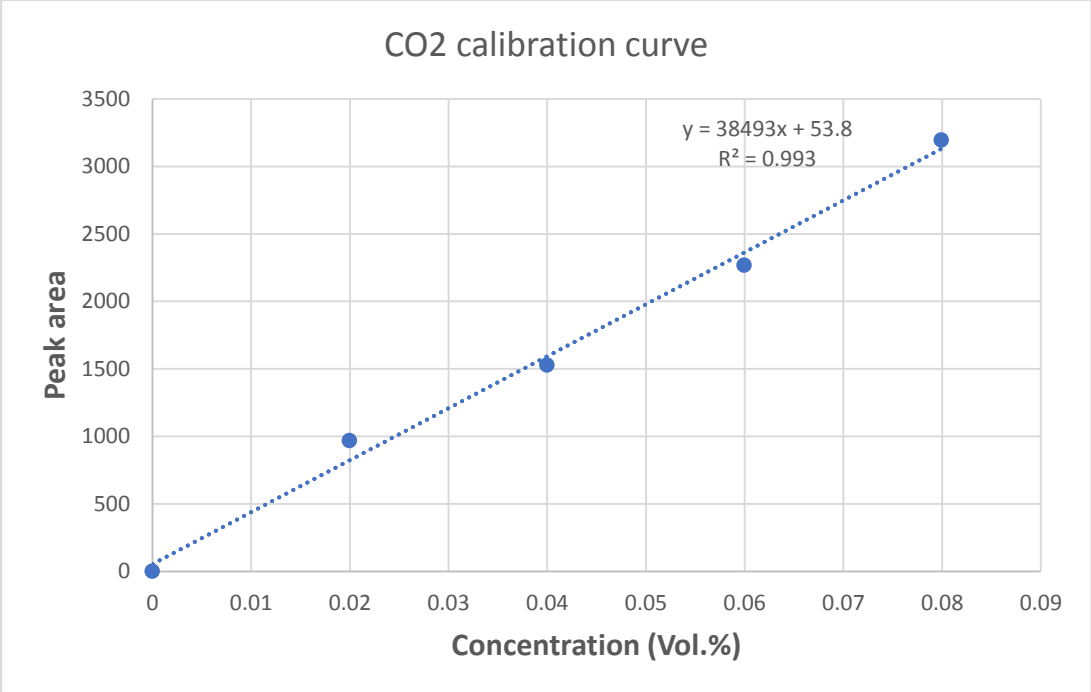

Appendix C.3 N_2 Calibration Curve

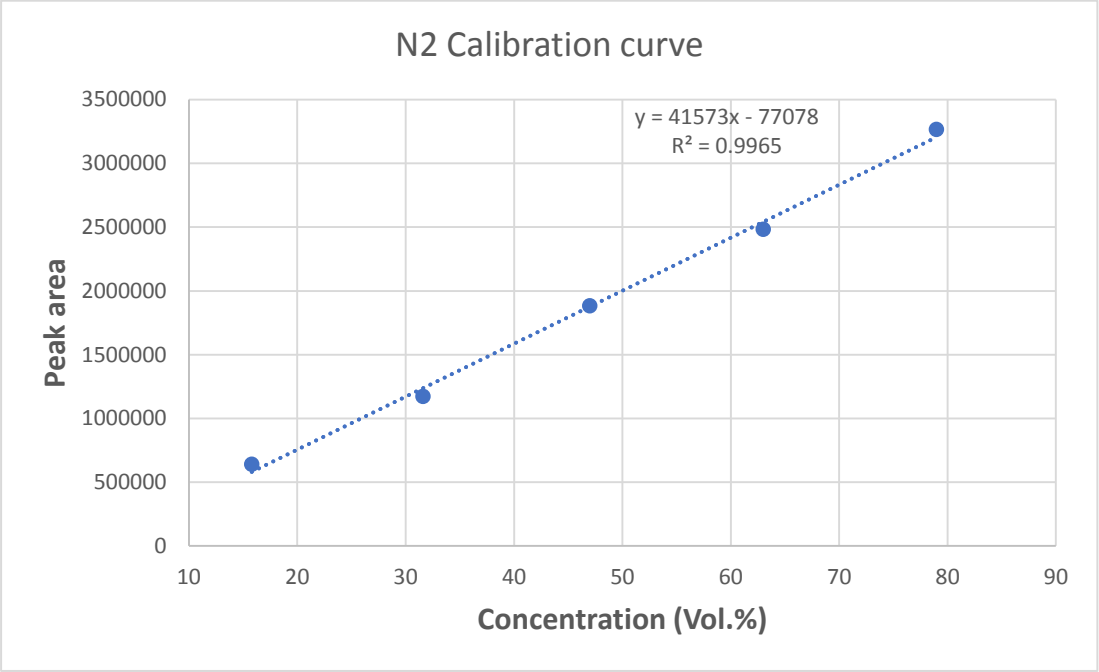

Appendix D: Journal articles published from this work

Kombe, E. Y., Lang'at, N., Njogu, P., Malessa, R., Weber, C.-T., Njoka, F., & Krause, U. (2022). Numerical investigation of sugarcane bagasse gasification using Aspen Plus and response surface methodology. *Energy Conversion and Management*, *254*, 115198. https://doi.org/10.1016/j.enconman.2021.115198

Kombe, E. Y., Lang'at, N., Njogu, P., Malessa, R., Weber, C.-T., Njoka, F., & Krause, U. (2022). Process modeling and evaluation of optimal operating conditions for production of hydrogen-rich syngas from air gasification of rice husks using aspen plus and response surface methodology. *Bioresource Technology*, *361*, 127734. https://doi.org/10.1016/j.biortech.2022.127734

Energy Conversion and Management 254 (2022) 115198

Contents lists available at ScienceDirect

Energy Conversion and Management

journal homepage: www.elsevier.com/locate/enconman

ELSEVIER

Numerical investigation of sugarcane bagasse gasification using Aspen Plus and response surface methodology

Emmanuel Yeri Kombe [a,b], Nickson Lang'at [c], Paul Njogu [d], Reiner Malessa [e], Christian-Toralf Weber [b], Francis Njoka [a,*], Ulrich Krause [f]

Impact Factor 11.533

Bioresource Technology 361 (2022) 127734

Contents lists available at ScienceDirect

Bioresource Technology

journal homepage: www.elsevier.com/locate/biortech

ELSEVIER

Process modeling and evaluation of optimal operating conditions for production of hydrogen-rich syngas from air gasification of rice husks using aspen plus and response surface methodology

Emmanuel Yeri Kombe [a,b], Nickson Lang'at [c], Paul Njogu [d], Reiner Malessa [e], Christian-Toralf Weber [b], Francis Njoka [a,*], Ulrich Krause [f]

Impact Factor 11.889

Appendix E: Research Aproval from graduate school

KENYATTA UNIVERSITY
GRADUATE SCHOOL

KENYATTA UNIVERSITY RECEIVED 05 APR 2019 DEPT. OF ENERGY TECHNOLOGY P.O. Box 43844 - NAIROBI

E-mail: dean-graduate@ku.ac.ke
Website: www.ku.ac.ke

P.O. Box 43844, 00100
NAIROBI, KENYA
Tel. 810901 Ext. 57530

Internal Memo

FROM: Dean, Graduate School

DATE: 1st April, 2019

REF: J98/39229/16

TO: Mr. Emmanuel Y. Kombe
C/o Energy Technology Dept.
Kenyatta University

SUBJECT: APPROVAL OF RESEARCH PROPOSAL

This is to inform you that Graduate School Board at its meeting of 27th March, 2019 approved your Research Proposal for the Ph.D. Degree, entitled "Thermodynamic Modelling and Optimization of Biomass Gasification System for Fischer-Tropsch Synthesis".

You may now proceed with your Data collection, subject to clearance with the Director General, National commission for Science & Technology.

As you embark on your data collection, please note that you will be required to submit to Graduate School completed supervision Tracking Forms per semester. The form has been developed to replace the progress Report Forms. The Supervision Tracking Forms are available at the University's Website under Graduate School webpage downloads.

By copy of this letter, the Registrar (Academic) is hereby requested to grant you substantive registration for your Ph.D. studies.

Thank you.

REUBEN MURIUKI
FOR: DEAN, GRADUATE SCHOOL

c.c. Registrar (Academic) Att. Ms. Lucy Njenga
Chairman, Department of Energy Technology

Supervisors:

1. Dr. Nickson Lang'at
C/o Agric & Biosystem Engineering Dept.
KENYATTA UNIVERSITY

2. Prof. Chrispus Ndiema
Mechanical & Industrial Engineering
Masinde Muliro University of Science & Tech
C/o Energy Technology Dept.
KENYATTA UNIVERSITY

RM/cao

Appendix F: Research Permit from NACOSTI

REPUBLIC OF KENYA

NATIONAL COMMISSION FOR SCIENCE,TECHNOLOGY & INNOVATION

Ref No: **472463**

Date of Issue: **15/December/2020**

RESEARCH LICENSE

This is to Certify that Mr.. Emmanuel Yeri Kombe of Kenyatta University, has been licensed to conduct research in Nairobi on the topic: Thermodynamic Modelling and Optimization of Biomass Gasification system for Fischer-Tropsch Synthesis for the period ending : 15/December/2021.

License No: **NACOSTI/P/20/8197**

472463

Applicant Identification Number

Director General
NATIONAL COMMISSION FOR SCIENCE,TECHNOLOGY & INNOVATION

Verification QR Code

NOTE: This is a computer generated License. To verify the authenticity of this document, Scan the QR Code using QR scanner application.

THE SCIENCE, TECHNOLOGY AND INNOVATION ACT, 2013

The Grant of Research Licenses is Guided by the Science, Technology and Innovation (Research Licensing) Regulations, 2014

CONDITIONS

1. The License is valid for the proposed research, location and specified period
2. The License any rights thereunder are non-transferable
3. The Licensee shall inform the relevant County Director of Education, County Commissioner and County Governor before commencement of the research
4. Excavation, filming and collection of specimens are subject to further necessary clearence from relevant Government Agencies
5. The License does not give authority to tranfer research materials
6. NACOSTI may monitor and evaluate the licensed research project
7. The Licensee shall submit one hard copy and upload a soft copy of their final report (thesis) within one year of completion of the research
8. NACOSTI reserves the right to modify the conditions of the License including cancellation without prior notice

National Commission for Science, Technology and Innovation
off Waiyaki Way, Upper Kabete,
P. O. Box 30623, 00100 Nairobi, KENYA
Land line: 020 4007000, 020 2241349, 020 3310571, 020 8001077
Mobile: 0713 788 787 / 0735 404 245
E-mail: dg@nacosti.go.ke / registry@nacosti.go.ke
Website: www.nacosti.go.ke